British Geological Survey
NATURAL ENVIRONMENT RESEARCH COUNCIL

Results of laboratory carbonation experiments on NRVB cement

Minerals and Waste Programme

Open Report OR/14/048

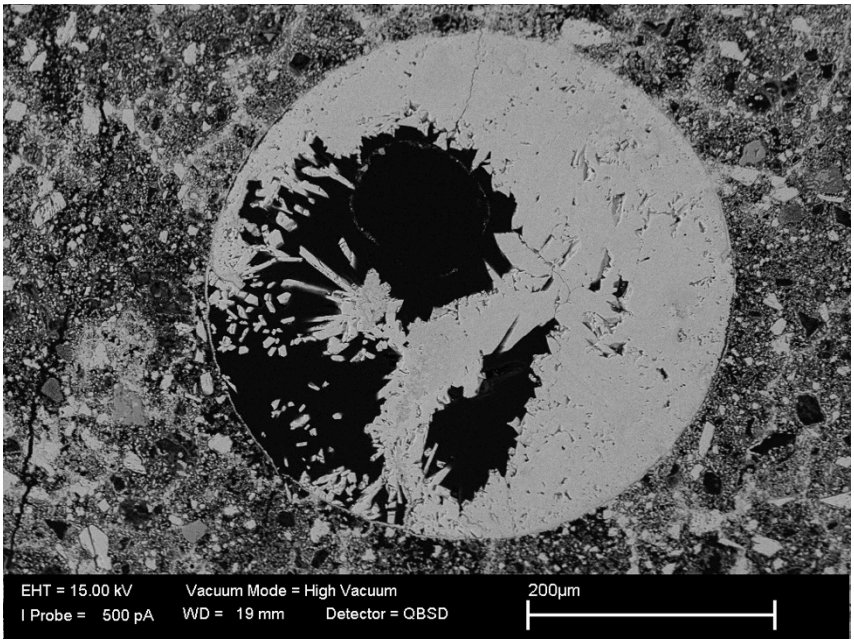

BRITISH GEOLOGICAL SURVEY

ENERGY SCIENCE PROGRAMME

OPEN REPORT OR/14/048

Results of laboratory carbonation experiments on Nirex Reference Vault Backfill cement

C.A. Rochelle, G. Purser and A.E. Milodowski

Key words

Radioactive waste, repository, backfill, carbon dioxide, experimental study, cement, carbonation, CO_2, geochemistry, NRVB.

Front cover

Scanning electron microscope image showing an air bubble entrained in cement, now largely filled by coarse secondary calcite (carbonation over 40 days at 40°C and 80 bar pressure).

Bibliographical reference

ROCHELLE, C.A., PURSER, G., AND MILODOWSKI, A.E. 2014. Results of laboratory carbonation experiments on NRVB cement. *British Geological Survey Open Report*, OR/14/014. 60 pp.

Keyworth, Nottingham British Geological Survey 2014

BRITISH GEOLOGICAL SURVEY

The full range of our publications is available from BGS shops at Nottingham, Edinburgh, London and Cardiff (Welsh publications only) see contact details below or shop online at www.geologyshop.com

The London Information Office also maintains a reference collection of BGS publications, including maps, for consultation.

We publish an annual catalogue of our maps and other publications; this catalogue is available online or from any of the BGS shops.

The British Geological Survey carries out the geological survey of Great Britain and Northern Ireland (the latter as an agency service for the government of Northern Ireland), and of the surrounding continental shelf, as well as basic research projects. It also undertakes programmes of technical aid in geology in developing countries.

The British Geological Survey is a component body of the Natural Environment Research Council.

British Geological Survey offices

BGS Central Enquiries Desk

Tel 0115 936 3143 Fax 0115 936 3276

email enquiries@bgs.ac.uk

Environmental Science Centre, Keyworth, Nottingham NG12 5GG

Tel 0115 936 3241 Fax 0115 936 3488

email sales@bgs.ac.uk

Murchison House, West Mains Road, Edinburgh EH9 3LA

Tel 0131 667 1000 Fax 0131 668 2683

email scotsales@bgs.ac.uk

Natural History Museum, Cromwell Road, London SW7 5BD

Tel 020 7589 4090 Fax 020 7584 8270

Tel 020 7942 5344/45 email bgslondon@bgs.ac.uk

Columbus House, Greenmeadow Springs, Tongwynlais, Cardiff CF15 7NE

Tel 029 2052 1962 Fax 029 2052 1963

Maclean Building, Crowmarsh Gifford, Wallingford OX10 8BB

Tel 01491 838800 Fax 01491 692345

Geological Survey of Northern Ireland, Colby House, Stranmillis Court, Belfast BT9 5BF

Tel 028 9038 8462 Fax 028 9038 8461

www.bgs.ac.uk/gsni/

Parent Body

Natural Environment Research Council, Polaris House, North Star Avenue, Swindon SN2 1EU

Tel 01793 411500 Fax 01793 411501

www.nerc.ac.uk

Website www.bgs.ac.uk

Shop online at www.geologyshop.com

Towards D3.16:

Results of laboratory carbonation experiments on Nirex Reference Vault Backfill cement

C.A. Rochelle, G. Purser and A.E. Milodowski

Towards FORGE Report D3.16 – VER. 3

	Name	Organisation	Signature	Date
Compiled	C. Rochelle	British Geological Survey	C. Rochelle	26/1/2014
Verified				
Approved				

Keywords

Radioactive waste, repository, backfill, NRVB, cement, carbon dioxide, CO_2, carbonation, experimental study, geochemistry.

Bibliographical reference

Rochelle, C.A. Purser, G. and Milodowski, A.E. 2014. Towards D3.6: Results of laboratory carbonation experiments on Nirex Reference Vault Backfill cement. FORGE Report D3.16. 60 pp.

Euratom 7th Framework Programme Project: FORGE

Fate of repository gases (FORGE)

The multiple barrier concept is the cornerstone of all proposed schemes for underground disposal of radioactive wastes. The concept invokes a series of barriers, both engineered and natural, between the waste and the surface. Achieving this concept is the primary objective of all disposal programmes, from site appraisal and characterisation to repository design and construction. However, the performance of the repository as a whole (waste, buffer, engineering disturbed zone, host rock), and in particular its gas transport properties, are still poorly understood. Issues still to be adequately examined that relate to understanding basic processes include: dilational versus visco-capillary flow mechanisms; long-term integrity of seals, in particular gas flow along contacts; role of the EDZ as a conduit for preferential flow; laboratory to field up-scaling. Understanding gas generation and migration is thus vital in the quantitative assessment of repositories and is the focus of the research in this integrated, multi-disciplinary project. The FORGE project is a pan-European project with links to international radioactive waste management organisations, regulators and academia, specifically designed to tackle the key research issues associated with the generation and movement of repository gasses. Of particular importance are the long-term performance of bentonite buffers, plastic clays, indurated mudrocks and crystalline formations. Further experimental data are required to reduce uncertainty relating to the quantitative treatment of gas in performance assessment. FORGE will address these issues through a series of laboratory and field-scale experiments, including the development of new methods for up-scaling allowing the optimisation of concepts through detailed scenario analysis. The FORGE partners are committed to training and CPD through a broad portfolio of training opportunities and initiatives which form a significant part of the project.

Further details on the FORGE project and its outcomes can be accessed at www.FORGEproject.org.

Contact details:

C.A. Rochelle
British Geological Survey
Tel: +44 (0)115 9363259 Fax +44 (0)115 9363200
email: caro@bgs.ac.uk
web address: www.bgs.ac.uk
Address Kingsley Dunham Centre, Keyworth, Nottingham, NG12 5GG, UK.

.

Foreword

The multiple barrier concept is the cornerstone of all proposed schemes for underground disposal of radioactive wastes. The concept invokes a series of barriers, both engineered and natural, between the waste and the surface. Achieving this concept is the primary objective of all disposal programmes, from site appraisal and characterisation to repository design and construction. However, the performance of the repository as a whole (waste, buffer, engineering disturbed zone, host rock), and in particular its gas transport properties, are still poorly understood. Issues still to be adequately examined that relate to understanding basic processes include: dilational versus visco-capillary flow mechanisms; long-term integrity of seals, in particular gas flow along contacts; role of the Engineering Damaged Zone (EDZ) as a conduit for preferential flow; laboratory to field up-scaling. Understanding gas generation and migration is thus vital in the quantitative assessment of repositories and is the focus of the research in this proposal for an integrated, multi-disciplinary project.

FORGE is a pan-European project with links to international radioactive waste management organisations, regulators and academia, specifically designed to tackle the key research issues associated with the generation and movement of repository gasses. Of particular importance are the long-term performance of bentonite buffers, plastic clays, indurated mudrocks and crystalline formations. Further experimental data are required to reduce uncertainty relating to the quantitative treatment of gas in performance assessment. FORGE will address these issues through a series of laboratory and field-scale experiments, including the development of new methods for up-scaling, allowing the optimisation of concepts through detailed scenario analysis.

This report has been prepared by the British Geological Survey (BGS) as a product towards FORGE deliverable 3.16 (‘Results of the tests on concrete [part 2]’), and is a more extensive description of the work outlined in the previous report ‘Results of the tests on concrete [part 1]’ (towards FORGE deliverable 3.6). It outlines fluid chemical and mineralogical changes resulting from experiments of durations from 10 days to 1 year, reacting CO_2 with a repository backfill cement and synthetic cement porewaters.

Contents

FIGURES

PLATES

TABLES

Summary

Some repository concepts envisage the use of large quantities of cementitious materials – both for repository construction and as a buffer/backfill. However, some wastes placed within a subsurface repository will contain a significant amount of organic material that may degrade to produce carbon dioxide. This will react with cement buffer/backfill to produce carbonate minerals such as calcite, which will reduce the ability of the buffer/backfill to maintain highly alkaline conditions and as a consequence its ability to limit radionuclide migration. The reaction may also alter the physical properties of the buffer/backfill. The work involved in this study investigates these processes through elevated pressure laboratory experiments conducted at a range of likely future *in situ* repository conditions. These will provide information on the reactions that occur, with results serving as examples with which to test predictive modelling codes. This report details a series of batch experiments to study carbonation of Nirex Reference Vault Backfil (NRVB) cement.

Thirty-two static batch experiments were pressurised with either CO_2, or with N_2 for 'non-reacting' comparison tests at 20°C or 40°C, and 40 or 80 bar. Twenty-six of these were left to react for durations of between 10-40 days, with six more left to react for a year. The aim of them was to help investigate mineralogical and fluid chemical changes due to the diffusional ingress of CO_2 into unconfined NRVB samples measuring 2.5 cm in diameter and 5 cm long.

All the cement samples showed rapid reaction with CO_2, manifested by a colour change from grey to light brown. Petrographic analysis of the reacted cement revealed that this colour change reflected the breakdown and dissolution of primary calcium ferrite and calcium alumina-ferrite (CAF) cement clinker phases (e.g. brownmillerite, $Ca_2(Al,Fe)_2O_5$ to form calcium carbonates and finely-disseminated free ferric oxide (probably hematite, Fe_2O_3), as a result of reaction with CO_2 to give a 'rusty' colour. It should be noted that his is not an oxidation reaction as the iron is present as Fe^{3+} in the original cement phases.

The cement blocks remained intact, even after prolonged exposure to CO_2-rich fluids. Carbonation was associated with an increase in weight of up to 8.5% during CO_2 uptake, though the samples did not change in overall size. There is potential therefore, for carbonation to immobilise $^{14}CO_2$ if that were present. Free-phase CO_2 gave slightly more reaction than dissolved CO_2, possibly because of its higher concentration and greater ability to penetrate the samples. In terms of major reactions during carbonation, these were the breakdown of portlandite, calcium silicate hydrate (CSH) phases, calcium aluminate (or calcium aluminate hydrate) phases, and ettringite-like phases, and the formation of carbonate phases and silica gel. Carbonation also revealed that heterogeneity within the cement samples had a major impact on migration pathways and extent of carbonation. This heterogeneity may have been a result of casting, and was only observed in some of the samples studied. It led to faster carbonation in some areas, and may account for some of the differences observed in the reacted cement samples. Such heterogeneity may be present within a repository, and should be taken into account when assessing repository performance.

Carbonation resulted in a series of reaction fronts that moved through the cement over time. These fronts separated several reaction zones: Zone 1 = minor carbonation with minimal apparent volume change, Zone 2 = partial carbonation and very localised shrinkage, Zone 3 = complete conversion of portlandite and CSH with localised shrinkage associated with the development of abundant calcium carbonate-sealed microfractures, Zone 4 = dissolution of initially-formed carbonate minerals in the outermost parts of the sample by the surrounding, slightly-acidic water. The shrinkage in Zone 2 was expressed as small fractures (typically several mm long), though these do not appear to extend beyond this zone. Zone 3 contained an intense anastomising '3D chickenwire' meshwork of interconnected, higher-density, carbonate-filled

microfractures (typically on a 10s-100s μm scale) that separated silica-rich areas having lower-density and high porosity, and sub-parallel 'relic' reaction fronts. The small fractures of Zone 2 appear to have filled with secondary precipitates in Zone 3. It would be useful to understand how these reaction zones evolve over longer timescales, and investigate whether they have the potential to become narrower (or even merge together), with more efficient sealing of porosity that might 'armour' the cement from further carbonation.

Appreciable amounts of two Cl-rich phases were formed at the boundary of Zones 2 and 3. At least one of these phases appears to have been enhanced by the presence of CO_2. The formation of Cl-rich phases within a repository could be beneficial as it might help to immobilise ^{36}Cl leaching from the waste. Further work is needed to precisely-identify these Cl-rich phases and ascertain the impact such phases could have on ^{36}Cl retardation and repository safety.

Carbonation features and secondary phases observed in these experiments using a relatively porous/permeable cement, bear many similarities to those found in far lower porosity/permeability borehole cements used in CO_2-storage operations. There are also similarities to samples of naturally-occurring CSH phases which have been naturally-carbonated over prolonged timescales. A number of common carbonation processes may be operating in all these systems.

1. Introduction

Some repository concepts envisage the use of large quantities of cementitious materials – both for repository construction and as a buffer/backfill. Key aspects of these materials are their good mechanical properties, and their ability to buffer pH to alkaline conditions. Such high pH conditions are important as they greatly limit metallic corrosion and radionuclide solubility - and as a consequence, radionuclide migration. Some wastes placed within a subsurface repository will contain a significant amount of organic material (e.g. ion-exchange resins, contaminated clothing etc). Over time, these may degrade to produce carbon dioxide (CO_2), which will rapidly react with cement buffer/backfill to produce carbonate minerals such as calcite. The conversion of cement minerals to carbonates will reduce the ability of the buffer/backfill to maintain highly alkaline conditions and as a consequence its ability to limit radionuclide migration. However, the reaction may also alter the physical properties of the buffer/backfill, possibly changing its permeability and strength. Although carbonation reactions might improve some properties, it is currently unclear whether the *overall* changes due to carbonation will be beneficial to long-term radionuclide immobilisation, or deleterious. The work involved in this study investigates these processes through laboratory experiments. These were conducted at a range of possible future *in situ* repository conditions, including those expected over glacial timescales, which might influence the form of the CO_2 (i.e. dissolved, gas, liquid or supercritical). The results of the experiments will serve as examples with which to test predictive modelling codes that incorporate reaction kinetics, and coupling between geochemical reaction, porosity changes and fluid flow (such as in the BGS-developed PRECIP code).

Two types of experiments were conducted as part of the FORGE work:

- Numerous batch experiments aimed at providing information on changing mineralogy and porosity upon reaction with free phase and dissolved gaseous, liquid and supercritical CO_2.
- A few flow experiments with mainly free phase and dissolved supercritical CO_2 aimed at providing information on changing permeability upon reaction

This report will only describe results from former of these, with Purser *et al.* (2013), describing the flow experiments.

2. Starting materials

2.1 CEMENT

The cement composition used is that of the 'Nirex reference backfill cement' (NRVB) (Francis *et al.*, 1997). This was chosen so that the results from the present study would be comparable with different measured parameters/datasets from earlier studies. It is acknowledged however, that the compositions of backfill cements used in any future repository may well be different to the composition used in this study, but it is thought that many of the mineralogical reactions we may observe are likely to be common to a wide-range of cements.
The composition of the starting cement is as follows:

- Portland Cement ('Ordinary Portland cement', from Hanson) = 450 kg/m^3
- Limestone flour ('Superlon 100', from Longcliffe Ltd) = 495 kg/m^3
- Lime ('Hydralime', from Lafarge) = 170 kg/m^3
- Water (mains tap water) = 615 kg/m^3

These were thoroughly mixed together over several minutes in a portable mixer to form fine slurry (Figure 1). A sufficient quantity (approximately 50 kg) of cement slurry was prepared in a single batch to provide an excess of material for use in the FORGE project. The cement was then

poured into several plastic moulds and allowed to set (Figure 2). As the cement was prepared as a single batch, all the resulting cylinders of cement should have identical composition.

Figure 1. Adding the cement components to a portable cement mixer.

Figure 2. Pouring the cement slurry into plastic moulds.

Once in the moulds the cement was left to set at 40°C for 24 hours. The plastic moulds were then removed, and the cylinders of cement cured for 40 days immersed in water saturated with $Ca(OH)_2$ at 40°C and 1 bar pressure. The presence of the $Ca(OH)_2$ was to minimise the potential for the outer parts of the cement to dissolve in the water. Being immersed in water also allowed pores within the cement to be fully saturated, and also to uptake extra water as remaining high

temperature clinker phases slowly hydrated. After curing, the cement was stored in $Ca(OH)_2$-saturated water in a sealed container at room temperature (20°C) and 1 bar.

2.2 AQUEOUS SOLUTIONS

The fluids used in the experiments were of three types:

1) A synthetic, young near-field porewater (YNFP) representative of the initial Na/K/Ca-rich pore fluid composition.
2) A slightly modified version of the above with chloride added (YNFP+Cl) to represent a fluid having a composition intermediate between (1) and (3).
3) A synthetic evolved near-field groundwater (ENFG) representative of the later Ca-rich pore fluid that will exist once local groundwater starts to perculate through the cement backfill.

The fluids used in this study were based on those reported in Francis *et al.* (1997). They are representative of those anticipated in the vicinity of a cementitious waste repository, and are broadly similar to those used in previous experimental studies Rochelle *et al.*, 1994, 1997, 1998a,b,c) which in turn used compositions based upon previous modelling studies (Bond *et al.*, 1995a,b) (see Table 1 for composition, and Appendix 1 for fluid chemical analytical results).

2.3 GASES

Two gases were used in the experiments: carbon dioxide (CO_2) and nitrogen (N_2).

CO_2

The CO_2 used in this study was sourced from high purity (99.99%) liquid CO_2 (Air Products, 4.5 Grade). This liquid CO_2 was obtained in a cylinder fitted with a dip tube and pressurised with 2000 psi (approximately 14 MPa) of helium. However, the actual experimental pressure was controlled by an ISCO syringe pump, which has its pressure transducer periodically 'zeroed' to minimise drift. As the liquid CO_2 at room temperature was piped to the experiments in the incubator, the increase in temperature caused it to become a lower density (supercritical) phase. Recorded pressures were taken from the ISCO pump controller readout.

N_2

The N_2 used in this study was obtained from BOC Gases and classified as 'oxygen free' (99.998% pure). It was delivered in a cylinder pressurised to 230 bar (23 MPa). However, the actual experimental pressure was controlled by an ISCO syringe pump, which has its pressure transducer periodically 'zeroed' to minimise drift. Recorded pressures were taken from the ISCO pump controller readout.

Chemical component	YNFP (mol l^{-1})	YNFP+Cl (mol l^{-1})	ENFG (mol l^{-1})
pH	c. 13 (at room temp.)	c. 12.5 (at room temp.)	12.4 (at room temp.)
Na	7.1×10^{-2}	7.1×10^{-2}	3.9×10^{-1}
K	9.3×10^{-2}	9.3×10^{-2}	3.9×10^{-3}
Ca	3.6×10^{-3}	3.6×10^{-3}	5.2×10^{-2}
Sr			3.0×10^{-4}
Cl		1.64×10^{-1}	4.3×10^{-1}
Br			3.2×10^{-4}
SO_4^{2-}			1.1×10^{-2}
SiO_2	8.0×10^{-4}	8.0×10^{-4}	2.6×10^{-5}

Chemical component	YNFP (grammes added per 2 litres of distilled de-ionised water)	YNFP+Cl (grammes added per 2 litres of distilled de-ionised water)	ENFG (grammes added per 2 litres of distilled de-ionised water)
CaO	0.3366	0.3366	-
$CaCl_2.2H_2O$	-		22.7739
NaOH	5.6249		3.7147
NaCl	-	8.2988	37.5767
KOH	10.4344		
KCl	-	13.8660	0.5341
$SrCl_2.6H_2O$	-		0.1602
SiO_2	† 96.125	† 96.1738	† 3.2019
Na_2SO_4	-		3.1246
KBr	-		0.0762

† g BDH 1000 mg l^{-1} standard SiO_2 solution added.

Table 1 Target compositions and recipes of the 'young' near-field porewater (YNFP), 'young' near-field porewater plus additional chloride (YNFP+Cl), and the 'evolved' near-field groundwater (ENFG) used in the experiments.

3. Description of the batch experiments

3.1 CEMENT SAMPLES

The larger cylinders of cement were removed from the $Ca(OH)_2$-saturated water and sub-cored to produce samples of 25 mm diameter for the batch experiments. There were then accurately machined to a length of 50 mm.

3.2 EXPERIMENTAL EQUIPMENT

Laboratory experiments were conducted within the Hydrothermal Laboratory of the British Geological Survey, Keyworth, UK. Prior to performing the experiments, it was necessary to consider the use of equipment that would perform well. Although dry CO_2 is relatively inert, in the presence of water or NaCl solution it is much more reactive. Previous investigations within the BGS Hydrothermal Laboratory and other studies (e.g. Schremp and Roberson, 1975) have shown that steel can corrode and standard O-ring seals can blister and fail. To minimise both corrosion and experimental failure, exposed surfaces were chosen so as to be as inert as practicable. Therefore, the pressure vessels were made of 316 stainless steel with wetted parts lined with PTFE (polytetrafluoroethene) 'cups', high pressure tubing was made of either 316 stainless steel or PEEK™ (polyetheretherketone), and O-ring seals were made of Viton®.

The batch equipment used is relatively simple and generally free from day-to-day maintenance. As a consequence, the vessels are well-suited for running over prolonged time periods. Indeed, similar equipment has also been used successfully in previous studies of CO_2-water-rock reaction (e.g. Gunter *et al.*, 1993; Rochelle *et al.*, 2004, 2006a). A schematic diagram of the equipment is given in Figure 3.

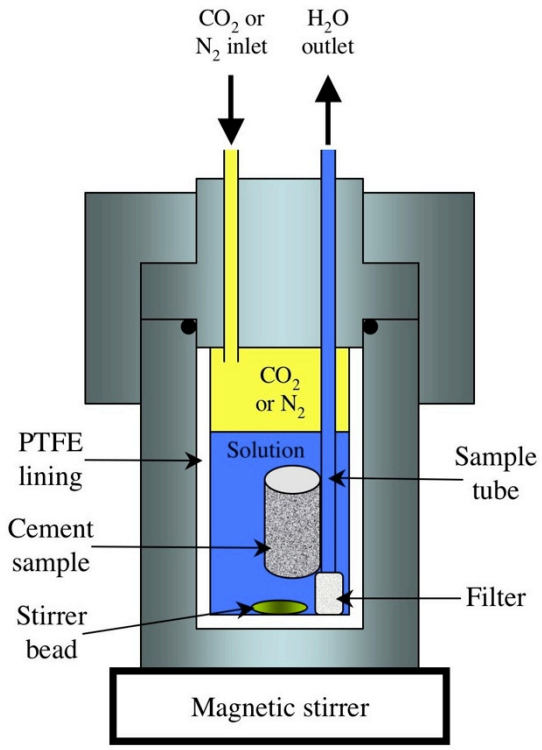

Figure 3. Schematic diagram of an assembled batch reactor.

Assembly of the experiment involved first securing a small cylinder of cement (25 mm diameter and 50 mm long, approximately 40 g in weight) to the lower part of the sampling tube attached to the head of the vessel. This was positioned so that it would not touch the base of the vessel once assembled. Raising the cement off the bottom of the vessel was important during fluid extraction and sample depressurisation. At the end of the experiment depressurisation results in degassing of CO_2 dissolved in the aqueous phase, and as a consequence the supersaturation of minerals such as carbonates. It is possible therefore, that if precipitation of these was rapid during the depressurisation process, then they might appear on the sample as an artefact and complicate subsequent interpretation. Although care was taken to remove as much fluid as possible prior to depressurisation (and hence reduce the potential for precipitation artefacts),

experience has shown that CO_2 break-through into the filter often results in a few millilitres of aqueous fluid remaining in the bottom of the vessel. By simply raising the cement sample above this remaining fluid, the potential for carbonate precipitation artefacts is greatly reduced.

Where used, a quantity (approximately 230 g) of cement porewater was placed into the PTFE liner of the vessel, together with a small magnetic stirrer bead. This amount of porewater was sufficient to cover the sample of cement. The porewaters used were one of; a synthetic 'young' cement porewater (rich in Na and K), a synthetic 'young' cement porewater with additional Cl, or a synthetic 'evolved' cement porewater (rich in Ca). The total volume of the solid and aqueous samples filled about 75% of the space within the vessels. For experiments involving both cement and porewater, the fluid:solid mass ratio was thus approximately 6:1. No porewater was added to the experiments reacting cement with dry gases.

Final assembly of the vessels involved a fresh O-ring being inserted into its groove in the head of the vessel, and the lid securely fastened down. The vessels were then placed into either a LMS thermostatically-controlled incubator for experiments at 20°C, or a Gallenkamp Plus2 oven for experiments at 40°C (both accurate to better than ±0.5°C) and connected to the appropriate pressure line (Figures 4 and 5).

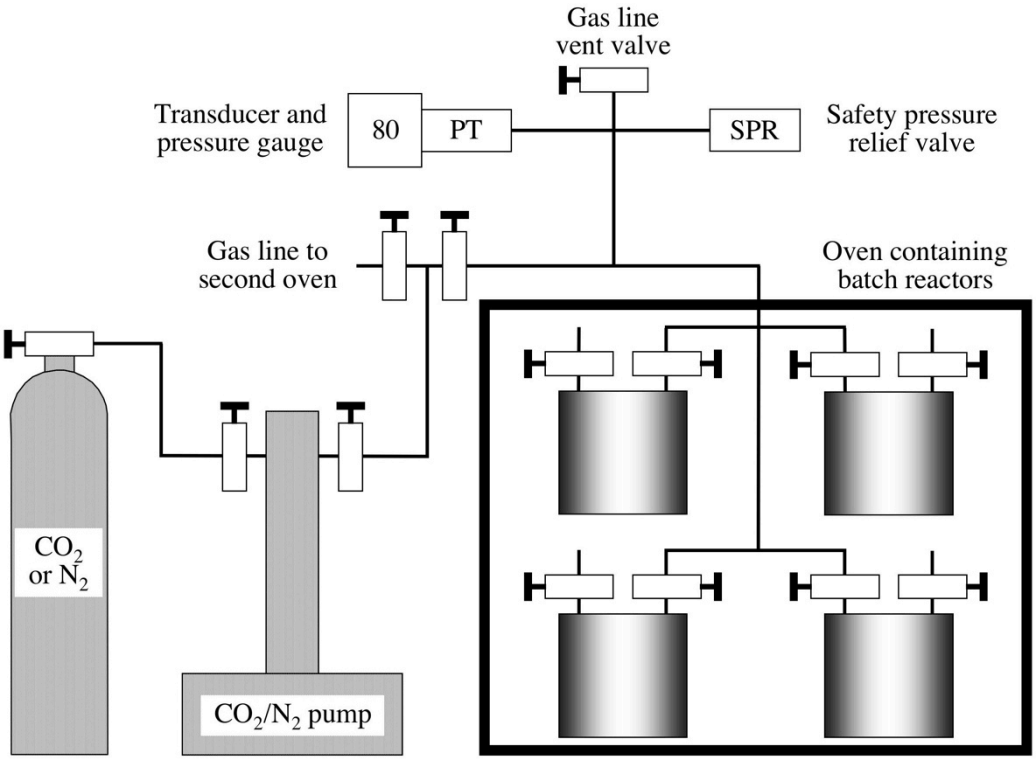

Figure 4. Schematic diagram of the typical arrangement of batch reactors inside an oven.

Figure 5. Photograph of batch reactors inside an oven.

The CO_2 and N_2 were supplied to the reactors from ISCO 500D syringe pumps running in 'constant pressure' mode. The computerised controller allowed the pressure to be controlled to within 0.1 bar (0.01 MPa). Several vessels were connected to the same pressure lines to ensure they experienced identical conditions. Pressure connections were placed at the top of the vessels so that aqueous fluids (denser than high pressure N_2 or CO_2) could not move out of, or between, the vessels.

The vessels pressurised with CO_2 represented the 'reactive cases' and those pressurised with N_2 the 'non-reactive cases'. This facilitated discrimination between reactions purely due to CO_2, and artefacts that might be introduced by the nature/arrangement of the experiments.

Good mixing of the CO_2 and synthetic porewater was achieved via the stirrer bead in each vessel. Although the base of the stainless steel pressure vessels was in the order of 1-1.5 cm thick, it still allowed for good 'coupling' between a magnetic stirrer and the stirrer bead. The vessels were stirred for several short periods each day - two minutes of stirring were used every 4 hours, which was controlled via an electronic time switch. Previous studies (Toews *et al.*, 1995) indicate that stable CO_2 concentrations can be obtained in high pressure water-CO_2 experiments within timescales as short as 30 minutes, though slightly longer timescales of just a few hours may be more realistic (Ellis and Golding, 1963; Stewart and Munjal, 1970; Czernichowski-Lauriol *et al.*, 1996). However, given the relatively long duration of the batch experiments (i.e. several weeks) and the relatively frequent stirring, it is reasonable to assume that the aqueous fluids within them were saturated with CO_2 at the pressure and temperature of the experiments.

The batch experiments were run under a range of conditions that are thought to be broadly representative of all possible future repository conditions at depths of 400 m and 800 m (Figure 6):

1) 20°C and 80 bar pressure [liquid CO_2 stable].

2) 40°C and 40 bar pressure [gaseous CO_2 stable].

3) 40°C and 80 bar pressure [supercritical CO_2 stable].

We acknowledge however, that of this selection, (2) is by far the most likely, and were the conditions under which flow experiments were also conducted (see Purser *et al.*, 2013). Conditions in (1) and (3) would require high CO_2 production rates, which may be unlikely. That said, running experiments under these conditions would enhance reaction, and place limits on maximum amounts of carbonation. Also, if reactions mechanisms appear similar for gaseous, liquid and supercritical CO_2, then that will provide robust evidence for a good understanding of cement carbonation over a wide range of conditions.

The other possible set of conditions would have been 20°C and 40 bar. However, as this would have also contained CO_2 in its gaseous state (as per [2] above) and was relatively close to the liquid/gas phase boundary (Figure 6), it was decided not to run experiments under these set of conditions.

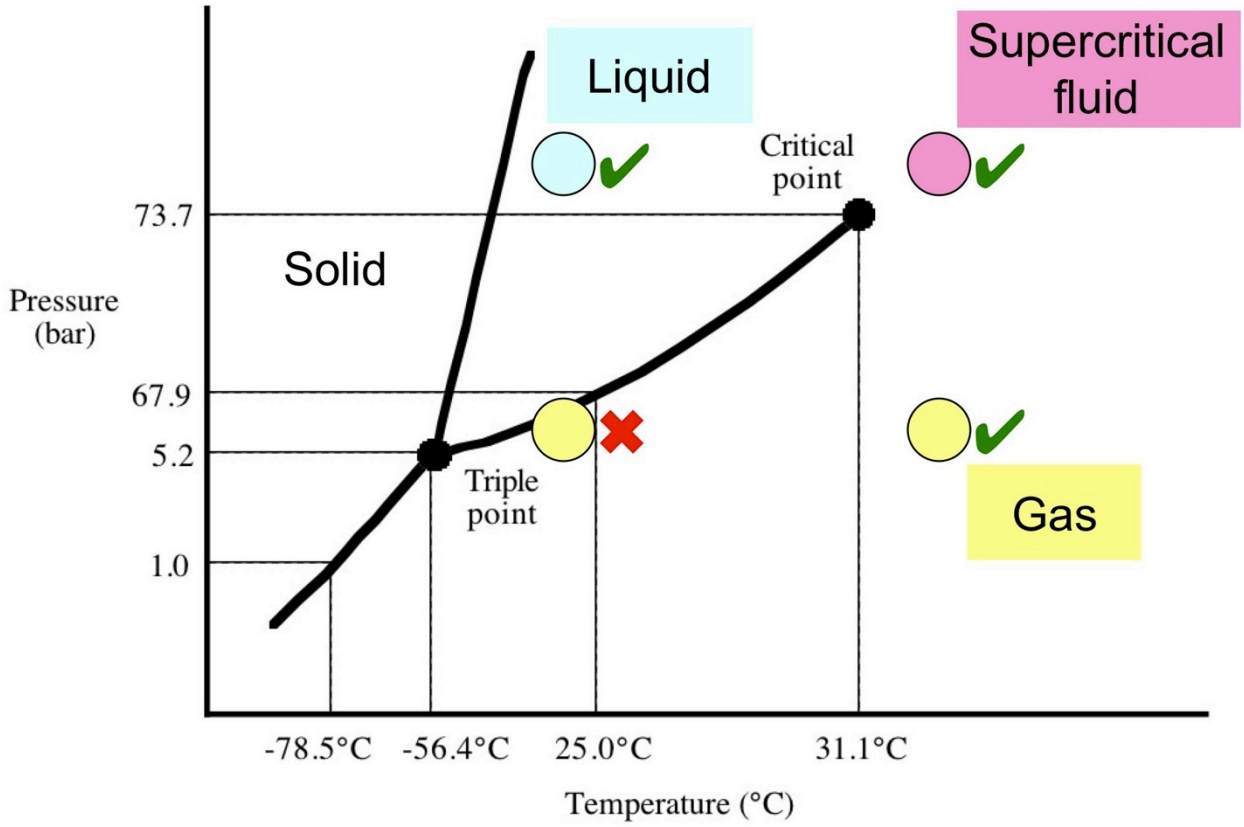

Figure 6. Experimental run conditions plotted on a phase diagram for CO_2.

The above conditions were mainly used in shorter (10-40 day) experiments to assess the effects of gaseous / liquid / supercritical CO_2 on the cement. Given the 2 types of porewater, some experiments being dry, and two gases, this gave a total of six experiments per set of conditions. However, a further six experiments were also run over longer timescales (12 months) to assess the maximum degree of reaction over as long a time as practicable within the work programme. The matrix of experiments is as detailed in Table 2.

At the end of the experiments sampling of the aqueous phase was carried out via a PEEK™ dip tube (with a 20 µm pore size polypropylene filter at the end), which ran to the base of the PTFE liner. Fluid samples were extracted whilst the reactor was still under run conditions, pressure being maintained through the injection of extra CO_2 into the headspace of the vessel. The vessel was then depressurised, dismantled and the cement sample extracted.

CO_2			Temperature °C							
			20°C				40°C			
			YNFP	YNFP+Cl	ENFG	DRY	YNFP	YNFP+Cl	ENFG	DRY
Pressure (bar)	40 Bar		Gaseous CO_2				Gaseous CO_2			
		40 Days		-	-	-	1423	1353	1357	1355
		1 Year		-	-	-		-	-	-
	80 Bar		Liquid CO_2				Supercritical CO_2			
		10 Days	-	-	-	-	1430	-	-	-
		20 Days	-	-	-	-	1427	-	-	-
		40 Days	1428	1364	1362	1360	1424	1346	1343	1348
		1 Year	-	-	-	-	-	1341	1345	1339
							Also, Run 1351: Just de-ionised water + CO_2, 40°C & 80 bar			

N_2			Temperature °C							
			20°C				40°C			
			YNFP	YNFP+Cl	ENFG	DRY	YNFP	YNFP+Cl	ENFG	DRY
Pressure (bar)	40 Bar		Gaseous N_2				Gaseous N_2			
		40 Days		-	-	-	1425	1352	1356	1354
		1 Year		-	-	-		-	-	-
	80 Bar		Gaseous N_2				Gaseous N_2			
		40 Days	1429	1365	1363	1361	1426	1347	1342	1349
		1 Year	-	-	-	-	-	1340	1344	1338
							Also, Run 1350: Just de-ionised water + N_2, 40°C & 80 bar			

Table 2. Batch experiment run numbers and their associated conditions and durations. The two experimental blanks (Runs 1350 and 1351) were run for 40 days as a check for experimental or analytical problems.

4. Sampling and analyses

4.1 SAMPLING PROCEDURE AND SAMPLE PRESERVATION

4.1.1 General

For each set of batch experiments, fluid samples from both CO_2-pressurised and N_2-pressurised experiments were treated in the same way. This involved degassing a sample of aqueous fluid (if present) straight into a sterile polythene syringe.

At the end of each experiment, as much as possible of the remaining fluid (if present) inside the vessel was removed whilst still at pressure. This was to minimise the potential for carbonate mineral precipitation as this could result from the solution degassing, and hence an artefact of sampling. However, previous experience has indicated that such degassing tends to result in carbonate precipitation only after a few hours. Consequently, for solution samples that were taken and preserved in a matter of a few tens of minutes, such precipitation is not thought to represent a significant problem.

Solid samples were extracted after slow depressurisation of the vessel by venting the CO_2 or N_2 to the atmosphere. Depressurisation was done slowly to maximise the ability of trapped CO_2 to exit the cement samples – not doing this increased the risk of hydrofracturing the sample.

4.1.2 Preservation of solid products

On opening a pressure vessel, the (slightly damp) sample of reacted cement was very gently dried with an absorbent paper towel, weighed, and its length and diameter measured. The cores were then immediately placed in flat-roll plastic tubing, which was flushed with Ar before being sealed by crimp-welding. Each sample was sealed and stored within a two layers of Ar-flushed

crimp-welded flat-roll plastic tubing, to prevent reaction with atmospheric CO_2 prior to petrographical analysis.

The cores of cement were then vacuum-dried at 20°C using an Edwards Modulyo freeze drying unit. However, the samples were not freeze-dried, as the pre-freezing process would have potentially created damage to the fabric of the samples. This is because the cement plugs were too large to allow rapid freezing throughout the mass of the sample, and slow freezing of the porewater within the core of cement plugs would have led to the slow but disruptive growth of ice crystals. Instead, the moist cement plugs were placed directly in the freeze drier unit, which was then evacuated, allowing the samples to gently dry at approximately 20°C, free from any contact with atmospheric CO_2, over a period of 48 hours at which point a constant vacuum of approximately $1x10^{-1}$ Torr was achieved, indicating no further loss of water from the samples. The dried cement plugs were then transferred into a glass desiccator containing soda lime prior to further preparation for mineralogical analysis. The soda lime served to adsorb any atmospheric CO_2 in the vessel, thereby preventing any potential carbonation of the solids during storage prior to analysis. The unreacted cement reference sample, which had been stored in a sealed container in water saturated with $Ca(OH)_2$ for the duration of the experiments, was also opened and treated in the same way as the reacted cement samples.

4.1.3 Preservation of fluid samples

After sampling, each of the reacted fluids was split into several sub-samples:

Approximately 1 ml was taken for immediate analysis of pH.

Approximately 2-4 ml was taken for immediate analysis of alkalinity/carbonate/bicarbonate.

Approximately 10-12 ml was filtered using a 0.2 μm 'Acrodisc®' nylon syringe filter. A volume (in the order of 8 ml) of this sample was placed into a polystyrene tube and acidified with 2% v/v (i.e. in the order of 0.08-0.4 ml) of concentrated 'ARISTAR®' nitric acid. This was analysed subsequently for major and trace cations by inductively coupled plasma - optical emission spectroscopy (ICP-OES).

A further aliquot of the filtered sample (in the order of 1-2 ml) was taken and placed in a polyethylene tube for analysis of anions by ion chromatography (IC). This sample was diluted (typically to 20-50% concentration) to minimise the potential for carbonate mineral precipitation prior to analysis.

Samples were stored in a fridge (at about 5°C) prior to analysis.

4.2 ANALYTICAL TECHNIQUES

4.2.1 Petrographic characterisation of the solid components

General

The reacted cement plugs, together with reference starting cement plugs, were initially photographed with a digital camera. The morphology and nature of any alteration products on the surfaces of the plugs were then examined in by optical binocular stereo microscope, which was then followed by more detailed observation using scanning electron microscopy (SEM) with secondary electron imaging (SEI). Alteration profiles through the reacted cement plugs were examined in polished thin sections prepared as longitudinal slices through the plugs. These sections were examined initially by optical petrographic (polarizing) microscope in transmitted-light, and then in more detail by backscattered scanning electron microscopy (BSEM). Identification of phases observed during SEM (BSEM and SEI) observation was aided by energy-dispersive X-ray microanalysis (EDXA) to provide semi-quantitative microchemical analysis of reacting materials and alteration products. During SEM analysis, selected areas of some polished thin sections of the reacted cement samples were also imaged by X-ray

microchemical mapping using EDXA, to examine the distribution of major chemical components and to provide further information on the movement of reaction fronts through the cement plugs.

Polished thin section preparation

Petrographic polished thin sections were prepared from each of the vacuum-dried reacted cement plugs and a reference unreacted cement plug. The plugs were longitudinally-sliced through the median line by dry-cutting with a diamond rock saw. One half of the cement plug was then vacuum-impregnated with epoxy-resin in order to stabilise the material for thin section preparation. A blue dye was added to the epoxy-resin so that the porosity in the cement could be readily identified and discriminated from artefacts of section preparation (e.g. grain-plucking), during examination of the polished thin sections in transmitted light under the optical microscope. Thin slices were cut from the resin-impregnated blocks and mounted on glass microscope slides with colourless epoxy-resin, and ground and polished to a thickness of 30 μm. The sections were finished to a high-quality polish with 0.45 μm diamond paste. All section cutting and polishing was conducted in the absence of water, using alcohol as a lubricant, to prevent further cement hydration reactions occurring during section preparation.

The cement plugs used in these experiments (25 mm diameter, 50 mm long) were too large to fit in their entirety onto the standard-size (28 mm x 48 mm slices) polished thin sections prepared from the cement plugs. However, the thin sections were cut so that they presented a profile that allowed the plug to be examined from at least the centre of plug to outer surface of the cement plug, to include the both sides and one end of each plugs.

Optical petrography

Prior to detailed petrographical observations by BSEM-EDXA, the polished thin sections were examined in transmitted light using a Zeiss Axioplan 2 optical petrographic (polarising) microscope. Low magnification images of whole thin sections were also be recorded by digitally scanning of the thin section using an Epsom Perfection 1240U flatbed scanner equipped with a transmitted light (transparency) scanning attachment.

Scanning electron microscopy

Scanning electron microscopy (SEM) analyses was carried out using either:

1) A LEO 435VP variable pressure digital scanning electron microscope (VPSEM) fitted with a KE Developments solid-state 4-element (diode) backscattered electron (BSEM) detector. The SEM instrument was also equipped with an Oxford Instruments INCA Energy 450 energy-dispersive X-ray microanalysis (EDXA) system with a thin window Si-Li X-ray detector capable of detecting elements from boron to uranium.
2) A FEI QUANTA 600 environmental scanning electron microscope (ESEM), equipped with both a conventional Evert-Thornley secondary electron detector and an environmental (large field) secondary electron detector, and a solid-state 2-element (diode) BSEM detector. The ESEM instrument was also equipped with an Oxford Instruments INCA Energy 450 EDXA system with an Oxford Instrunment X-MAX large area (50 mm^2) silicon drift detector (SDD) capable of detecting elements from boron to uranium.

SEI observations of the reacted core surfaces were made by direct observation of the whole (intact) cement core samples in the FEI QUANTA 600 ESEM instrument, under low-vacuum (variable pressure) mode, using a water-vapour atmosphere at a pressure of 0.95 Torr, and with an electron beam accelerating voltage of 15 kV and beam current of 7.5 pA. The polished thin

sections were examined under BSEM using both the FEI QUANTA 600 ESEM and the LEO 435VP variable pressure SEM instruments. Uncoated polished thin sections were examined in the variable pressure (low vacuum) mode: (a) on the FEI QUANTA 600 ESEM using a water-vapour atmosphere at a pressure of 0.95 Torr, and with an electron beam accelerating voltages of 15-20 kV and beam current of 40-100 pA; or (b) on the LEO 435VP VPSEM using a nitrogen atmosphere of 0.4 Torr, and with an electron beam accelerating voltages of 15-20 kV and beam current of 500-800 pA. Higher-resolution BSEM-EDXA imaging of the polished thin sections was also undertaken using the SEM instruments in high-vacuum mode, after coating the sections with a thin layer of carbon (approximately 25 nm thick). The BSEM image brightness is proportional to the average atomic number of the material, thus allowing the differentiation of phases on the basis of their chemistry (Goldstein *et al.*, 1981). Phase identification was also be aided by microchemical information obtained from observation of semi-quantitative EDXA spectra recorded from features of interest. EDXA data were acquired and processed using the Oxford Instruments Microanalysis Suite (version: Issue 18d+SP3) software package.

4.2.2 Chemical analysis of experimental fluids

Appropriate fluid samples were taken for chemical analysis of cations using inductively coupled plasma - optical emission spectroscopy (ICP-OES), and for anions using ion chromatography (IC). Bicarbonate/carbonate analysis was by titration against a known volume of sulphuric acid.

pH measurements were made on cooled and depressurised samples using either an Orion® '900A' pH meter or an Orion® '3 Star' pH meter. Both were calibrated using NBS traceable buffers chosen from pH 4, 7 10 and 12.46.

Details of major elements/species that will be analysed, typical detection limits and associated analytical errors are given in Table 3. The errors are based on long-term internal quality control standards.

5. Results of cement size and weight change analyses

5.1 DIMENSIONS OF CEMENT CORES AFTER REACTION

Prior to the start of the experiments each core sample had several measurements taken of their diameter and length using a Linear Tools electronic calliper accurate to 0.01 mm. This process was repeated at the end of the experiments, after the core samples had been carefully dried, in order to ascertain if reaction with CO_2 had caused ay swelling or shrinkage of the cement.. All cores were measured, apart from those that broke apart during the tests / during depressurisation. Care was taken when measuring post reaction samples so as to not damage delicate precipitates on the surfaces of the cement cores. We found that none of the cement cores changed size during the experiments pressurised with N_2 or on exposure to CO_2.

5.2 WEIGHT OF CEMENT CORES AFTER REACTION

Prior to the start of the experiments each core sample was weighed on a Mettler AT460 digital balance accurate to 0.0001 g. The average values for each core sample are given in Table 4. This process was repeated at the end of the experiments (after the core samples had been gently and carefully dried using a clean tissue) in order to ascertain if reaction with CO_2 had caused ay swelling or shrinkage of the cement (Table 4). All cores were measured, apart from those that broke apart during the tests / during depressurisation. Care was taken when measuring post reaction samples so as to not damage delicate precipitates on the surfaces of the cement cores. In order to give a clearer indication of the direction and degree of weight change, the information in Table 4 has been recast as percentage changes in Table 5.

Analyte	Detection limits (instrument) # (mg l^{-1})	Likely detection limits # mg l^{-1}	mol l^{-1}	Likely percentage ± uncertainty †
Na	0.35	7.0	3.1×10^{-4}	<5
K	0.5	10.0	2.6×10^{-4}	<5
Mg	0.01	0.2	8.2×10^{-6}	<5
Ca	0.1	2.0	5.0×10^{-5}	<5
Sr	0.002	0.5	5.7×10^{-6}	<5
Mn	0.002	0.04	7.2×10^{-8}	5-10
Total Fe	0.01	0.2	3.5×10^{-6}	5-10
Al	0.01	0.2	7.4×10^{-6}	5-10
Total S	0.25	5	1.6×10^{-4}	<5
Si	0.075	1.5	5.4×10^{-5}	<5 to 5-10
SiO_2	0.16	3.21	5.4×10^{-5}	<5 to 5-10
Cl^-	0.1	100	2.8×10^{-3}	<5
SO_4^{2-}	0.3	30	3.3×10^{-4}	5-10
HCO_3^-	5	10	1.6×10^{-4}	<5 to 5-10
CO_3^{2-}	5	10	1.6×10^{-4}	5-10

Table 3. Listing of a selection of typical major analytes, instrument detection limits, likely detection limits given likely dilution factors, and an estimation of uncertainty.

Limits of quantification can be described in more than one way. Firstly there is the actual instrument limit for an 'ideal' dilute solution. However, more concentrated solutions (i.e. saline porewaters) have to be diluted prior to analysis as high concentrations of total dissolved solids cause analytical problems. Dilution causes an effective worsening of the detection limits. During this study, samples were typically diluted by; 20x for ICP analysis, 100x to 10000x for IC analysis, 2x for bicarbonate analysis, and 6x for TOC analysis.

† Illustrative uncertainties considered 'typical' for the concentration ranges likely to be found in this study. Concentrations <10x the detection limit have uncertainties ≥10%, concentrations >10x the detection limit have uncertainties typically ≤5%.

CO_2

Pressure (bar)			Temperature °C							
			20°C				40°C			
			YNFP	YNFP+Cl	ENFG	DRY	YNFP	YNFP+Cl	ENFG	DRY
	40 Bar		Gaseous CO_2				Gaseous CO_2			
		40 Days	- -	- -	- -	- -	41.0054 (42.9901)	40.5500 (41.5868)	40.6665 (41.7148)	40.4661 (43.7841)
		1 Year	- -	- -	- -	- -	- -		- -	- -
	80 Bar		Liquid CO_2				Supercritical CO_2			
		10 days	- -	- -	- -	- -	41.2338 (42.4954)		- -	- -
		20 days	- -	- -	- -	- -	41.5595 (43.4257)		- -	- -
		40 Days	41.6631 (43.4248)	40.4660 (42.5902)	40.4150 (41.8581)	39.9855 (broken)	41.1266 (43.4266)	41.4214 (44.6017)	42.0064 (43.8972)	41.9013 (45.0965)
		1 Year	- -	- -	- -	- -	- -	41.1893 (44.0077)	41.9299 (43.9366)	41.7545 (45.2746)
							Run 1351: N/A			

N_2

Pressure (bar)			Temperature °C							
			20°C				40°C			
			YNFP	YNFP+Cl	ENFG	DRY	YNFP	YNFP+Cl	ENFG	DRY
	40 Bar		Gaseous N_2				Gaseous N_2			
		40 Days	- -	- -	- -	- -	42.3932 (42.6875)	40.6397 (40.3360)	40.8163 (41.0549)	40.4923 (39.5256)
		1 Year	- -	- -	- -	- -	- -		- -	- -
	80 Bar		Gaseous N_2				Gaseous N_2			
		40 Days	41.4170 (41.6866)	40.2322 (40.6207)	40.2544 (41.0836)	40.4071 (39.1821)	41.7662 (41.8931)	41.1453 (41.1960)	41.5020 (41.4852)	41.7220 (40.0921)
		1 Year	- -	- -	- -	- -	- -	41.2876 (42.6775)	41.1727 (42.0810)	40.9702 (37.3522)
							Run 1350: N/A			

Table 4. Initial weights (in grammes) of cement samples at the start of the tests, together with their weights (in grammes) after reacting for 40 days and one year. Reacted weights are given in brackets.

CO_2			Temperature °C							
			20°C				40°C			
			YNFP	YNFP+Cl	ENFG	DRY	YNFP	YNFP+Cl	ENFG	DRY
Pressure (bar)	40 Bar		Gaseous CO_2				Gaseous CO_2			
		40 Days	-	-	-	-	+4.84%	+2.56 %	+2.58 %	+8.20 %
		1 Year	-	-	-	-	-	-	-	-
	80 Bar		Liquid CO_2				Supercritical CO_2			
		10 Days	-	-	-	-	+3.06%		-	-
		20 Days	-	-	-	-	+4.49%		-	-
		40 Days	+4.23%	+5.25 %	+3.57 %	N/A	+5.59%	+7.68 %	+4.50 %	+7.63 %
		1 Year	-	-	-	-	-	+6.84 %	+4.79 %	+8.43 %
							Run 1351: N/A			

N_2			Temperature °C							
			20°C				40°C			
			YNFP	YNFP+Cl	ENFG	DRY	YNFP	YNFP+Cl	ENFG	DRY
Pressure (bar)	40 Bar		Gaseous N_2				Gaseous N_2			
		40 Days	-	-	-	-	+0.69%	-0.75 %	+0.58 %	-2.39 %
		1 Year	-	-	-	-	-	-	-	-
	80 Bar		Gaseous N_2				Gaseous N_2			
		40 Days	+0.65%	+0.97 %	+2.06 %	-3.03 %	+0.30%	+0.12 %	-0.04 %	-3.91 %
		1 Year	-	-	-	-	-	+3.37 %	+2.21 %	-8.83 %
							Run 1350: N/A			

Table 5. Percentage weight changes of cement samples relative to their initial weights after reacting for 40 days and one year.

Several observations are apparent from the measurements of weight changes:

1) For tests with dry N_2 gas (non-carbonation experiments), all the cement samples lost weight. This seems to have been more pronounced with increasing pressure, temperature and especially timescale. This seems to be related to simple dehydration of the cement samples in the dry N_2 gas.

2) For tests with alkaline waters pressurised with N_2 gas (non-carbonation experiments), there is more variation in sample weights. Generally speaking, most samples remained roughly the same weight (within ±1%). There are 3 exceptions to this:

   - The sample reacted at 20°C and 80 bar for 40 days (+2.06%). This weight increase is not typical of similar samples, and may be a consequence of a slightly under-saturated sample at the start of the test, and which took up a little extra water when it saturated during the 40 days of the test.
   - The two samples reacted for a year at 80 bar (+3.37% and +2.21%). These weight increases are thought to represent slow and continuous hydration of previously unreacted cement 'clinker' phases present within the cement during the long duration of the tests.

3) All the tests involving CO_2 (i.e. carbonation experiments) gave cement weight increases (except for the one test where the sample broke up), and these were over and above the weight changes observed in the N_2-pressurised experiments. This is interpreted as carbonation of the cement minerals such as portlandite and CSH gels, with the weight gain being associated with incorporation of the CO_2 into secondary phases, e.g.

$$Ca(OH)_2 + CO_2 \Rightarrow CaCO_3 + H_2O \quad [1]$$
portlandite calcite

$$Ca_5Si_6O_{16}(OH)_2.9.5H_2O + 5\,CO_2 \Rightarrow 5CaCO_3 + 6\,SiO_2 + 10.5\,H_2O \quad [2]$$
tobermorite (a CSH gel) calcite silica gel

4) Reaction with CO_2 resulted in weight increases that were more pronounced with increasing timescale, and especially increasing pressure and temperature. The latter two parameters probably increasing the degree of reaction through more CO_2 being present in the reactors, and increased reaction kinetics.
5) The largest weight increases were found in tests with just dry CO_2 (weight increases of approximately 8%). In terms of molar quantities, the carbonation reaction produces at least as much water as amounts of CO_2 consumed (equations [1] and [2]). A dry CO_2 atmosphere would have helped remove this water from the cement sample, facilitating access of more CO_2 to continue the reaction (see Reardon *et al*., 1989).
6) There are broadly similar weight gains for samples reacted with dry supercritical CO_2 for 40 days and for 1 year. This suggests that the vast majority of the cement carbonation was completed in the first few weeks or reaction.
7) Given that the cement samples did not change size appreciably during carbonation, but did change weight, then their *average* density must have increase.

6. Results of fluid chemical analyses

The full set of analytical data for the experiments is given in Appendix 1. The following sub-sections describe some of the more important changes that were observed in the chemistry between pre- and post-reacted solutions, and between 'reactive' (i.e. pressurised by CO_2) and 'non-reactive' (i.e. pressurised by N_2) experiments. Most reactivity was relatively early in the experiments, and so just the 40 day data are shown on the following figures.

In terms of a broad summary, the changes observed are consistent with our understanding of chemical reactions during CO_2-cement reaction, and the data obtained for reaction of the NRVB matches data from other studies studying different cement formulations.

6.1 CHANGES IN pH

The observed trends in pH (Figure 7) over the course of the experiments were as follows:

- The two starting solutions had very similar pH values.
- Solutions from the N_2-pressurised experiments showed a very slight increase in pH at the end of the experiments.
- Solutions from the CO_2-pressurised experiments however, showed a very marked decrease in pH to values of approximately 6.5-7.

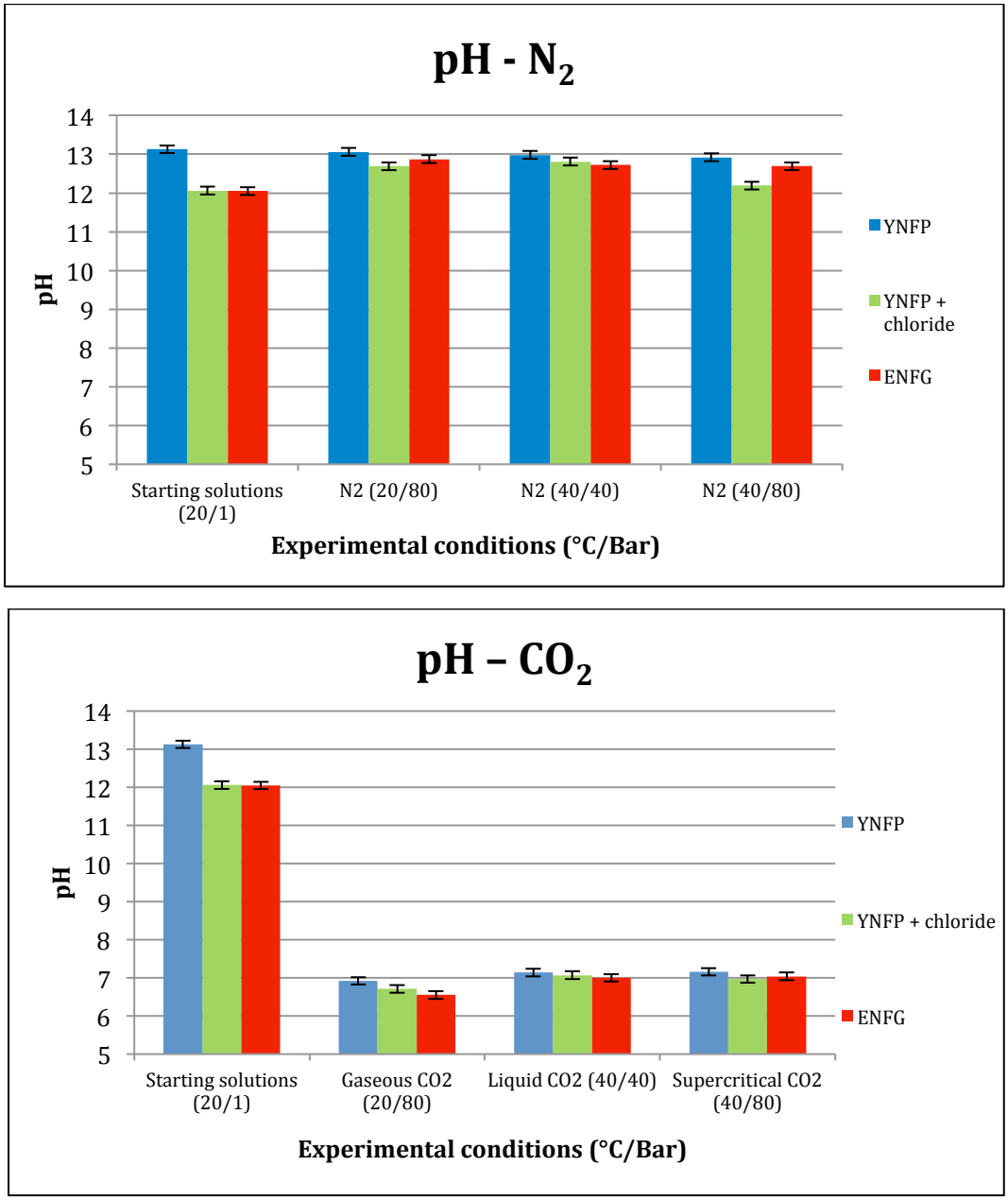

Figure 7. Changes in pH during the 40 day experiments (as measured at room temperature and pressure). Upper graph - nitrogen experiments, lower graph - CO_2 experiments.

Though the composition of the 'young' pore fluid with additional chloride was prepared based on previous work (Francis *et al.*, 1997), it ended up having a lower pH value (12.06) than an anticipated value in excess of pH 13. The reasons for this are not clear, though in terms of representing the repository environment however, a slightly reduced pH is still relevant. As groundwater percolates through, and interacts with, the repository cement, the cement porewater composition will vary over time, and the pH will fall. Thus this porewater composition represents porewater compositions intermediate between 'very young' porewaters and 'evolved' porewaters.

The slight increase in pH in the N_2-pressurised experiments appears to represent (at least partial) equilibration of the solution with $Ca(OH)_2$ and CSH phases in the sample of cement. Given the differences in solubility of these phases between lab pressure and temperature (P&T) and the P&T of the tests, then the observed slight variation in final pH is to be expected.

The large reduction in pH values in the CO_2-pressurised experiments reflects equilibration of the solution with the fixed pressure of CO_2 in the autoclaves. This observation mirrors those from

previous studies where CO_2 was reacted with samples of cement used to seal the gaps between steel borehole linings and the surrounding rocks (Rochelle *et al.*, 2004, 2006, 2007). As the (acidic) CO_2 was present in excess, then it would have provided the dominant control of pH. Initially there would have been extensive reaction between the alkaline solution and the initial CO_2 that dissolved into it. This can be represented by a series of reactions; first CO_2 dissolution, then reaction of CO_2 with water, and finally neutralisation of hydroxyl ions:

$$CO_{2(g)} \Leftrightarrow CO_{2(aq)} \quad [3]$$

$$CO_{2(aq)} + H_2O \Leftrightarrow HCO_3^- + H^+ \quad [4]$$

$$OH^- + H^+ \Leftrightarrow H_2O \quad [5]$$

Subsequently the rate of this reaction would have been dictated by the rate of production of OH^- (or H^+ consumption) by the sample of cement. A consequence of these reactions is an increase in concentration of dissolved bicarbonate (see below). The actual final *in-situ* pH values within the experiments would have been lower than those measured in the laboratory. This is because the solutions degassed CO_2 as they were depressurised, increasing solution pH in the process.

6.2 CHANGES IN BICARBONATE CONCENTRATIONS

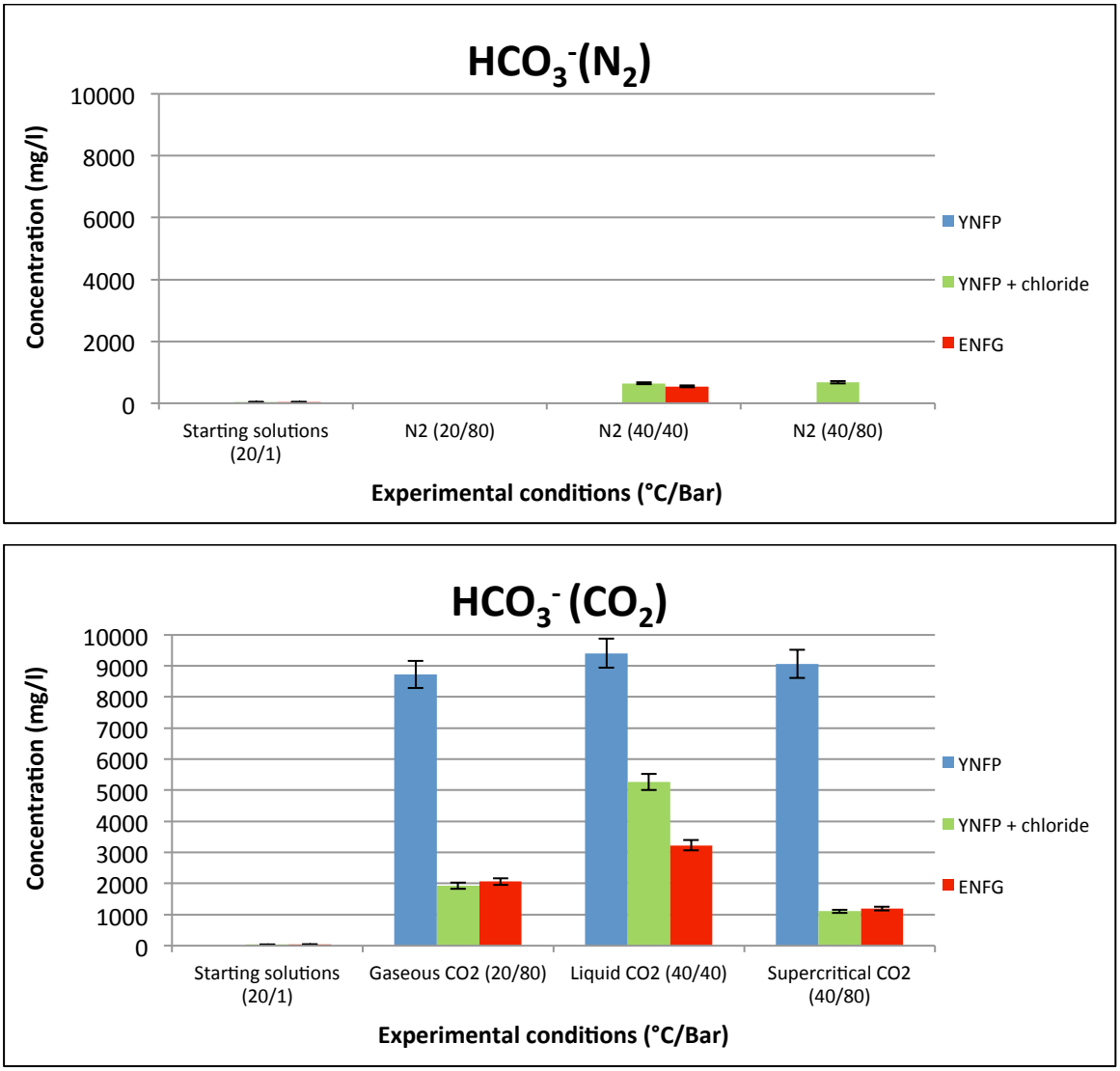

Figure 8. Changes in HCO_3^- concentrations during the 40 day experiments.

The observed trends in bicarbonate (Figure 8) over the course of the experiments reflect the pH conditions. Initially no bicarbonate was added to the starting solutions. In the N_2 experiments where pH values were high, the stable dissolved carbon phase is carbonate rather than bicarbonate. However, concentrations of this would also have been low as; a) additional CO_2 was not added to these experiments, b) high pH conditions and presence of Ca favour precipitation of all inorganic carbon as $CaCO_3$ minerals.

The presence of excess CO_2 caused pH values to decrease and reaction with hydroxyl ions. This caused the formation of significant amounts of bicarbonate ions, especially in the highest pH YNFP. The lower pH in these experiments would have meant that virtually all the dissolved inorganic carbon was bicarbonate. The high concentrations of bicarbonate would have facilitated saturation with carbonate minerals even for solutions of relatively low pH, provided that sufficient Ca was available in solution (see below).

6.3 CHANGES IN CALCIUM CONCENTRATIONS

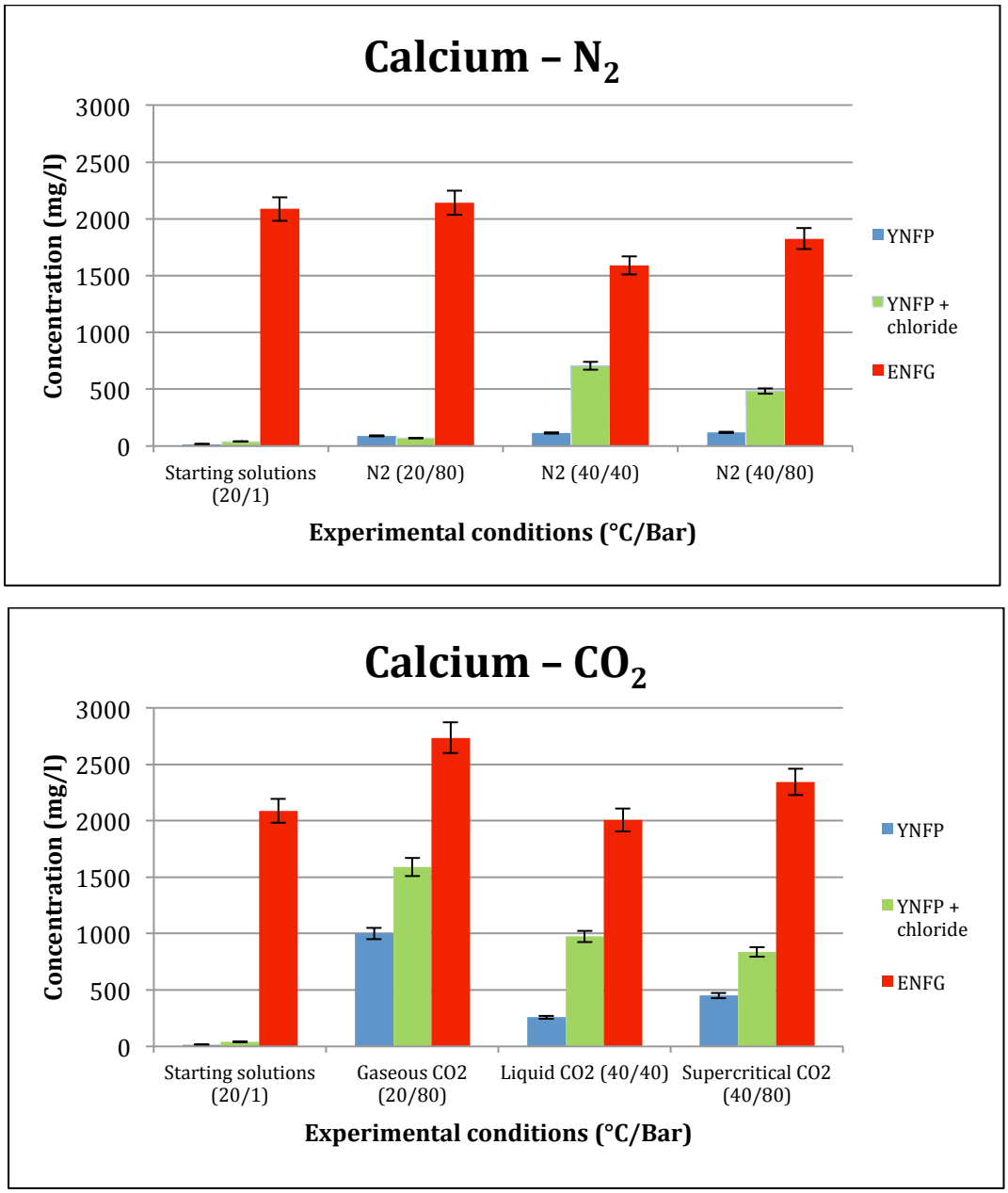

Figure 9. Changes in Ca concentrations during the 40 day experiments. Upper graph - nitrogen experiments, lower graph - CO_2 experiments.

The observed trends in Ca concentrations (Figure 9) over the course of the experiments were as follows:

- Solutions from the N_2-pressurised experiments showed some variability. In broad terms however, they exhibited an increase in Ca concentrations for the 'young' pore fluid, and approximately unchanged concentrations for the 'evolved' pore fluid.
- Solutions from the CO_2-pressurised experiments also showed some variability. In broad terms they also exhibited an increase in Ca concentrations for the 'young' pore fluid, and either unchanged or increased concentrations for the 'evolved' pore fluid.

It is not straightforward to explain all the trends in Ca concentrations in the N_2-pressurised experiments. For the 'young' pore fluid, data from the 20°C experiment and starting fluid show broad similarities, but these values are much lower than for the two experiments at 40°C. This suggests that the phase controlling Ca concentrations (presumably either calcite, portlandite [$Ca(OH)_2$] or a CSH phase) has a different solubility at these two temperatures, and may have undergone some dissolution to release Ca (see comments in the SiO_2 section below). The concentrations for the 'evolved' pore fluids show less variability and are around 2000 mg/l. However, the concentrations seem to be slightly lower in the 40°C experiments compared to the starting fluid and the 20°C experiment.

The trends in Ca concentrations in the CO_2-pressurised experiments show certain similarities to data from the N_2-pressurised experiments. However, the increases in the 'young' pore fluid experiments are much larger than in the N_2-pressurised experiments. Given the lower pH in these experiments, then portlandite and CSH phases would not be stable, and so the phase buffering Ca concentrations seems likely to have been calcite. The higher Ca concentration in the 20°C experiment compared to the 40°C experiments may reflect the higher solubility of CO_2 at lower temperatures (leading to slightly more acidic conditions, and a higher solubility of calcite). However, this is a somewhat tentative conclusion as CO_2 solubility also increases with pressure, and it is less easy to judge at this stage how much influence increasing the pressure would have – though data from the 40°C experiments suggests that this is smaller than for temperature). The Ca concentrations for the 'evolved' pore fluids are approximately double those of the 'young' pore fluids. Though the data are somewhat scattered, they also seem to show a slightly higher value at 20°C compared to 40°C. If the Ca concentrations were also buffered by calcite as per the 'young' pore fluid experiments, then it is not clear why one set of values are approximately twice those of the other.

6.4 CHANGES IN MAGNESIUM CONCENTRATIONS

The observed trends in Mg concentrations (Figure 10) over the course of the experiments were as follows:

- Solutions from the N_2-pressurised experiments showed no detectable dissolved Mg.
- Solutions from the CO_2-pressurised experiments however, showed a very marked increase in Mg concentrations (50-100 mg/l) compared to the starting solutions.

No useful Mg data were obtained from the N_2-pressurised experiments because the concentrations were below the detection limits. This is consistent with previous studies that show that highly alkaline conditions stabilise brucite [$Mg(OH)_2$], the low solubility of which is very effective in removing Mg from solution.

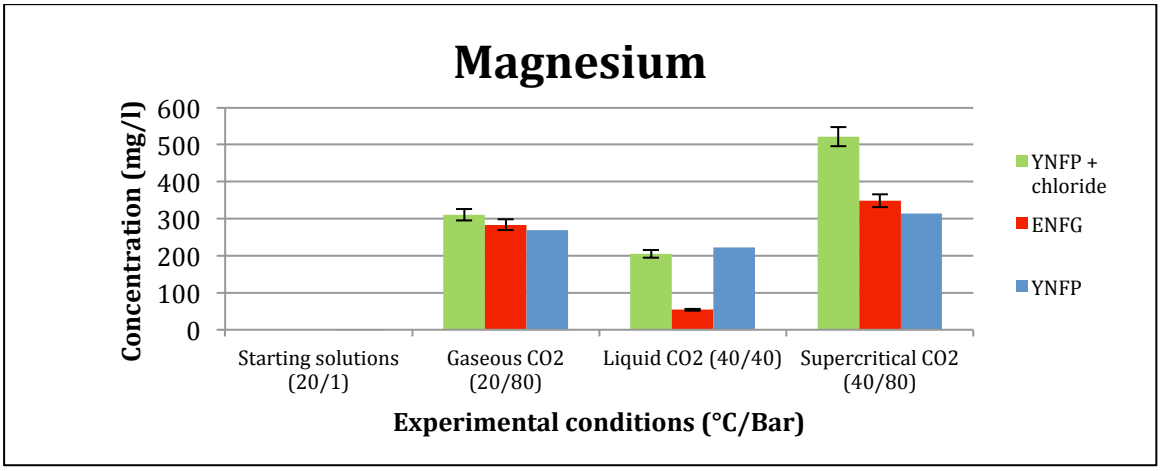

Figure 10. Changes in Mg concentrations during the 40 day CO_2 experiments.

The CO_2-pressurised experiments show a very different situation, with increases in Mg concentrations in all the experiments. This is due to leaching of Mg from the cement driven by the low pH caused by the presence of CO_2. The phase in the cement that is dissolving is probably brucite, which is anly stable under alkaline conditions. That Mg concentrations after 40 days reaction vary by about an order of magnitude between the experiments, may reflect variable degrees of leaching of the cement samples. As per the Ca data (see the previous section), a possible (though tentative) explanation could be that the experiments were not yet at equilibrium, and that complete leaching of Mg from the cement cores would require timescales in excess of 40 days to be completed. Data from 12 month long experiments (to be described in a subsequent report) may help clarify this issue.

6.5 CHANGES IN SILICA CONCENTRATIONS

The observed trends in SiO_2 concentrations (Figure 11) over the course of the experiments were as follows:

- The only N_2-pressurised experiment that showed any dissolved SiO_2 was the 20°C 'young' pore fluid experiment.
- All solutions from the CO_2-pressurised experiments however, showed significant amounts of dissolved SiO_2.

In the N_2-pressurised experiments the general lack of dissolved SiO_2 can be explained by equilibrium with respect to CSH phases. The high pH conditions within these experiments maintain the stability of CSH phases within the cement. These phases moderate both SiO_2 and Ca concentrations, such that significant concentrations of either are mutually exclusive. Thus elevated SiO_2 concentrations can only happen when Ca concentrations are relatively low, and vice versa. This exclusivity has been noted in previous work (Savage *et al.*, 1992). It would be expected that if the 20°C 'young' pore fluid experiment had run for longer and Ca concentrations started to increase, then there would have been a related decrease in SiO_2 concentrations.

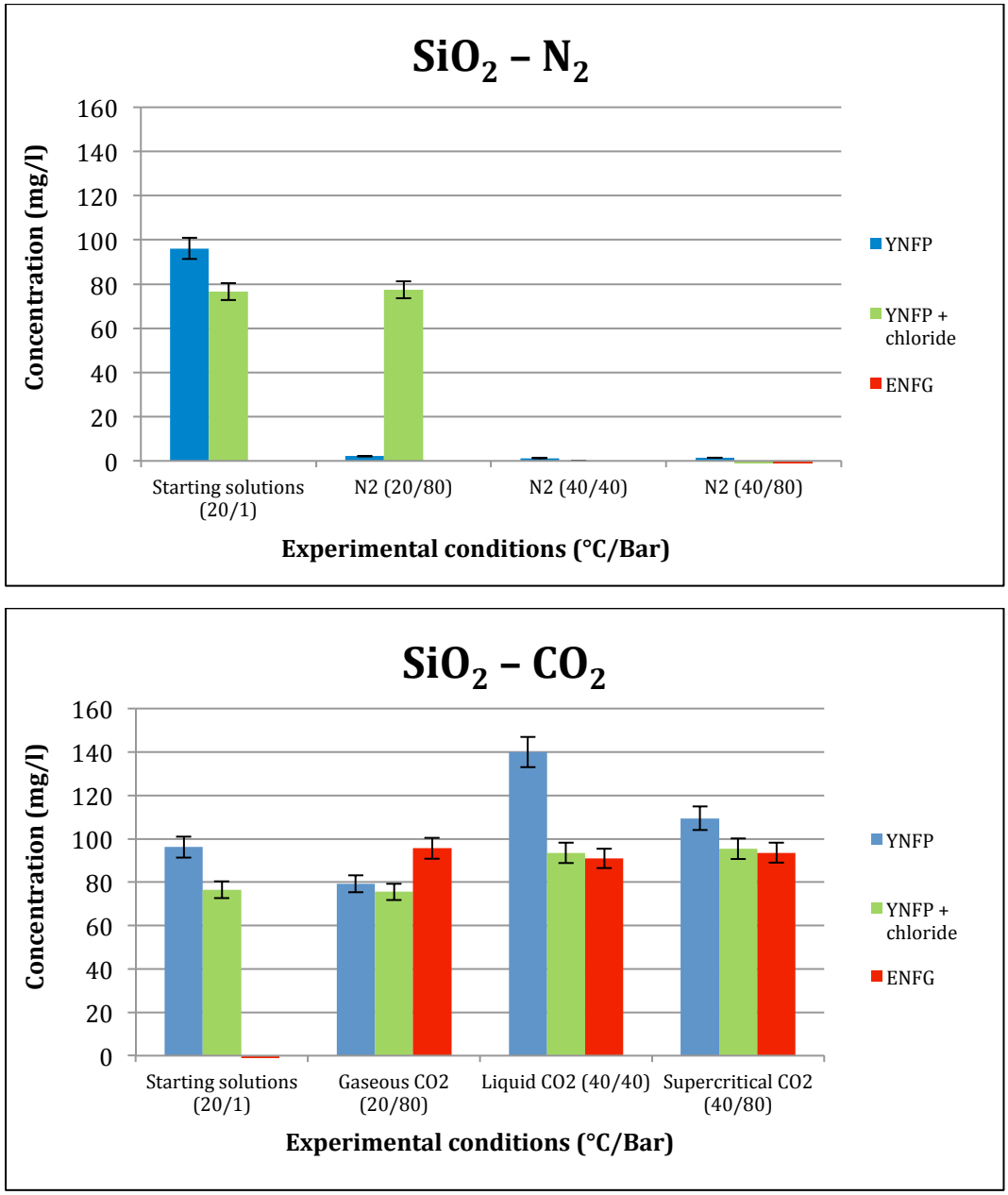

Figure 11. Changes in SiO_2 concentrations during the 40 day experiments. Upper graph - nitrogen experiments, lower graph - CO_2 experiments.

The CO_2-pressurised experiments show a very different situation, with the dissolved SiO_2 concentrations in the 80-100 mg/l range. The lower pH in these experiments would destabilise CSH phases, releasing both SiO_2 and Ca to solution. The broad consistency in dissolved SiO_2 concentrations suggests equilibrium with a common secondary Si phase, which in this case is likely to be silica gel formed through the breakdown of CSH:

$$Ca_5Si_6O_{16}(OH)_2.9.5H_2O + 5\ CO_{2(aq)} \Rightarrow 5\ CaCO_3 + 6\ SiO_2 + 10.5\ H_2O \qquad [6]$$

CSH (e.g. tobermorite) calcite silica

6.6 CHANGES IN SULPHATE CONCENTRATIONS

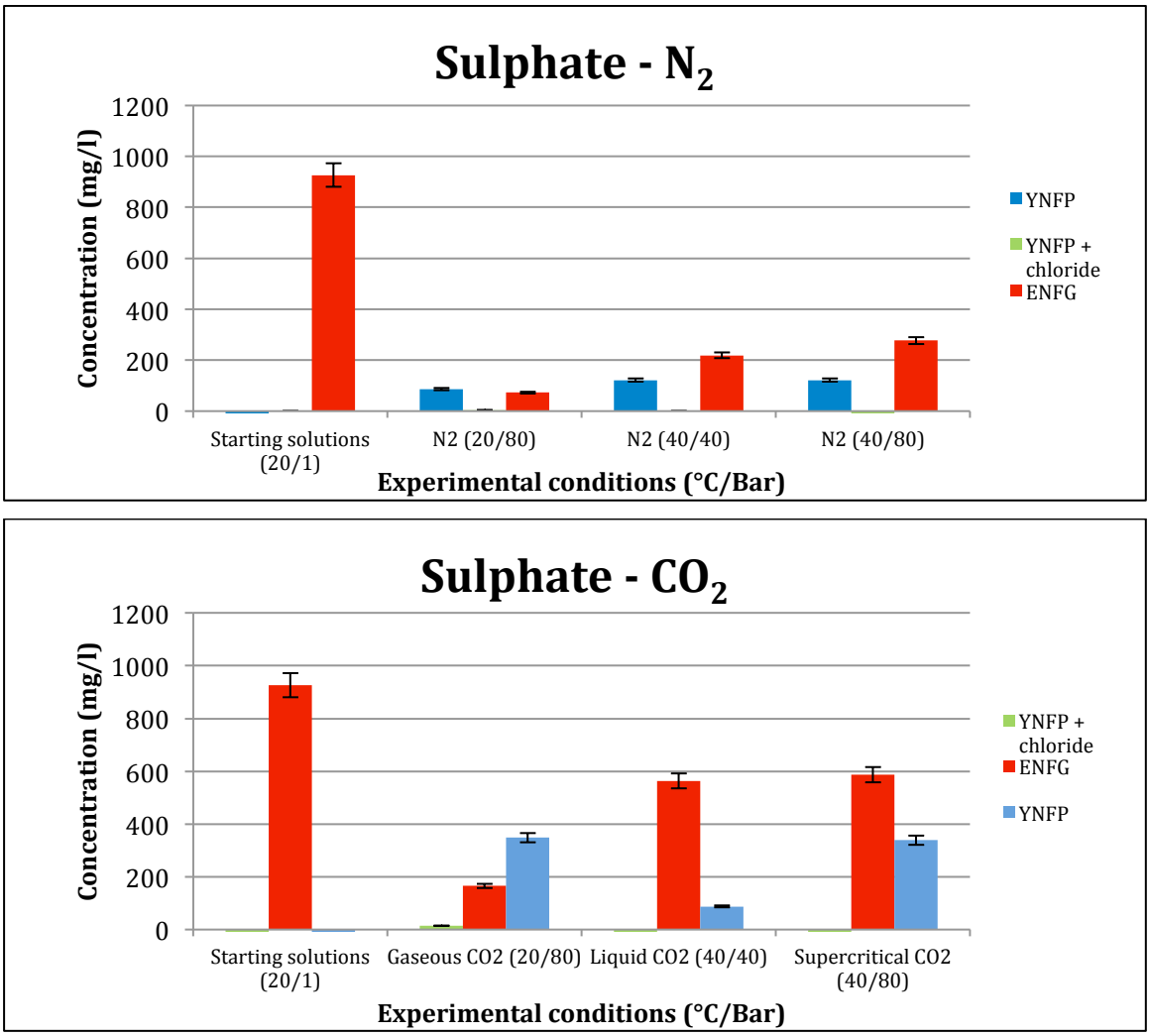

Figure 12. Changes in SO_4^{2-} concentrations during the experiments.

Only the 'evolved' pore fluid experiments contained appreciable dissolved SO_4^{2-}, and the observed trends in SO_4^{2-} concentrations (Figure 12) over the course of the experiments were as follows:

- All the N_2-pressurised experiments showed large decreases in concentrations, and this was particularly marked in the 20°C experiment.
- A similar pattern of decreases was found in the CO_2-pressurised experiments, however the decreases in concentration were not as great as for the N_2-pressurised experiments.

The concentration decreases in the N_2-pressurised 'evolved' pore fluid experiments suggests that a secondary phase containing SO_4^{2-} was being formed. Fluid chemical data alone cannot uniquely identify this phase, but possibilities could include an ettrignite group phase (due to the high pH) or gypsum (due to the high Ca concentrations). That about 15-20% more of the phase appears to have formed at 20°C compared to 40°C is suggestive that its solubility has a fairly strong dependence on temperature.

The concentration decreases in the CO_2-pressurised 'evolved' pore fluid experiments again suggest that a secondary phase containing SO_4^{2-} was being formed, and a similar dependence on temperature was observed. The generally higher concentrations however, indicate that less of

this phase formed compared to the N_2-pressurised experiments (about 60% of that in the N_2-pressurised experiments). The presence of CO_2 in these experiments would have made the pore water slightly acidic, and if the same phase was controlling SO_4^{2-} concentrations as in the N_2-pressurised experiments, then its solubility has a dependence on acidity as well as temperature. However, the slightly acidic pore fluid would have made phases such as ettringite unstable. This suggests that either: a phase such as gypsum was controlling SO_4^{2-} concentrations, or that ettringite had formed but it was partly protected inside the remaining unreacted parts of the cement block. If the latter were the case, then further reaction of the cement would be expected to release the SO_4^{2-} to solution.

Fluid chemical data alone cannot uniquely identify this phase, but possibilities could include an ettrignite group phase (due to the high pH) or gypsum (due to the high Ca concentrations). That more of the phase appears to have formed at 20°C compared to 40°C is suggestive that its solubility has a fairly strong dependence on temperature.

6.7 CHANGES IN CHLORIDE CONCENTRATIONS

The observed trends in Cl^- concentrations (Figure 13) over the course of the experiments bear many similarities to the SO_4^{2-} concentrations, and were as follows:

- All N_2-pressurised experiments showed decreases in Cl^- concentrations relative to the starting solutions, but the decreases in the 20°C experiments were far larger than in the 40°C experiments.
- All the CO_2-pressurised experiments also showed decreases in Cl^- concentrations relative to the starting solutions, and the decreases in the 20°C experiments were again far larger than in the 40°C experiments. Concentration decreases in these experiments were slightly larger compared to the N_2-pressurised experiments.

Although Cl^- is considered conservative in many studies, this is not the case when dealing with highly alkaline cementitious solutions, as several Cl-containing phases are stable at high pH. The high pH values in the N_2-pressurised experiments are consistent with the stability of Cl-containing phases such as hydrocalumite and Friedel's Salt, and the reduction in dissolved Cl-concentrations suggests that this type of phase formed during the experiments. The large decreases in the 20°C 'evolved' pore fluid experiment (approximately 13 g/l) suggests that a significant amount of secondary phase formed. The smaller decreases in the 40°C experiments suggests that the solubility (or stability) of this phase has a strong dependence on temperature.

The CO_2-pressurised experiments show a very similar situation, but with slightly larger decreases in Cl^- concentrations. At first sight such decreases would seem at odds with the low pH in these experiments, but they are consistent with other experimental studies (Rochelle *et al.*, 2006, 2009). The previous work found significant formation of a Cl-rich phase inside partially-reacted blocks of cement, which was concentrated particularly on the internal side of a major reaction front, and where high pH conditions would have existed. This could explain why minerals stable under alkaline conditions could exist (albeit for a limited time) within a block of cement submerged within slightly acidic water. If this were the case, then further reaction of CO_2 with the cement would be expected to consume the remaining $Ca(OH)_2$ and CSH phases, reducing pH within the (reacted) cement block, destabilising the Cl-rich phase, and releasing Cl^- back to solution. That the CO_2-pressurised experiments apparently favour the formation of a Cl-containing phase may suggest that the phase may also be part of a solid-solution series, one end-member of which may contain carbonate. Also, the similar pattern of SO_4^{2-} concentrations in the 'evolved' pore fluid experiments may be an indication that the phase also has a sulphate end-member (see the mineralogical information in the following sections).

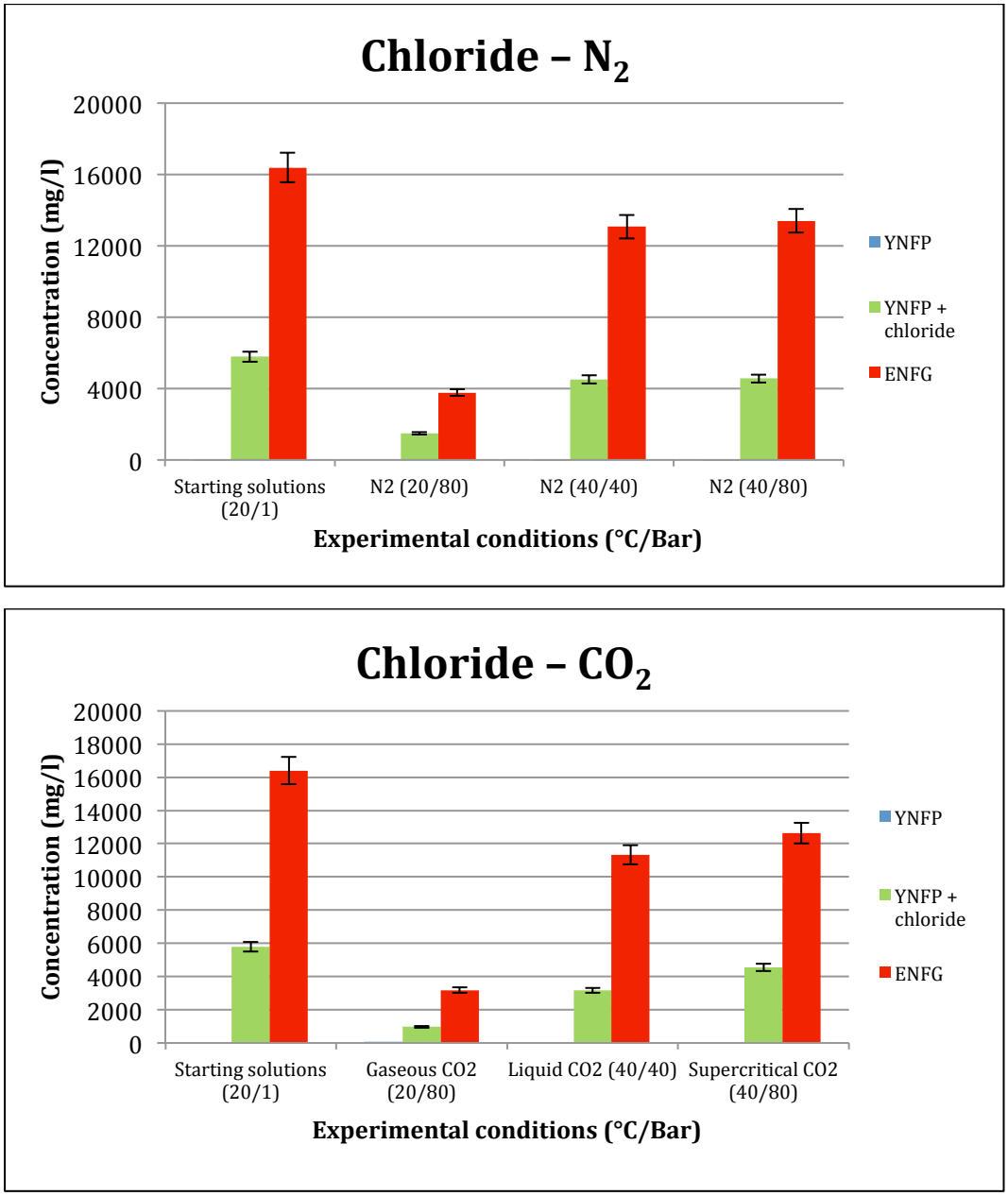

Figure 13. Chloride behaviour in 40 day static batch experiments. Note decreases relative to the starting solutions, especially at 20°C. Note also that concentrations in the YFNP experiments are too low to be visible on these plots. Upper graph - nitrogen experiments, lower graph - CO_2 experiments.

7. Results of petrographical analyses

7.1 UNREACTED STARTING CEMENT

The cured, but unreacted, NRVB cement cores used in the batch experiments were characteristically mid-to-light grey in colour (Plate 1A). Petrographic analysis shows that several (though by no means all) of the NRVB cement plugs used were significantly heterogeneous. The surfaces of the cement cores often displayed a 'marbled' or 'wood-grained' effect, which in thin section was seen to be due to fine lamination in the cement (Plate 1B). This lamination results from particle-size segregation of the cement paste into finer- and coarser-grained layers. The

segregation is clearly a primary feature of the hydrated cement produced by a combination of one or more of following factors:

- Incomplete or poor mixing during preparation of the cement paste. In this context it should be noted that the NRVB cement paste used in these experiments was prepared using only a basic portable builders cement mixer, rather than a high-shear cement blender system;
- Hydrodynamic flow-separation of cement paste on the basis of the difference in density and grain size differences of components within the cement paste, *during pouring* the cement into plastic moulds used for casting the blocks of cement, from which the core plugs were subsequently cut. In this context, it should be noted that no special additives were used that might prevent segregation of the NRVB cement components;
- Hydrodynamic segregation of material on the basis differences in particle size and density, as a result of settling and dewatering of the cement *after pouring* the cement paste into the plastic moulds. In places, the laminae are contorted and disturbed, and closely resembling soft-sediment deformation structures formed by dewatering of unconsolidated sediments (e.g. Allen, 1982; Mills, 1983), and suggests some gravitational settling and dewatering of the cement paste has occurred immediately after pouring the cement paste and before cement setting and hardening. Further evidence of post-pouring segregation of the cement can be found in the development of a thin layer of very fine cement paste, which appears to have settled out on the upper surface of some of the unreacted cement core sample. In this context, it should be noted that no special additives were used during cement preparation to inhibit any physical segregation occurring within the cement paste. It is possible therefore, that without additives such segregation features may occur within actual repository cement.

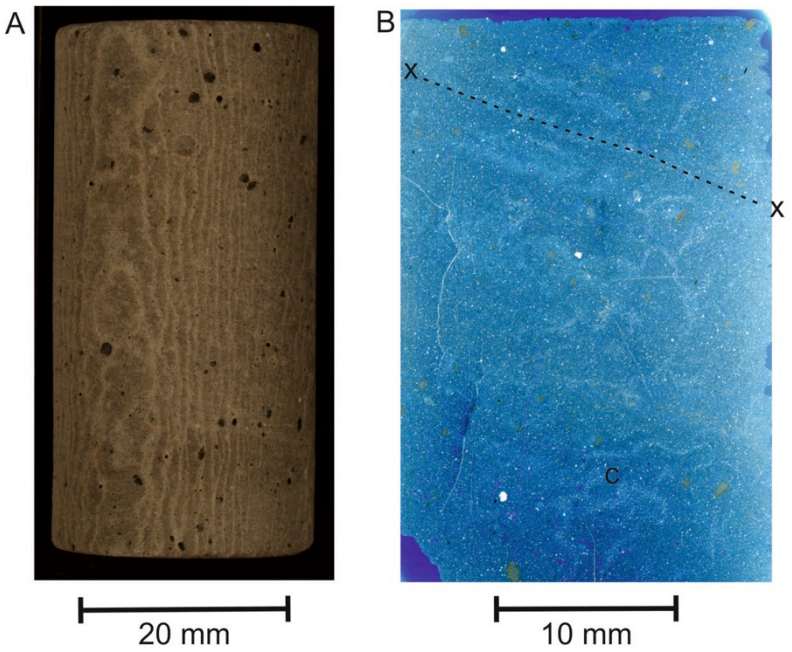

Plate 1. A: Photograph of a typical unreacted cured NRVB cement core used in the batch experiments displaying 'marbled' or 'wood-grain effect' surface and small dark grey particles of limestone aggregate. B: Transmitted light photomicrograph of a blue-dyed epoxy-resin impregnated polished thin section through an unreacted NRVB cement core showing fine lamination (e.g. X-X) reflecting heterogeneity due to particle size segregation in the cement paste. The lamination is locally contorted (c).

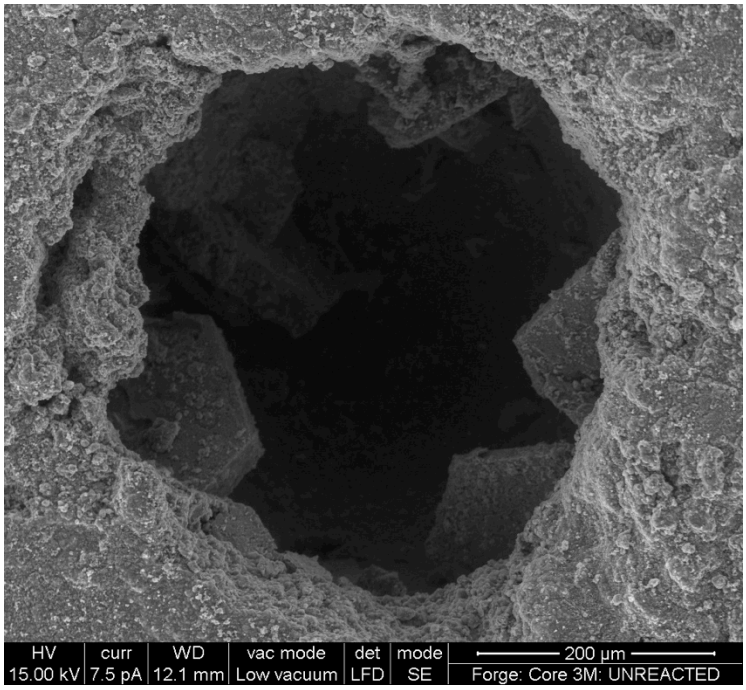

Plate 2. SEM (SEI) photomicrograph of an air bubble in NRVB cement paste. The cavity is partially filled with hexagonal plate-like crystals of portlandite ($Ca(OH)_2$). Unreacted NRVB cement paste starting material.

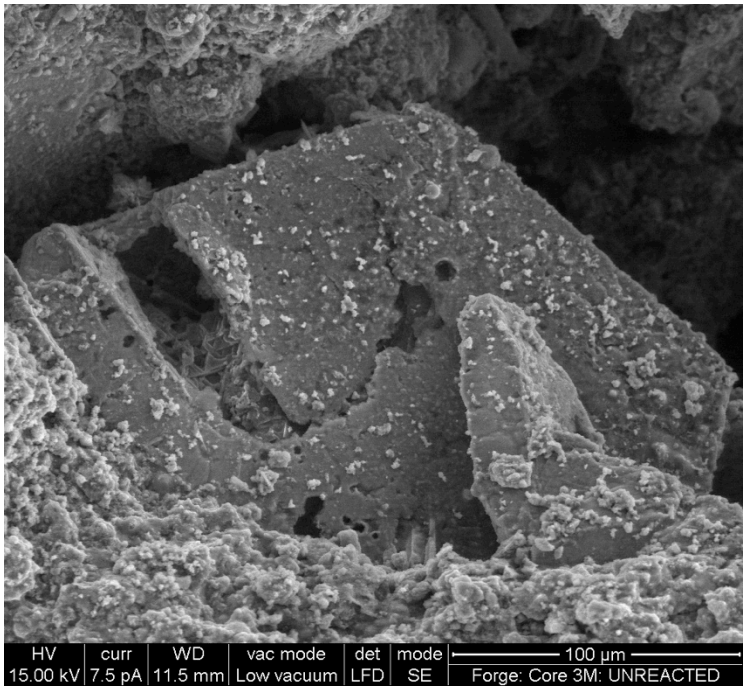

Plate 3. SEM (SEI) photomicrograph showing dissolution and corrosion of a portlandite crystal formed within an air bubble exposed in the outer surface of the NRVB cement core. The surfaces of the corroded portlandite crystal are coated with very fine secondary calcium carbonate. Unreacted NRVB cement paste starting material.

Small (0.1 to 2 mm diameter) dark grey particles of dense micritic limestone aggregate were visible in the core plug surface (Plate 1A) and were also apparent in thin section. The cement cores also contained entrained air bubbles that had been incorporated into the cement paste

during mixing. These represent macropores ranging in size from 0.2 to 1 mm diameter and are commonly partly filled or lined by euhedral, hexagonal plates of portlandite ($Ca(OH)_2$) (Plate 2). In the outer surface of the cement, the portlandite crystals are etched and corroded (Plate 3), and the corroded surfaces are partly encrusted with very fine secondary calcium carbonate crystals. Some of the calcium carbonate exhibits rhombohedral morphology and is, therefore, most probably calcite. This indicates that the outer surfaces of the cement had already reacted to a small degree with CO_2 prior to the batch experiment run. This CO_2 is likely to have been derived from direct exposure atmospheric CO_2 during core handling or by diffusion of atmospheric CO_2 into the storage containers prior to experimentation. Portlandite found lining entrained air bubbles in the centre of the cement plug generally had pristine crystal faces and showed no alteration.

The cement comprises fragments of fine silt to fine sand-grade limestone aggregate, within a very fine amorphous or nanocrystalline gel-like calcium silicate hydrate (CSH) matrix (Plate 4). Within this, remanant fragments of primary cement clinker grains are present. These consist of relatively unaltered calcium aluminate-ferrite (CAF) phases, probably brownmillerite ($Ca_2(Al,Fe)_2O_5$), intergrown with amorphous of microcrystalline CSH, hydrated calcium aluminate (CAH) and hydrated calcium aluminosilicate (CASH) hydration products (replacing the original primary anhydrous calcium silicates and aluminosilicates) (Plate 4).

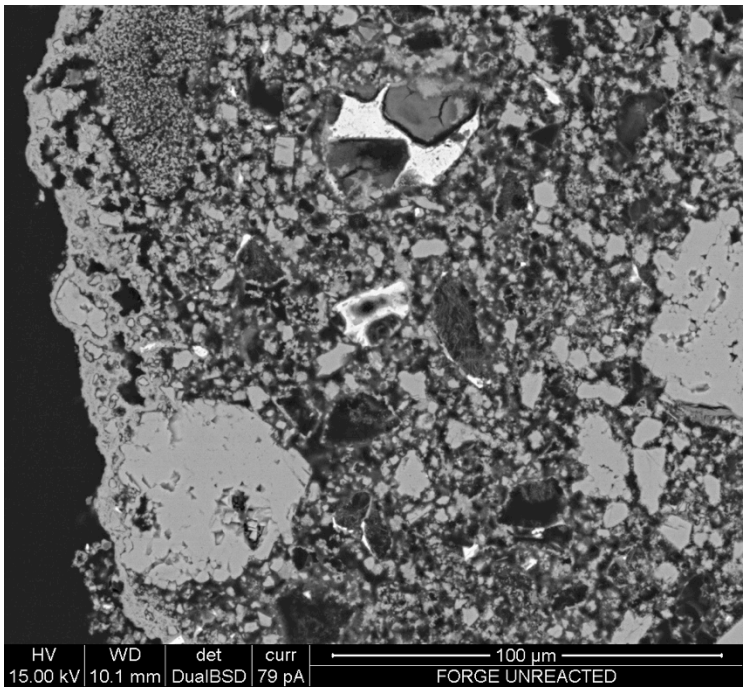

Plate 4. BSEM photomicrograph of showing a section through the outer edge of the cement plug (left edge of image). A thin dense layer of microcrystalline calcite (light grey) can be seen to form a continuous outer layer, with finely-disseminated calcite (light grey) permeating the CASH gel matrix (dark grey) of the cement. Coarse fragments of limestone aggregate can be seen as the relatively large grains of calcium carbonate (light grey). Remnants of primary cement clinker grains are present, with relatively unaltered brownmillerite (bright grains) intergrown with CSH hydration products (dull grey) replacing the original primary anhydrous calcium silicate. Immediately beneath the dense outer calcium carbonate skin, the cement has been dissolved with interconnected dissolution microporosity (black) Unreacted NRVB cement paste starting material.

Detailed observations of the laminated fabric observed in the cement reveal marked mineralogical and fabric differences between the laminations. The lighter and coarser laminae

observed in thin section (Plate 1B), have a higher proportion of coarser silt-grade limestone aggregate particles (Plate 5). They also contain patches of relatively coarsely-crystalline portlandite poikilotopically-cementing the intergranular microporosity, and which also displaces the gel-like CSH-rich interstitial matrix within these coarser bands (Plate5). These patches may coalesce to form relatively continuous bands at the thin section scale. In contrast, the darker finer laminations (Plate 1B) have a higher proportion of finer limestone aggregate particles and much less (and finer scaled) interstitial/intergranular portandite development.

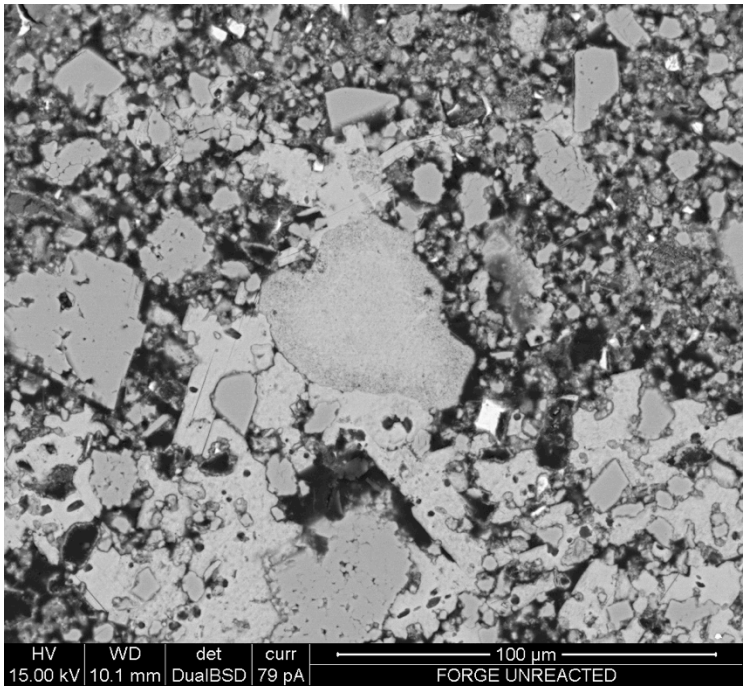

Plate 5. BSEM photomicrograph of showing patches of relatively coarsely-crystalline portlandite crystals (light grey) cementing the microporosity and enclosing silt-grade limestone aggregate particles, and growing displacively within the CSH-rich gel matrix. The image is characteristic of the apparently coarser and lighter laminae seen in thin section under transmitted light (Plate 1B). Unreacted NRVB cement paste starting material.

The petrographic observations show that this laminated fabric has developed as a result of physical separation of the finer and coarser particle sizes of the cement clinker and limestone flour aggregate. This clearly occurred as through hydrodynamic particle-size fractionation during manufacture of the stock NRVB cement starting material from which the cement cores were cut. This process appears to have produced a heterogeneous laminated fabric with coarser and pore porous (and presumably more permeable) laminae within which portandite precipitated in the intergranular porosity from the cement porewater during sample curing. Whereas, the finer and less permeable laminae developed much less portlandite during the curing process.

The segregation of the cement past into fine and coarse laminae influences the porosity distribution in the cement, and thereby will affect the permeability of gas flow pathways through the cement cores. Observation of the blue-dye epoxy-resin impregnation of the thin sections by transmitted-light optical microscopy suggests that the coarser laminae display greater degree of resin impregnation, and hence greater porosity than the finer laminae. This heterogeneity in the primary cement fabric, produced during the manufacture of the cement core samples, was observed to have had a significant influence on the pattern and extent of alteration and CO_2 diffusion pathways in several of the cement cores during the carbonation of the cement in the batch experiments.

BSEM-EDXA observations of the polished thin section profile from the rim to centre of the unaltered cement revealed that a thin layer of carbonated cement was already present on the external surfaces of the cement cores before the carbonation experiments started (Plate 4). The carbonated cement layer formed a near-continuous skin over the surface of the cement plug (Plate 4). It consisted of a dense outer layer of tightly-interlocking microcrystalline calcium carbonate up to 50 um thick, within which the original hydrated cement phases have been virtually completely replaced by calcium carbonate. This indicates that there has been almost complete migration and loss of Si and Al from within this narrow alteration zone. Beneath this, a band of more pervasive impregnation and partial replacement of the underlying CSH matrix by fine-grained calcium carbonate extends for up to 150 um from the surface of the cement. Immediately beneath the dense outer carbonated layer, the cement shows evidence of dissolution of the CASH and CAH/CASH phases, with subsequent enhanced porosity, extending over a zone up to 50 μm wide. Coarse clear colourless or white crystals up to 2 mm long were observed sporadically on the surfaces of the unfreacted cores after curing (Plate 6). SEM-EDXA showed that these were also calcium carbonate. This mineralogical alteration indicated that the cement had already undergone some reaction with atmospheric CO_2 and dissolution in the water during the curing and storage of the cement plugs prior to use in the experiments.

7.2 ANALYSES OF EXPERIMENTALLY CARBONATED CEMENT

The following sections describe observations made of different parts of the cement blocks after they had undergone carbonation tests.

7.2.1 Surface alteration characteristics of the cement cores

Upon reaction with CO_2 (gaseous, liquid or supercritical) most cement blocks showed a marked colour change from grey to brown (Plate 6). Petrographic analysis shows that this colour change results from the reaction of calcium ferrite or calcium aluminoferrite phases (e.g. brownmillerite) with CO_2 to produce secondary calcium carbonates accompanied by the liberation of finely-disseminated free ferric oxide (Fe_2O_3) or ferric oxhydroxide ($Fe_2O_3.nH_2O$) to give a 'rusty' colour.

$$\text{e.g.} \qquad [CaO]_2.Fe_2O_3 + 2\,CO_2 \Rightarrow 2\,CaCO_3 + Fe_2O_3$$

These preliminary observations are consistent with results from studies of CO_2 reaction with borehole cement as part of studies into the deep underground storage of CO_2 (e.g. Carey *et al.*, 2007; Rochelle *et al.*, 2007). It is possible therefore, that similar CO_2-cement mineral reactions are taking place. Should further analyses prove this to be the case, then there could potentially be useful exchange of data and modelling approaches between radioactive waste studies and carbon capture and storage studies.

All of the reacted cement cores exhibited extensive precipitation of secondary calcium carbonate reaction products on their external surfaces. The morphology of the carbonate varied considerably, from: dense crystalline calcite and aragonite encrustations with dry supercritical CO_2 (e.g. Plate 7), with supercritical CO_2 and YNFP (e.g. Plate 8), and supercritical CO_2 and ENFG; to encrustations of loosely-adhering microcrystalline sub-rounded rhombohedral calcite and rare coarse calcite rhombs after reaction with supercritical CO_2 and ENFG (e.g. Plate 9); to microporous bladed orthorhombic crystal aggregates of probable aragonite with dry liquid CO_2 (e.g. Plate 10); and fine tightly interlocking 'scaley' microcrystalline calcite and gelatinous (possibly amorphous) calcium carbonate seen with liquid CO_2 and ENFG (e.g. Plate 11).

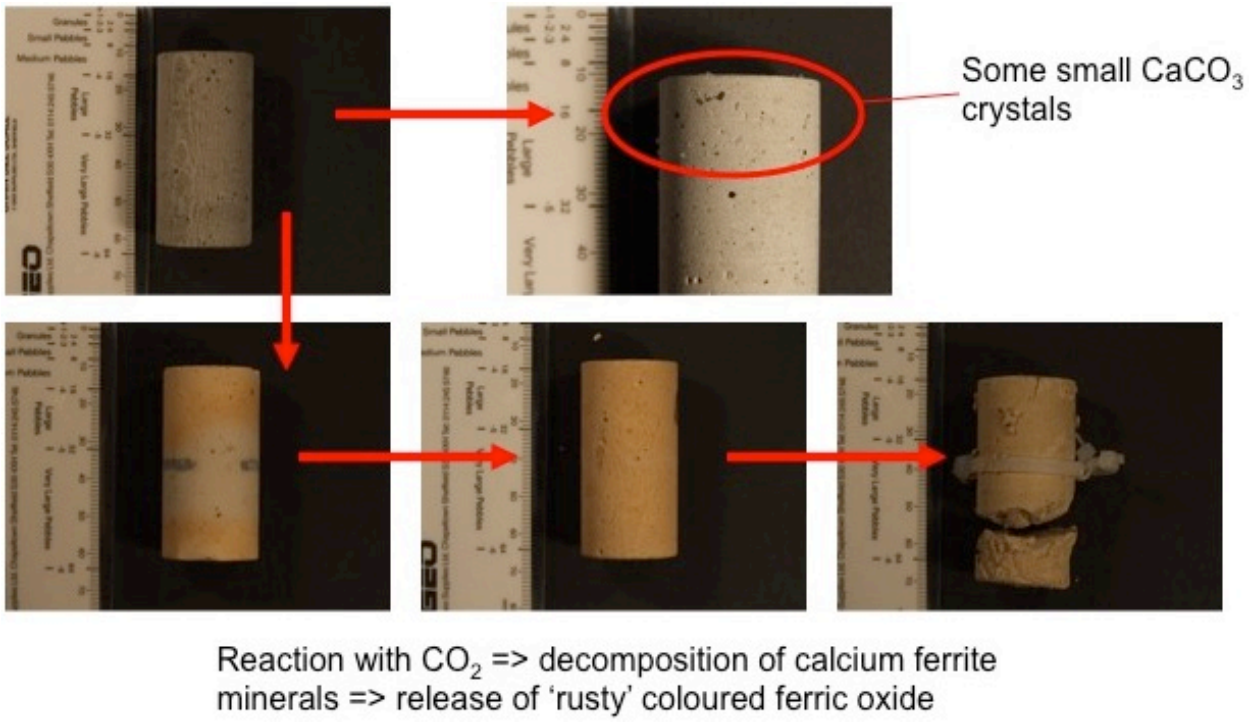

Plate 6. Examples of cement cores before reaction (upper left hand image) and after reaction. Note the grey to brown colour change upon reaction with CO_2, and the appearance of small calcium carbonate crystals on the surface of the cement.

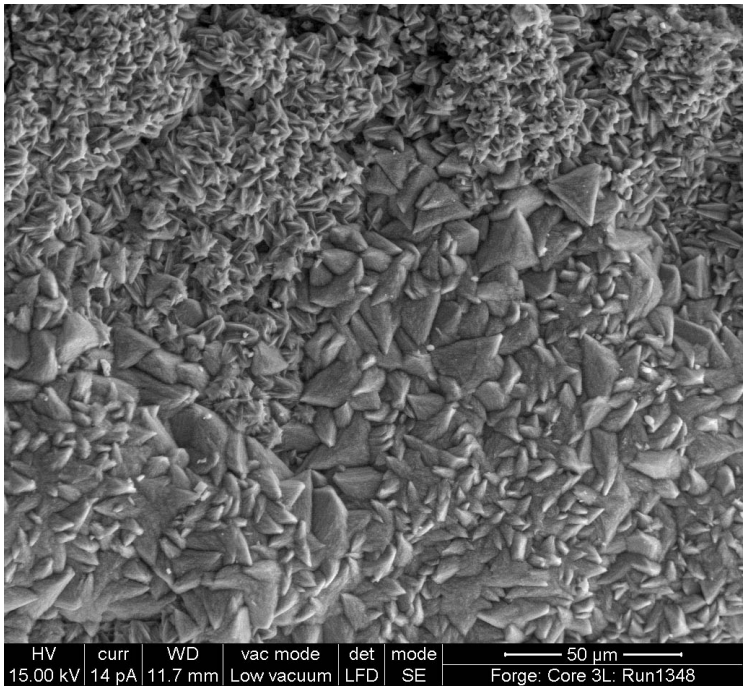

Plate 7. SEM (SEI) photomicrograph of the surface of cement plug after reaction with dry supercritical CO_2 after 40 days at 40°C and 80 bar. The surface is encrusted with tightly interlocking crystals of trigonal-rhombohedral calcite (lower half of image) and spheroidal radial-fibrous aggregates of acicular, bladed or elongated prismatic calcium carbonate (upper half of image) that are probably aragonite.

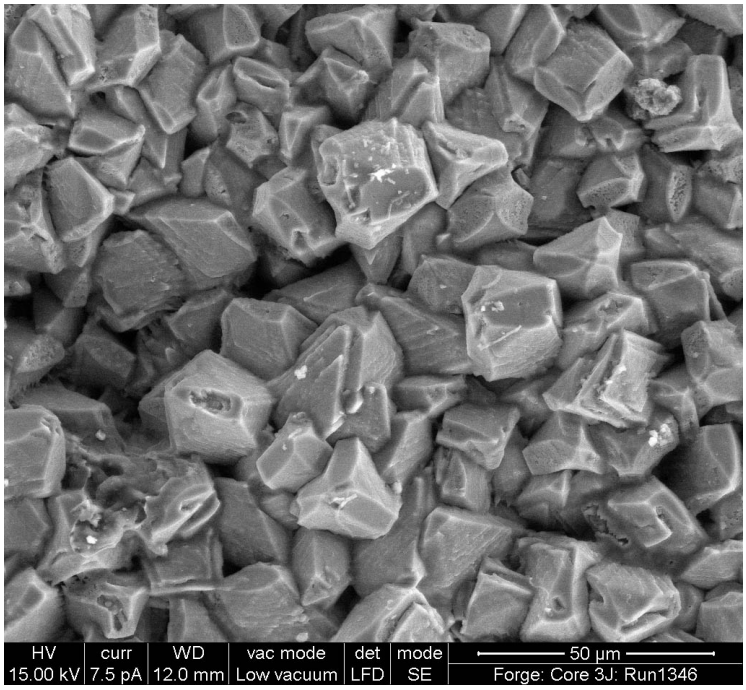

Plate 8. SEM (SEI) photomicrograph of the surface of cement plug after reaction with YNFP and supercritical CO_2 after 40 days at 40°C and 80 bar. The surface is encrusted with tightly-interlocking crystals of calcite.

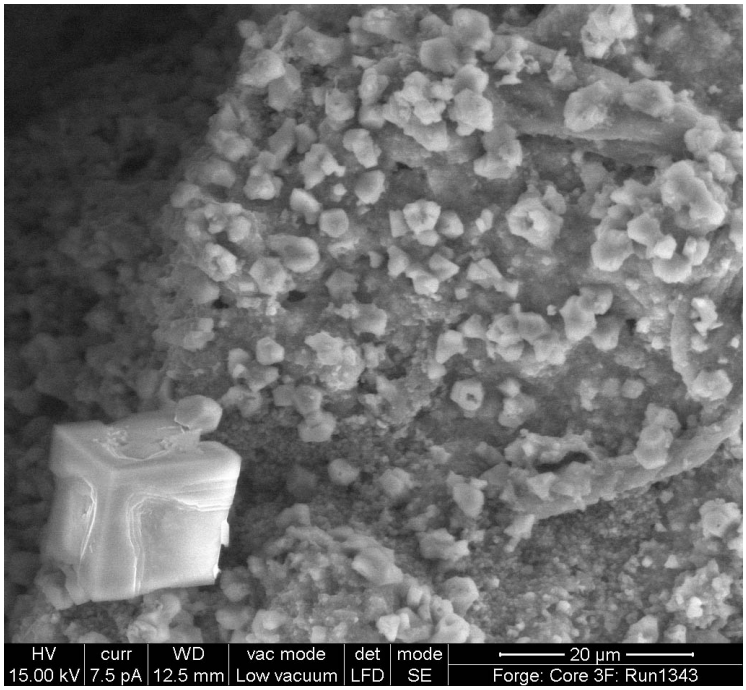

Plate 9. SEM (SEI) photomicrograph of the surface of cement plug after reaction with ENFG and supercritical CO_2 after 40 days at 40°C and 80 bar. The surface is encrusted with loosely-adhering, finely crystalline equant sub-rounded rhombohedral crystals of calcite.

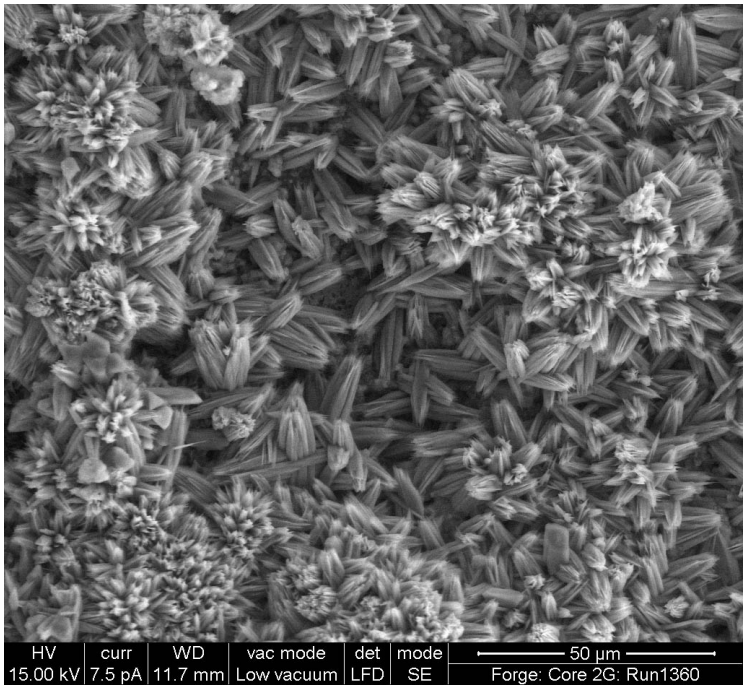

Plate 10. SEM (SEI) photomicrograph of the surface of cement plug after reaction with dry liquid CO_2 after 40 days at 20°C and 80 bar, showing encrustation of the surface by aggregates of elongated to bladed orthorhombic prisms of possible aragonite crystals.

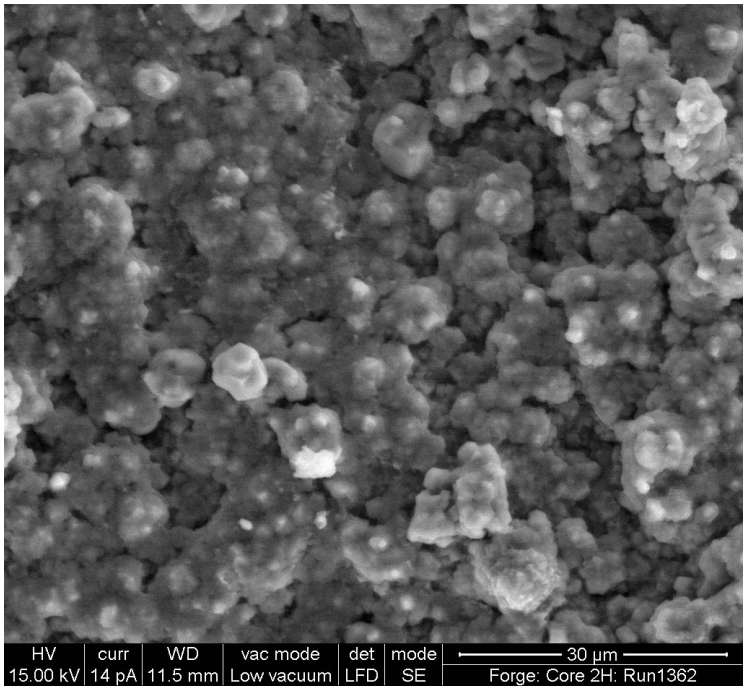

Plate 11. SEM (SEI) photomicrograph of the surface of cement plug after reaction with dry liquid CO_2 after 40 days at 20°C and 80 bar, showing coalescing, microcrystalline to amorphous calcium carbonate crystals coating reacted cement surface.

Calcium carbonate precipitation on the cement surfaces was observed in reacted cores from both CO_2 and N_2 control experiments. No consistent relationship was found between the morphology of the calcium carbonate coating the external surfaces of the cement cores and the experimental conditions. The carbonation observed in the N_2 control experiments suggests that either the N_2 experimental cells were not entirely free of atmospheric CO_2, or that the sealing of the reacted samples within the Ar-flushed crimp-welded flat-roll tubing was nor completely effective in preventing reaction with atmospheric CO_2 prior to petrographic analysis.

7.2.2 Carbonation with gaseous CO_2

Detailed petrographic analysis was undertaken on the cement cores reacted with YNFP and ENFG in the presence of gaseous CO_2 and with dry gaseous CO_2, all reacted for 40 days at 40°C under 40 bar pressure. Plate 12 compares transmitted light images of polished thin sections illustrating profiles through reacted cores for experiments with YNFP and ENFG in the presence of gaseous CO_2, with dry gaseous CO_2, and unreacted cement. The degree and pattern / pathway of alteration was observed to be markedly different between the three experiments 'YNFP + gaseous CO_2', 'ENFG + gaseous CO_2' and 'dry gaseous CO_2 only'. The transmitted light photomicrograph of the reacted cement core from experiment with 'YNFP(1) + CO_2', is also shown in Figure 13. This sample was not examined in detail but appears to show broadly similar alteration characteristics to that in the 'YNFP+Cl + gaseous CO_2' experiment.

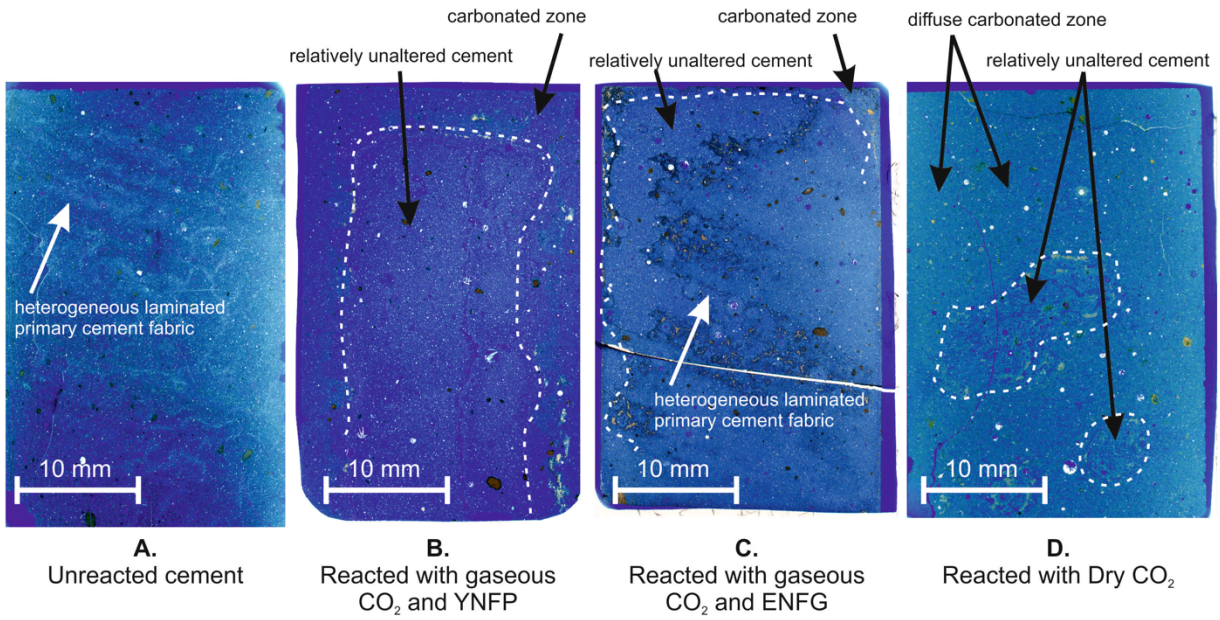

Plate 12. Comparison of transmitted light image of polished thin sections through cores of (A) unreacted NRVB and NRVB reacted with (B) YNFP in the presence of gaseous CO_2, (C) ENFG in the presence of gaseous CO_2, and (C) dry gaseous CO_2 at 40°C, 40 bar for 40 days. Top and sides of image represents outer edges of the cement cores. The position of the main reaction (carbonation) fronts are shown by dashed lines.

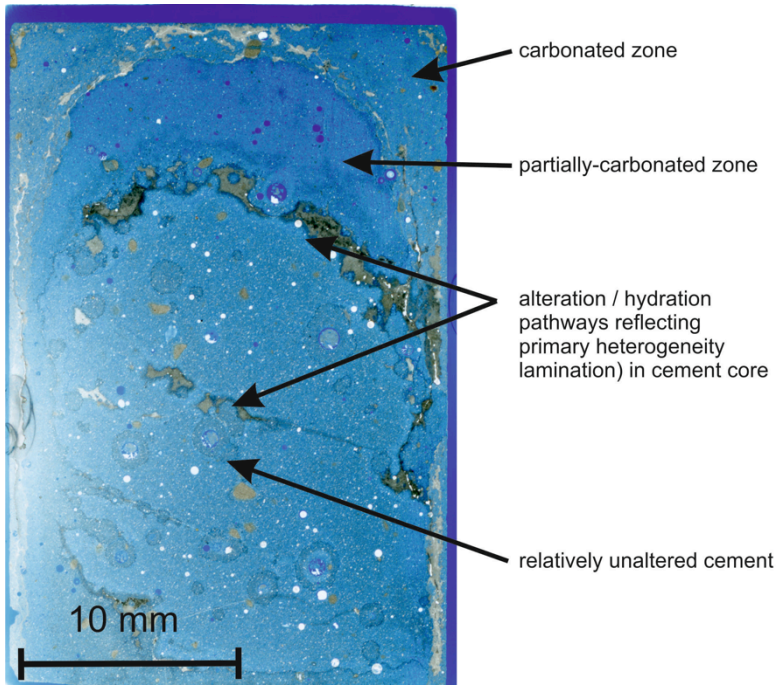

Plate 13. Transmitted light image of polished thin section through core of NRVB reacted with YNFP+Cl in the presence of gaseous CO_2, 40 days at 40°C under 40 bar pressure. Top and sides of image represents outer edges of the cement core. Patterns or pathways of changes in hydration and alteration in the relatively unaltered cement are influenced to some extent by pre-existing heterogeneity (particle size segregations / laminations) in the original cement.

The alteration pattern and pathways taken by the alteration in 'YNFP+Cl + gaseous CO_2' are strongly influenced by the heterogeneity (particle size laminations and segregations) in the original cement paste, which most probably controlled variation in primary permeability of the cement core.

The 'YNPF + gaseous CO_2' experiments showed the sharply-defined reaction fronts. Both 'YNFP+Cl + gaseous CO_2' and 'YNFP + gaseous CO_2' experiments show broadly similar alteration patterns (Plate 12B and Plate 13). The alteration is characterised by broadly concentric alteration fronts, with an outer zone of intensely carbonated cement up to 6 mm wide and an inner zone of relatively unaltered cement (although detailed BSEM-EDXA observations show at least some carbonation within this inner region of the cores). In the case of the 'YNFP+Cl + gaseous CO_2' experiment, a 0 to 8 mm wide zone of enhanced porosity (shown in the thin section by greater blue-dye resin impregnation in Figure 13) is seen between the outer carbonated zone and the relict unaltered core of the cement. In the case of the 'YNFP + gaseous CO_2' experiment, this zone of enhanced porosity is very poorly-developed to imperceptible, and where developed it is confined to an extremely narrow zone less than 250 um wide and immediately in front of and at the edge of the carbonation front (Plate 14). The reason for this difference observed in the alteration behaviour of these two similar experiments is unclear. However, this may in part be influenced by differences in the heterogeneity of the two cement cores. In constrast to the 'YNFP + gaseous CO_2' experiment, the cement core in the 'YNFP+Cl + gaseous CO_2' possessed significant primary heterogeneity due to lamination and particle size segregation in the original cement. This appeared to have influenced at least some of the diffusion pathways for CO_2 migration into the cement during the experiment, and may have provided greater access of CO_2 to the cement along the more permeable coarser laminations.

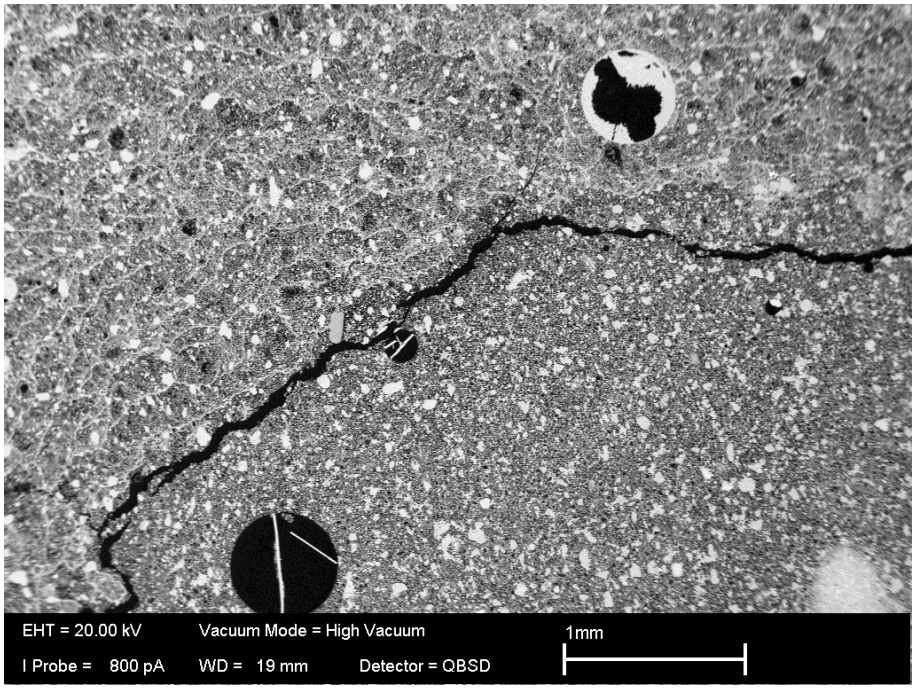

Plate 14. BSEM photomicrograph of the interface between the intensely-carbonated cement (top and left of image) and residual relatively unaltered core (bottom and right of image) of the reacted cement plug from the 'YNFP + gaseous CO_2', 40 days at 40°C under 40 bar pressure experiment. The carbonated cement zone displays a 'chicken-wire' alteration fabric of anastomising interconnected microfractures and shrinkage cracks sealed by microcrystalline calcium carbonate. Entrained air bubbles are mineralised by coarsely crystalline aragonite in the carbonated cement and by plates of portlandite in the unaltered cement.

In both 'YNFP+Cl + gaseous CO_2' and 'YNFP + gaseous CO_2' experiments, the carbonation of the cement is associated with the development of a series of carbonation reaction fronts, along which a an anastomising network of very fine (5-10 μm wide) microfractures is developed sub-parallel to the alteration front (Plate 14). As this front moves forward the microfractures are mineralised by calcium carbonate to produce a 'chicken-wire' meshwork fabric of microfractures within the carbonated cement behind the advancing reaction front. As it moves into the cement core (Plate 14 and Plate 15). Within the carbonated cement, the hydrated CSH and CASH/CAH hydrated cement compounds are progressively altered at the reaction front, to produce a matrix of finely-disseminated micro- to nanocrystalline calcium carbonate dispersed within an amorphous gel-like residual silica rich groundmass (Plate 16).

The matrix of the carbonated cement appears to have broadly similar matrix microporosity porosity to that of the unaltered cement. Although, as described above, the porosity may be enhanced locally by dissolution of CSH and CAH/CASH phases immediately ahead of the main carbonation front seen in the 'YNFP+Cl + gaseous CO_2' experiment. The macroporosity, represented by the entrained air bubbles in the cement past were observed to be unmineralised or partially-filled by hexagonal plates of portlandite in the residual unaltered cement ahead of the carbonation front (Plate 14). However, in the carbonated cement zone the portlandite has been removed and the cavities are now lined or filled by orthorhombic prisms or acicular calcium carbonate (Plate 14), which (on the basis of its morphology) is most probably aragonite.

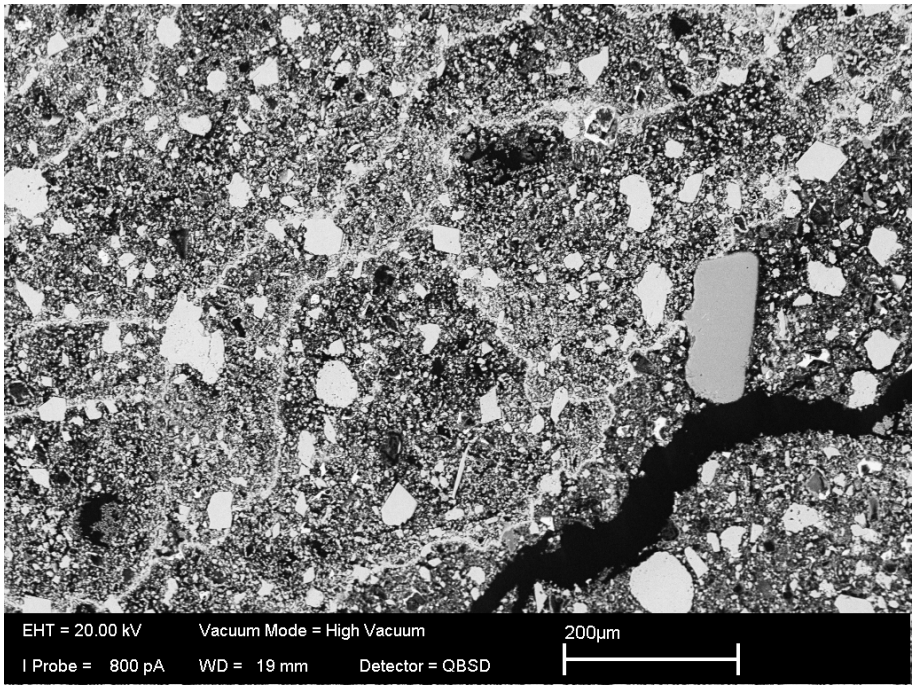

Plate 15. BSEM photomicrograph of the carbonated cement zone showing the 'chicken-wire' alteration fabric of anastomising interconnected microfractures and shrinkage cracks sealed by microcrystalline calcium carbonate (white), within a very fine matrix of microcrystalline calcite disseminated in a amorphous silica groundmass. 'YNFP + gaseous CO_2', 40 days at 40°C under 40 bar pressure experiment.

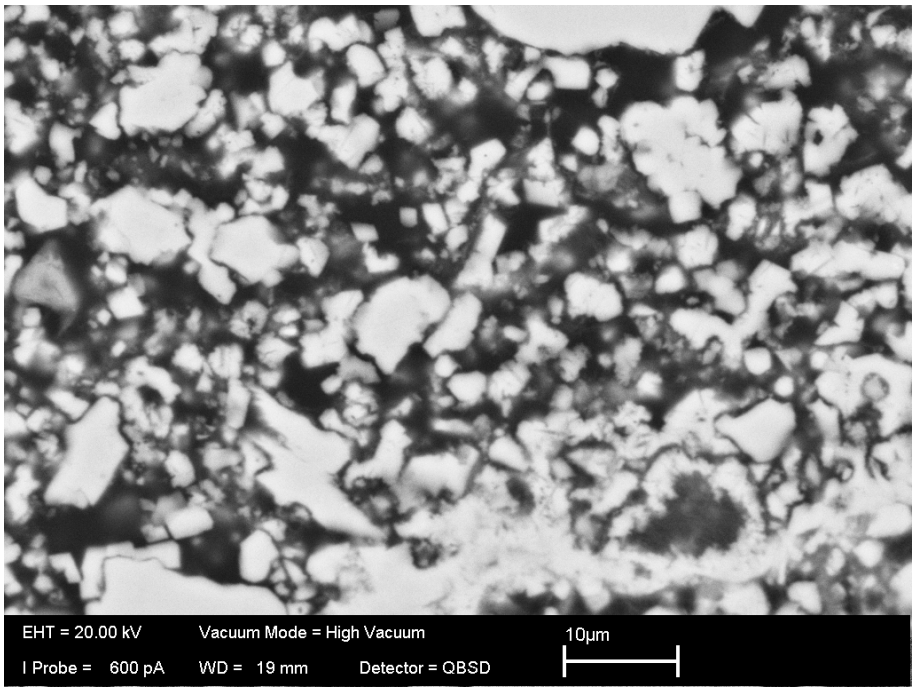

Plate 16. BSEM photomicrograph of the matrix of the carbonated cement showing microcrystalline calcium carbonate (white) in an amorphous or poorly-crystalline groundmass of hydrous silica (dark grey). YNFP + gaseous CO_2, 40 days at 40°C under 40 bar pressure experiment.

Although, the carbonation alteration is strongest within the fully-carbonated region of cement behind the sharply-defined carbonation front, it was clear that CO_2 had diffused further into the cement cores ahead of the main reaction front. This has resulted in patchy, diffuse alteration, and partial replacement of the hydrated CSH and CASH cement phases thoughout the cement core by very fine (sub-micron) calcium carbonate material.

EDXA showed enhanced concentration of Cl in the matrix of the alterated cement, at the leading edge of the carbonation front. However, unlike in the experiments with 'ENFG and gaseous CO_2', no discrete Cl-rich phase was found by BSEM-EDXA.

The 'ENFG + gaseous CO_2' experiment (40 days at 40°C under 40 bar pressure) produced a much narrower and less developed zone of carbonation in the reacted cement plug than in the two 'YNFP + gaseous CO_2' experiments (Plate 12 and Plate 17). However, the carbonation reaction front is sharply-defined (Plate 17), as was seen in the 'YNFP + gaseous CO_2' experiments. The carbonated zone varied from only 250 μm to about 1 mm in thickness (Plate 17). This experiment also produced a carbonated alteration zone with similar development of a 'chicken-wire- like' network fabric of anastomosing calcium carbonated sealed microfractures to that seen in the YNFP experiments. However, the degree of carbonation and alteration within this very narrow zone was much more intense with more complete replacement of the cement matrix by calcium carbonate (Plate 18) than was observed in the ENFG experiment. The secondary calcium carbonate appeared to be coarser than in the YNFP fluid experiments, and many of the microcrystals displayed rhombohedral form, suggesting that the secondary calcoum carbonate phase is dominantly calcite rather than the aragonite or vaterite polymorphs.The 'ENFG + gaseous CO_2' experiment also displayed more complicated alteration at the carbonation reaction front than was observed in the 'YNFP + gaseous CO_2' experiments. Detailed BSEM-EDXA observations revealed the formation of secondary calcium chloroaluminate alteration products at or immediately behind the leading edge of the carbonation front in this experiment (Plate 19 and Plate 20). A similar secondary calcium chloroaluminate alteration product was observed by Rochelle *et al.* (2009), in experiments on the interaction of CO_2 with Portland cement-based oilwell 'Type G' cement. XRD analysis of the altered oilwell cement tentatively identified the crystalline product observed previously by Rochelle *et al.* (2009) as hydrocalumite ($Ca_4Al_2O_6Cl_2.10H_2O$). This phase has nucleated within, and is enclosed by, a matrix of amorphous silica-rich gel and finely-disseminated calcium carbonate (Plate 20).

Detailed BSEM-EDXA petrographic analyses show that this reaction product is strongly growth-zoned (Plate 20, Figure 14). The early growth stages of the radial-fibrous crystals are Al-rich with only minor Fe (Figure 14). However, as growth proceeds, the crystals become increasingly enriched in Fe with a corresponding decrease in Al (Figure 14). This demonstrates that there is significant solid-solution, with Fe substitution for Al within this calcium chloroaluminate phase, and that Fe is being mobilised and enriched in the cement pore fluids with time as alteration at the leading edge of the carbonation front progresses.

The formation of this secondary calcium chloroaluminate is responsible for a concentration of chloride at or just behind the leading edge of the main carbonation front in these experiments with 'ENFG + gaseous CO_2'. However, this phase is transient and is absent in the fully-carbonated cement. As the carbonation front moves forward the calcium chloraluminate phase is dissolved and replaced by calcium carbonate and fine grained aluminous material. The chlorine then continues to migrate further into the cement, following the carbonation front, to reform and precipitate fresh crystals of calcium chloroaluminate

The precipitation of calcium chloroaluminate as a reaction product in these experiments accounts for the significant depletion of Cl^- observed in the fluid. Although only a transient phase, the formation of this reaction product may potentially be important as a mechanism of retarding the migration of ^{36}Cl from low- and intermediate-level radioactive waste.

Although Cl was observed to be lost from the fluid phase during the course of the control experiments with gaseous N_2, no petrographic evidence of Cl concentration or secondary Cl-rich

alteration products were observed. EDXA maps for Cl showed uniformly-distributed low concentration of Cl throughout the cement in the control experiments with gaseous N_2.

As seen in the 'YNFP + gaseous CO_2' experiments (see earlier), although the carbonation alteration is strongest within the fully-carbonated region of cement left in the 'wake' of the sharply-defined advancing carbonation front, diffuse alteration by CO_2 was observed to have penetrated deeper into cement cores ahead of the main reaction front. This, again resulted in patchy, diffuse and partial replacement of the hydrated CSH and CASH cement phases by very fine (sub-micron) calcium carbonate material.

The cement core that had been reacted with 'Dry CO_2'at 40° C displayed a marked colour change from initially grey cement to orange-brown stained cement (Plate 21). The alteration fabric is markedly different to that observed with either 'YNFP + gaseous CO_2' or 'ENFG + gaseous CO_2'. The cement from this sample appears to have been carbonated through much of the volume of the core, with only a small proportion of relatively unaltered cement remaining near the middle of core plug (Plate 12). The carbonation alteration is pervasive and diffuse, and extremely fine grained, and the altered cement has a nano-to-microporous matrix. The strong reaction fronts, with relatively coarse and tightly-interlocking crystalline calcite (or other calcium carbonates) observed in the 'YNFP + gaseous CO_2' or 'ENFG + gaseous CO_2'experiments were not developed in this experiment with dry CO_2.

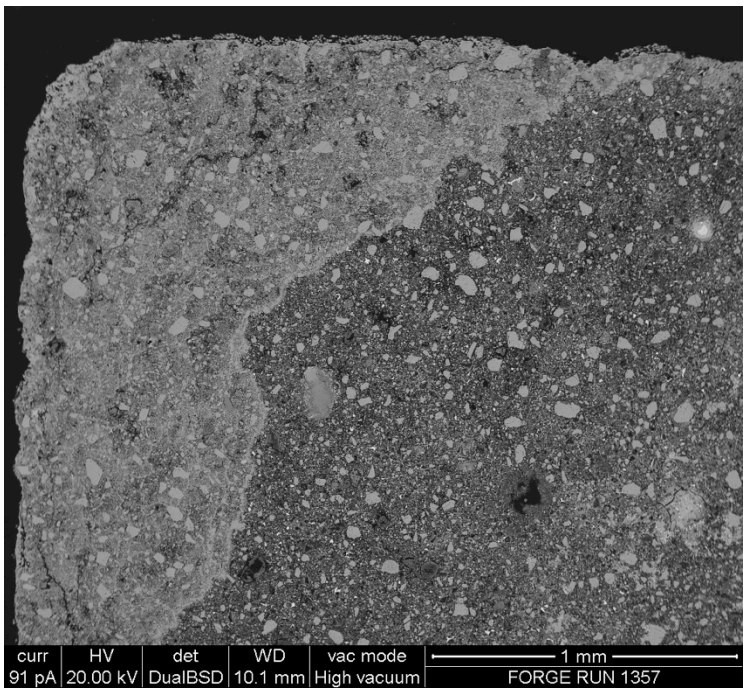

Plate 17. BSEM photomicrograph of the interface between the intensely-carbonated cement (brighter region at the top left of the image) and residual relatively unaltered core (predominantly duller region at the bottom and right of image) of the reacted cement plug from the 'ENFG + gaseous CO_2', 40 days at 40°C under 40 bar pressure experiment.

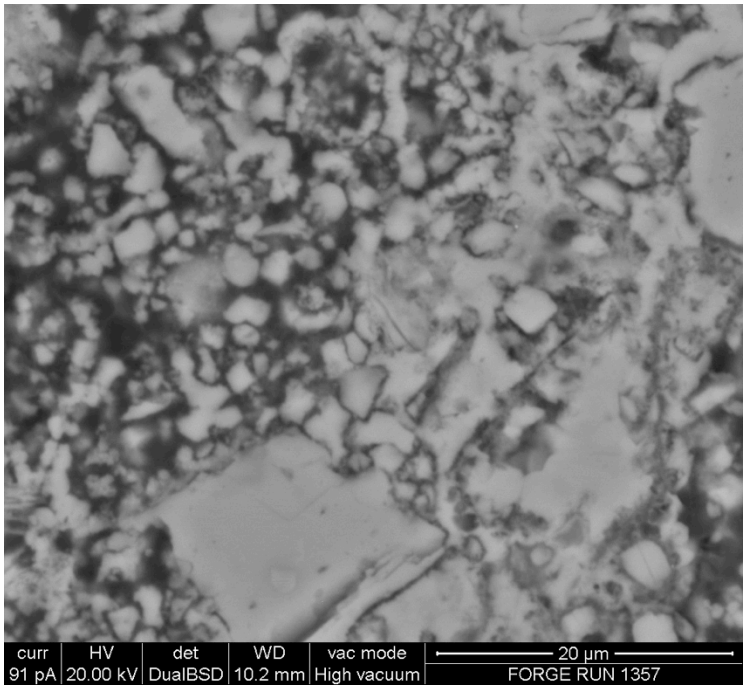

Plate 18. BSEM photomicrograph of the intensely-carbonated cement from the 'ENFG + gaseous CO_2', 40 days at 40°C under 40 bar pressure experiment, showing extensive replacement of the original CSH and CAH / CASH matrix by microcrystalline rhombs of calcite. The image also shows part of a tight, calcite-filled microfracture from close to the interface between altered and unaltered cement (bottom left of image).

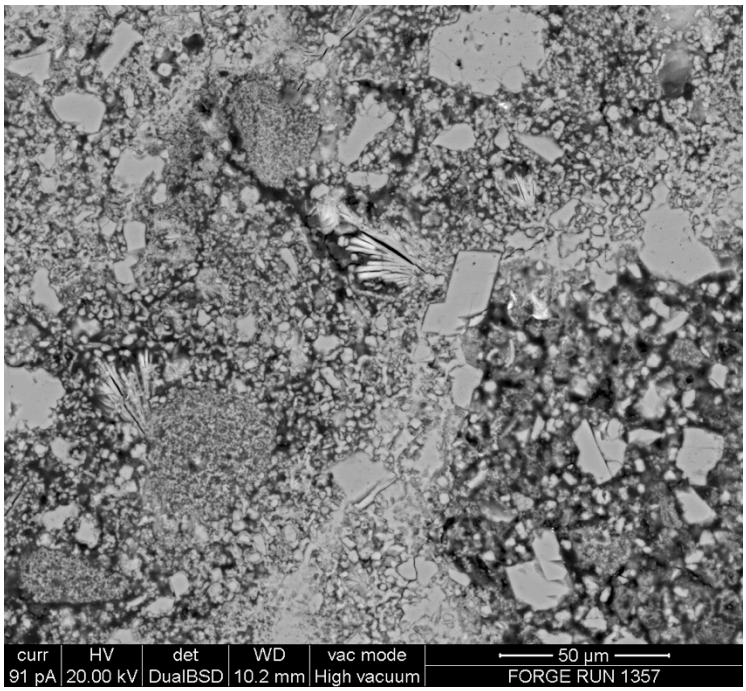

Plate 19. BSEM photomicrograph of the carbonation reaction front between intensely-carbonated cement (top left) and residual unaltered cement (bottom right) from the 'ENFG + gaseous CO_2', 40 days at 40°C under 40 bar pressure experiment. Dense microcrystalline calcium carbonate is developed at the leading edge of the front and a radial fibrous calcium chloroaluminate phase has formed within altered cement immediately behind the front.

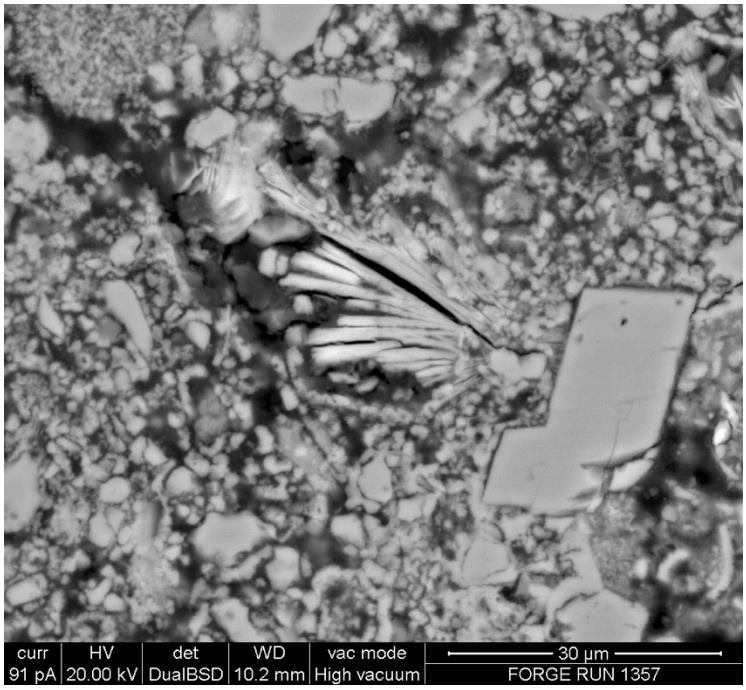

Plate 20. BSEM photomicrograph showing detail of the radial fibrous secondary calcium chloroaluminate phase formed within altered cement immediately behind the leading edge of the carbonation front. The BSEM brightness increases towards the outer edge of the phase as Fe:Al increases. The calcium chloroaluminate phase is enclosed in a matrix of Si-rich gel (dull grey) with finely-disseminated calcium carbonate (light grey) 'ENFG + gaseous CO_2', 40 days at 40°C under 40 bar pressure experiment.

7.2.3 Carbonation with supercritical CO_2

The alteration characteristics of NRVB cement with supercritical CO_2 in the presence of YNPF or ENFG are very similar. As with gaseous CO_2 (Section 7.2.1), the reaction with CO_2 is demarcated by very sharp reaction fronts (Plate 21), which migrate deeper into the cement with time. In the case of the 'YNPF+Cl + supercritical CO_2' experiment, the cement sample appears to be completely carbonated after 1 year (Plate 22). However, in the experiments with ENFG the carbonation fronts appear to advance more lowly than with YNPF, and even after a year of reaction, a relict core of only partially carbonated cement is still present (Plate 22). Transmitted light optical microscope observations show that there is an intermediate zone of of slightly more nano- to micro-porous cement developed ahead of the main carbonation front . This appears to be partially altered to very fine grained calcium carbonate but also partially leached of Ca in comparison to either the dense calcite-replaced outer reaction zone or the residual and partially altered cement in the core of the cement plugs.

The alteration by dry supercritical CO_2 does not produce discrete reaction fronts. Instead, it resulted in diffuse alteration to a highly-carbonated cement comprising a mixture of very fine grained calcium carbonate and secondary silica-rich material, and with finely disseminated iron oxide is produced (Plate 22). Within this fine-grained highly-carbonated matrix, irregular relicts of unreacted cement paste may be present. These unreacted relicts are heterogeneously distributed, and reflect the original heterogeneous character of the original fabric of the cement paste.

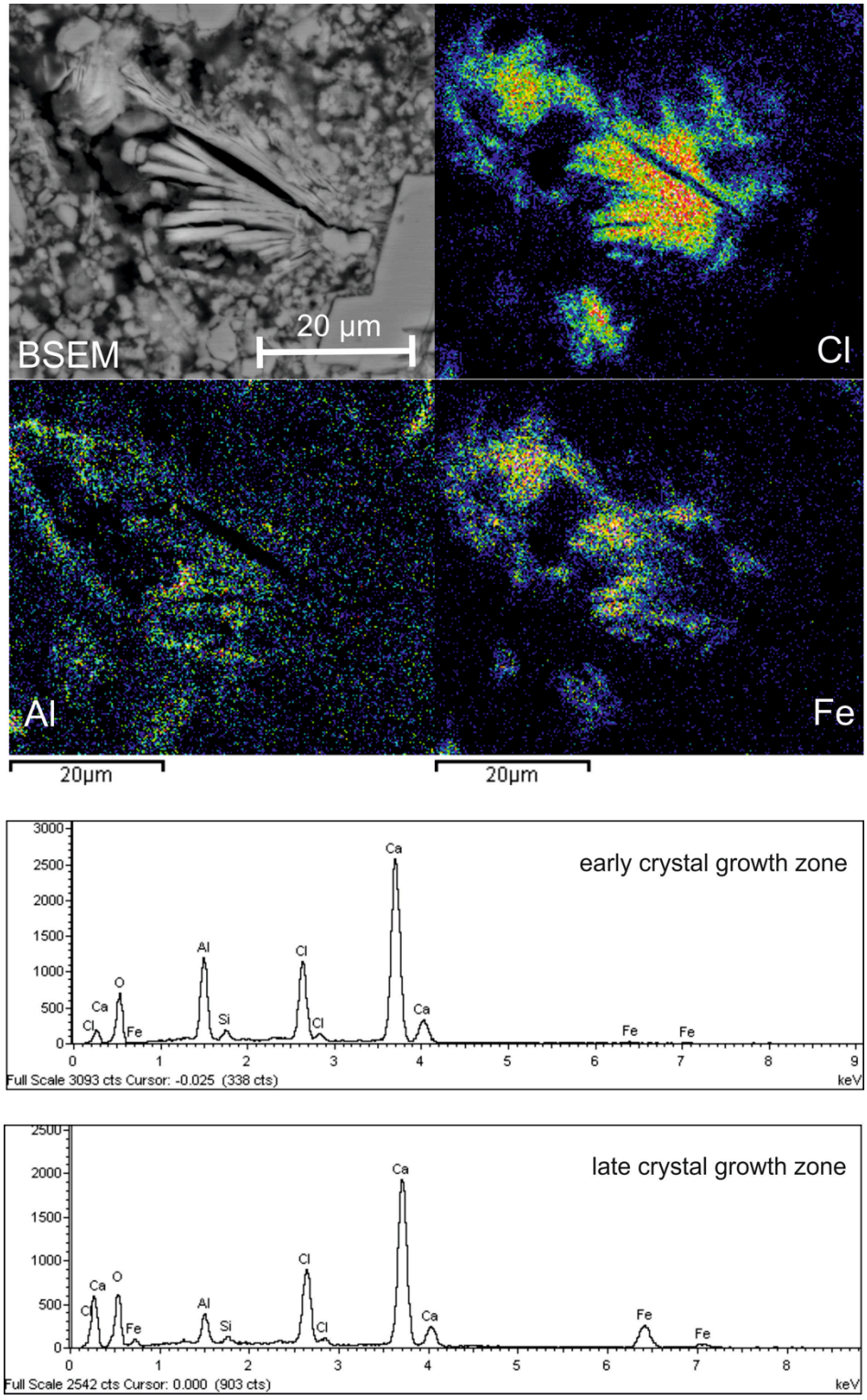

Figure 14. Top: BSEM photomicrograph and corresponding EDXA elemental distribution maps for Cl, Al, and Fe, showing zoned variation in Al and Fe in the secondary radial fibrous calcium chloroaluminate reaction product. Bottom: EDXA spectra from the early Al-rich growth zone and later Fe-rich growth zone of the secondary radial fibrous calcium chloroaluminate reaction product seen in the BSEM image and Xray elemental maps above. ENFG + gaseous CO_2', 40 days at 40°C under 40 bar pressure experiment. Dense microcrystalline calcium carbonate is developed at the leading edge of the front and has formed within altered cement immediately behind the front.

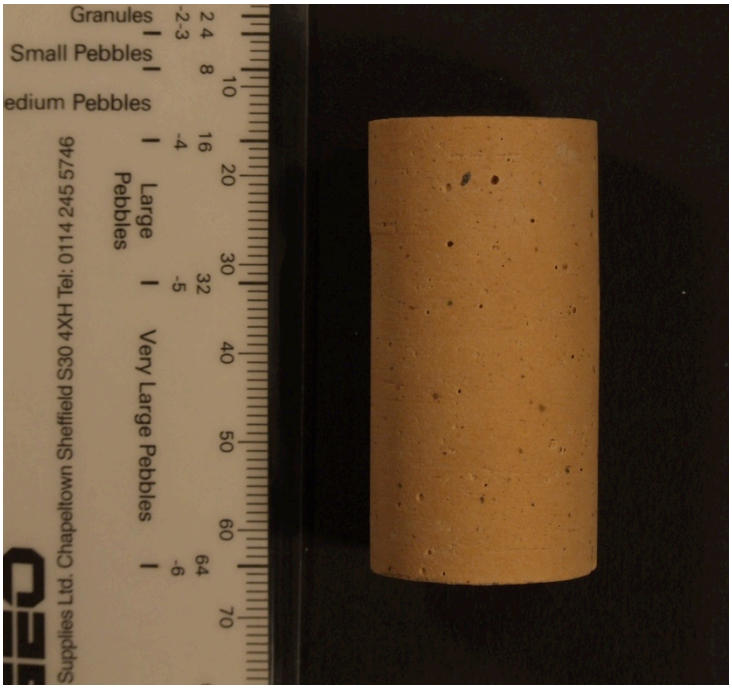

Plate 21. Photograph of the cement core reacted with 'Dry CO_2' at 40° C for 40 days. The core displays a marked orange-brown discolouration.

Detailed BSEM-EDXA observations show that the alteration fabric within the outer, and fully-carbonated regions of the cement plugs reacted in the presence of YNPF and ENFG are broadly similar. The alteration is characterised by the development of a 'chicken-wire- like' network fabric of anastomosing calcium carbonated sealed microfractures similar to that seen in the experiments with gaseous CO_2 (Plate 23). However, the degree of carbonation and alteration within this very narrow zone was much more intense with more complete replacement of the cement matrix by microcrystalline calcium carbonate and secondary amorphous silica (e.g. Plate 24). Within the altered cement, former air bubbles entrained within the original cement paste are largely infilled with coarse secondary calcite (Plate 25). Many of these are completely infilled, thereby almost completely destroying any macroporosity within the cement.

Detailed BSEM-EDXA observations show that the main carbonation front is characterised by a very sharp leading edge, which is very ragged and 'fingers' into the partially carbonated cement ahead (Plate 26). The trailing edge of this reaction front is characteristically diffuse, and over a distance of 0.1-0.5 mm it grades into highly altered cement characterised by the chicken-wire microfracturing and calcite mineralisation described above. The petrolographic features suggest that the processes of calcium carbonate precipitation observed at this reaction front are very complex and dynamic, and that calcium carbonate must be redissolving and redistributing within the anastomising network of calcite-mineralised veinlets behind the advancing reaction front.

The 'dry supercritical CO_2'experiments did not display sharply-defined reaction fronts (Plate 22). The carbonation alteration was pervasive through the whole cement plug. However, BSEM-EDXA observations revealed that the carbonated cement fabric was characterised by the development of a 'chicken-wire- like' network fabric of anastomosing calcium carbonated sealed microfractures similar to that seen in the experiments with supercritical and gaseous CO_2 experiments in the presence of an aqueous phase (Plate 27). However, in this case, little or no evidence of calcium carbonate precipitation was observed to seal air-bubbles that were entrained within the original cement paste. Consequently, much of the macroporosity in the cement plugs was preserved in these experiments.

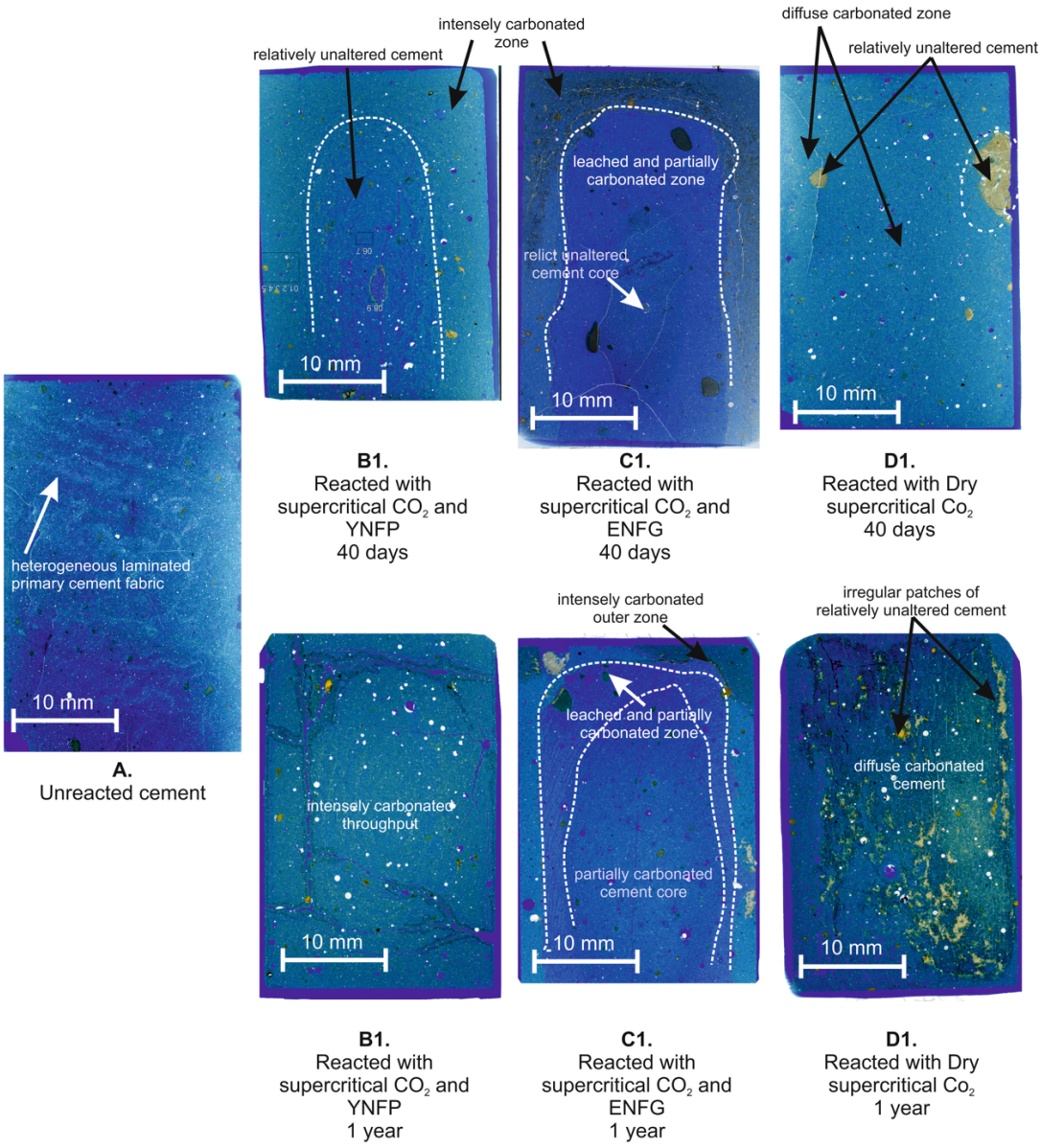

Plate 22. Comparison of transmitted light images of polished thin sections through cores of unreacted NRVB (left) and NRVB reacted with (B1, B2) YNFP +Cl in the presence of supercritical CO_2, (C1, C2) ENFG in the presence of supercritical CO_2, and (D1, D2) dry supercritical CO_2 at 40°C, 80 bar for 40 days (upper images) and 1 year (lower images). Top and sides of each image represents the outer edges of the cement cores. The position of the main reaction (carbonation) fronts are shown by dashed lines.

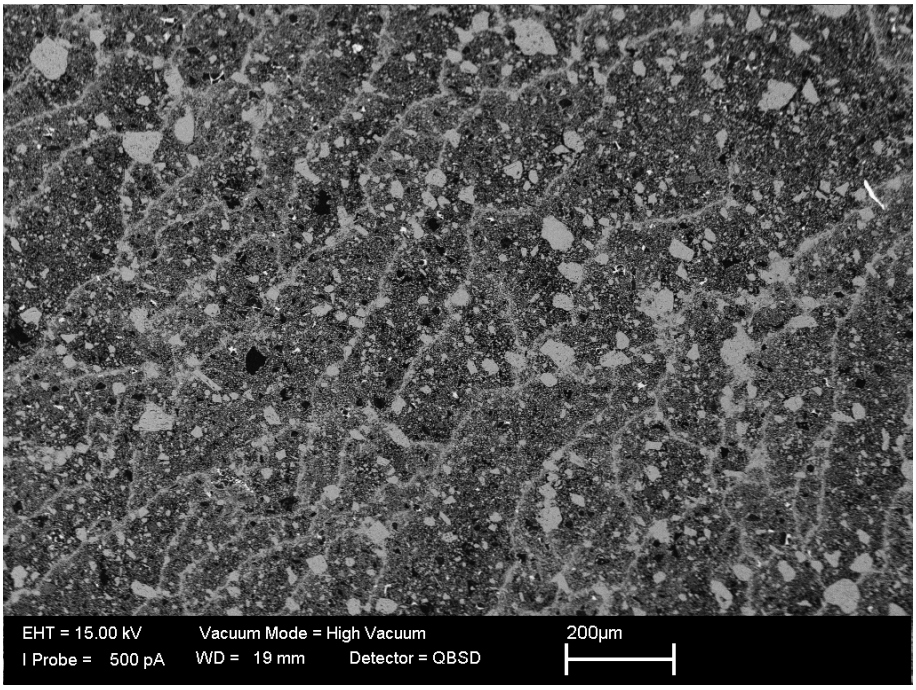

Plate 23. BSEM photomicrograph of the carbonated cement zone showing the 'chicken-wire' alteration fabric of anastomising interconnected microfractures and shrinkage cracks sealed by microcrystalline calcium carbonate (white), within a very fine matrix of microcrystalline calcite disseminated in an amorphous silica groundmass. 'YNFP+Cl + supercritical CO_2', 40 days at 40°C under 80 bar pressure experiment.

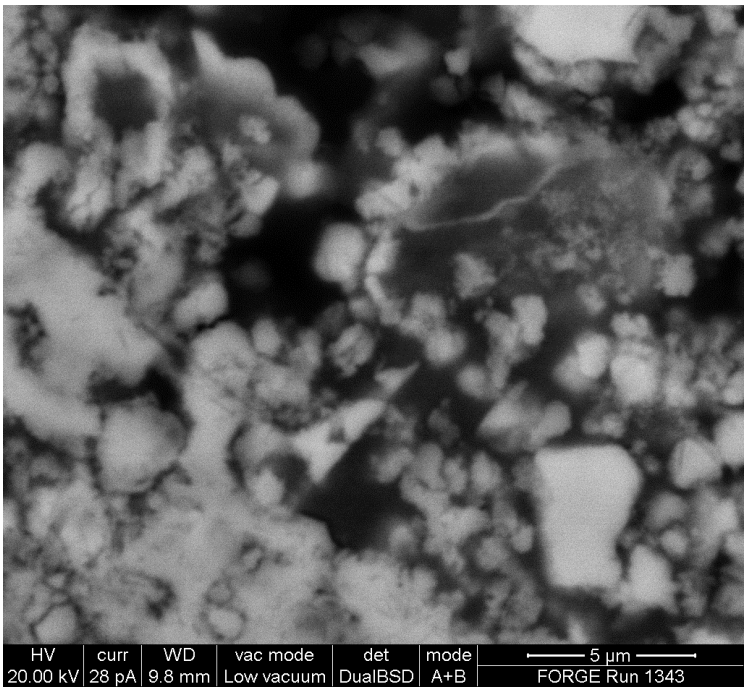

Plate 24. BSEM photomicrograph of the highly-altered matrix of the carbonated cement zone showing complete replacement of the CSH and CASH (and any partially-hydrated clinker phases) in the cement past by nano- to microcrystalline calcium carbonate (white), within a very fine matrix of amorphous silica (dull grey). Fine secondary cavities and microporosity (black) is also evident. 'ENFG + supercritical CO_2', 40 days at 40°C under 80 bar pressure experiment.

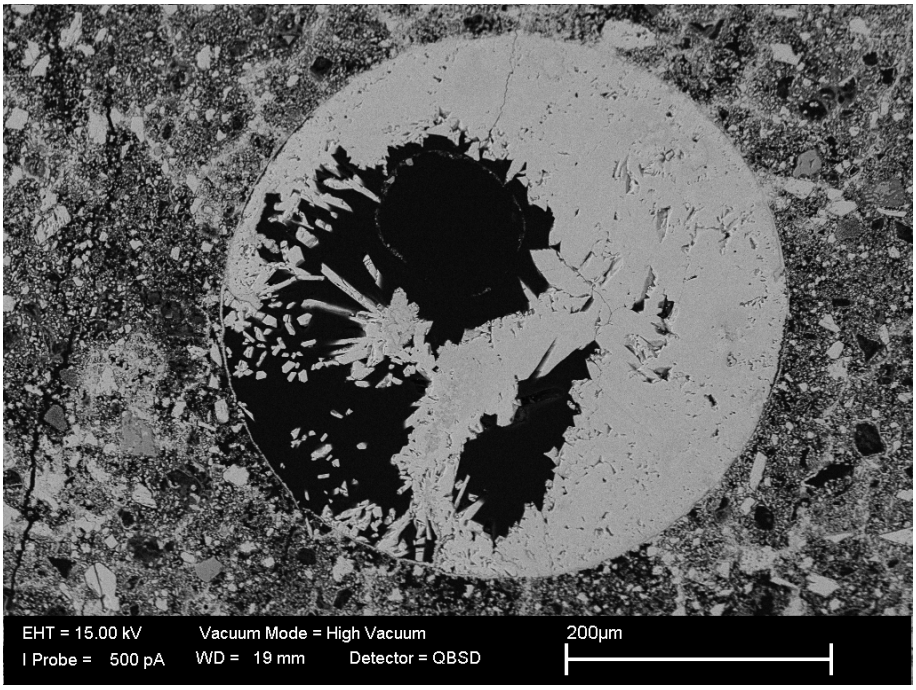

Plate 25. BSEM photomicrograph of the carbonated cement zone showing spherical voids after air bubbles entrained in the cement paste are now largely filled by coarse secondary calcite. 'YNFP+Cl + supercritical CO_2', 40 days at 40°C under 80 bar pressure experiment.

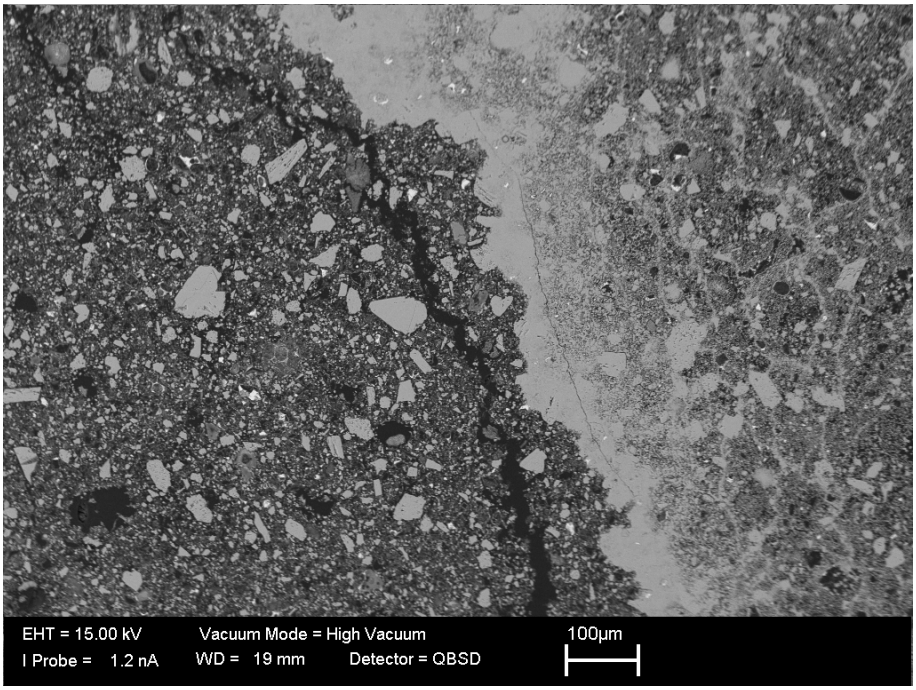

Plate 26. BSEM photomicrograph showing the very sharply-defined main carbonation reaction front demarcating the inner region of partially-carbonated cement (left) from the outer reaction zone of intensely carbonated cement (right). The reaction front is defined by a narrow zone of intense precipitation of dense microcrystalline calcite, with a sharp ragged leading edge, and a more diffuse tail. 'YNFP+Cl + supercritical CO_2', 40 days at 40°C under 80 bar pressure experiment. YNPF+Cl 40 days.

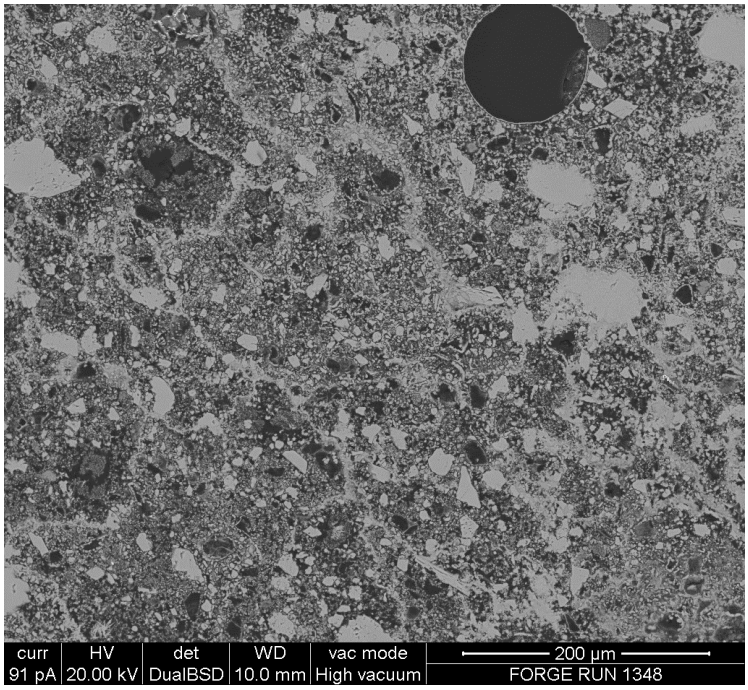

Plate 27. BSEM photomicrograph of the pervasively-carbonated cement showing the 'chicken-wire' alteration fabric of anastomising interconnected microfractures and shrinkage cracks sealed by microcrystalline calcium carbonate (white), within a very fine matrix of microcrystalline calcite disseminated in an amorphous silica groundmass. 'Dry supercritical CO_2', 40 days at 40°C under 80 bar pressure experiment.

As in the experiments with gaseous CO_2 in the presence of YNPF and ENFG, BSEM-EDXA analyses showed that the 'YNFP+Cl + supercritical CO_2' and 'ENFG + supercritical CO_2' experiments both demonstrated a concentration of Cl close to the leading edge of the main carbonation front (Figure 15). However, the distribution of Cl was found to be subtlety different, in that the Cl is concentrated *ahead* of the main calcium carbonate replacement front in these experiments, rather than behind the main reaction front. Also, no discrete Cl-bearing phase was found in the experiments with supercritical CO_2. The concentration of Cl at the leading edge of the reaction front in these carbonation experiments accounts for the significant depletion of Cl^- observed in the fluid. Although only a transient phase, the formation of this reaction product may potentially be important as a mechanism of retarding the migration of ^{36}Cl from low- and intermediate-level radioactive waste.

7.2.4 Carbonation with liquid CO_2

The alteration characteristics of NRVB cement with supercritical CO_2 in the presence of YNPF or ENFG are very similar. As with gaseous CO_2 (Section 7.2.1) and supercritical CO_2 (Section 7.2.2), the reaction with liquid CO_2 is demarcated by very sharp reaction fronts (Plate 28), which migrate deeper into the cement with time. In the case of the 'YNPF + liquid CO_2' experiment, the cement sample appears to be strongly carbonated after 40 days, with only a small relict of partially reacted cement paste in the centre of the core (Plate 28). With ENFG the carbonation reaction front appears to be less advanced than with YNPF, although there is diffuse pervasive carbonation of the cement matrix throughout he whole sample (Plate 28). Transmitted light optical microscope observations show that there is an intermediate zone of of slightly more nano- to micro-porous cement developed ahead of the main carbonation front in the experiment with ENFG (Plate 28), similar to that see in the same experiment with supercritical CO_2. This appears to be partially altered to very fine grained calcium carbonate but also partially leached of

Ca in comparison to either the dense calcite-replaced outer reaction zone or the residual and partially altered cement in the core of the cement plugs.

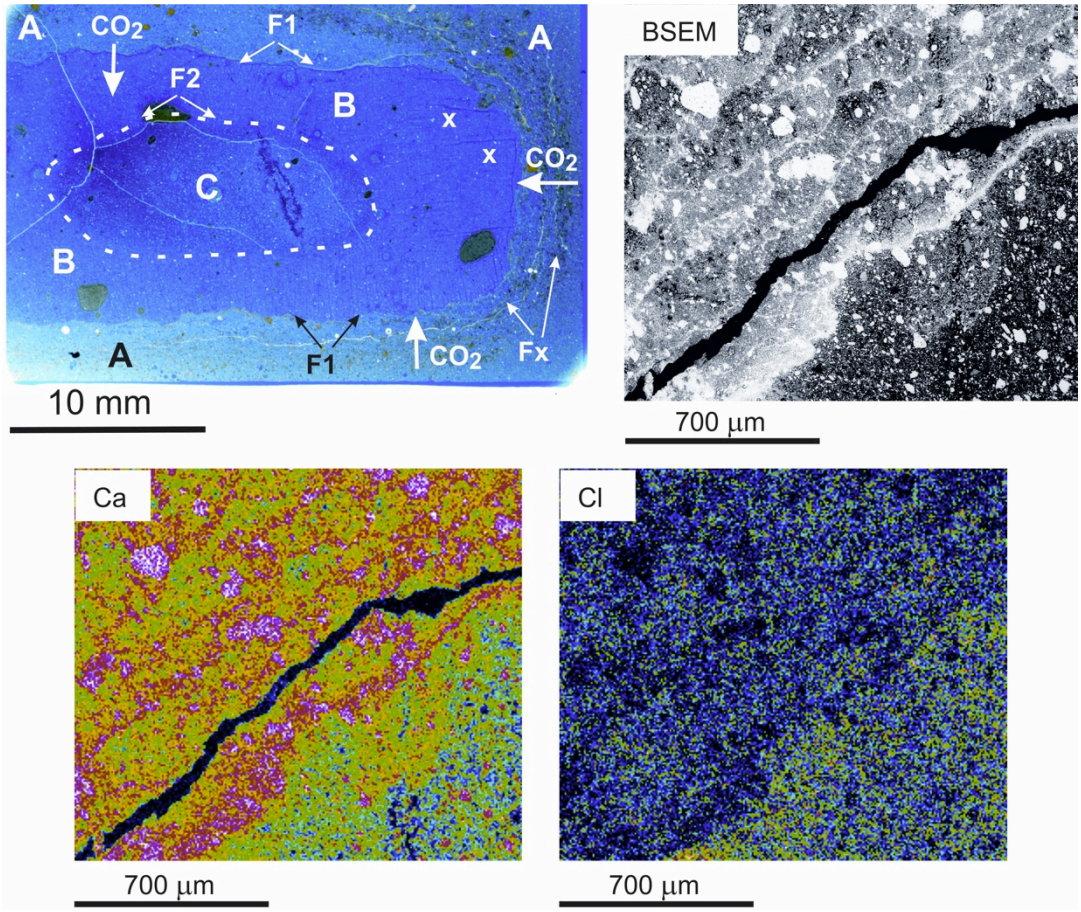

Figure 15. Top left: Transmitted light photomicrograph of thin section through NRVB cement reacted for 40 days with FORGE evolved cement porewater and exposed to supercritical CO_2. A = fully-carbonated cement; B = partially carbonated cement; C = residual weakly carbonated cement core; F1 = main carbonation reaction front; F2 = diffuse inner reaction front; Fx = position of old reaction fronts; x = shrinkage cracks developed perpendicular to main carbonation front Top right: BSEM image detail of reaction front between fully carbonated cement zone (top) and partially carbonated cement. Bottom: EDXA distribution maps for Ca and Cl corresponding to same area as in BSEM image (qualitative colour scale: red = high concentration; black = low concentration).

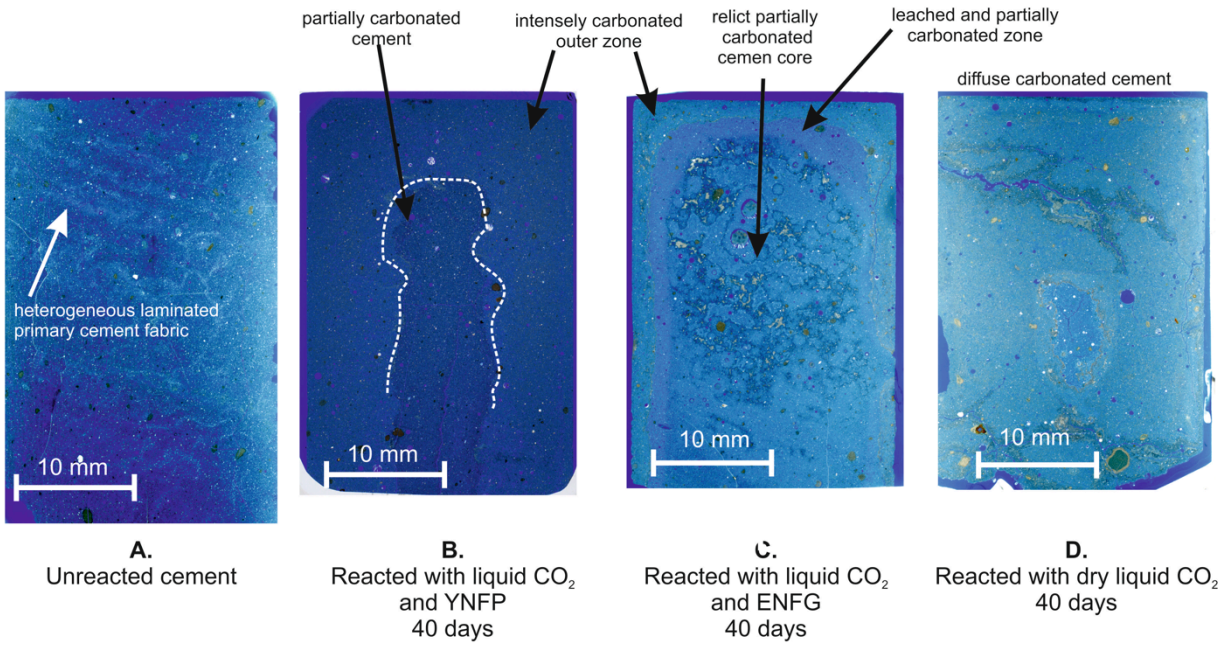

Plate 28. Comparison of transmitted light images of polished thin sections through cores of (A) unreacted NRVB and NRVB; (B) reacted with YNFP in the presence of liquid CO_2; (C) ENFG in the presence of liquid CO_2; and (D) dry supercritical CO_2 at 20°C, 80 bar for 40 days (upper images) and 1 year (lower images). Top and sides of each image represents the outer edges of the cement cores. The position of the main reaction (carbonation) fronts are shown by dashed lines.

The alteration by dry liquid CO_2 is similar to that observed with dry supercritical CO_2. It did not produce a discrete reaction front. The experiment resulted in diffuse alteration to a highly-carbonated cement comprising a mixture of very fine grained calcium carbonate and secondary silica-rich material, and with finely disseminated iron oxide is produced (Plate 22). Within this fine-grained highly-carbonated matrix, irregular relicts of unreacted cement paste may be present. These unreacted relicts are heterogeneously distributed, and reflect the original heterogeneous character of the original fabric of the cement paste.

In thin section the petrographic fabrics of the alteration in the presence of the YNPF and ENFG aqueous fluids are very similar to those observed with supercritical CO_2 and gaseous CO_2. The alteration is characterised by the development of a 'chicken-wire-like' network fabric of anastomosing calcium carbonated sealed microfractures. However, the replacement of the carbonated cement paste by calcium carbonate was seen to be notably more intense with ENFG as the aqueous phase (Plate 29). The carbonated matrix of the cement is replaced by an intimate mixture of amorphous silica-rich material with finely dispersed nano- to micro-crystalline calcium carbonate. Many of the air bubbles that were entrained in the original cement paste are open and unminerlised, even in the intensely carbonated outer regions of the cement plugs (Plate 29)

The main reaction front is defined by a narrow sharp front of microcrystalline calcium carbonate (probably calcite). However, in the experiment with ENPF fine fibrous needles of calcium carbonate – probably aragonite (based on morphological considerations) – is formed. This was not seen in the other experiments.

As with the experiments with supercritical CO_2 and gaseous CO_2, BSEM-EDXA observations indicate that Cl may be concentrated immediately ahead of the main reaction front in the 'ENFG + liquid CO_2' experiment. However, no discrete Cl-bearing phase could be differentiated.

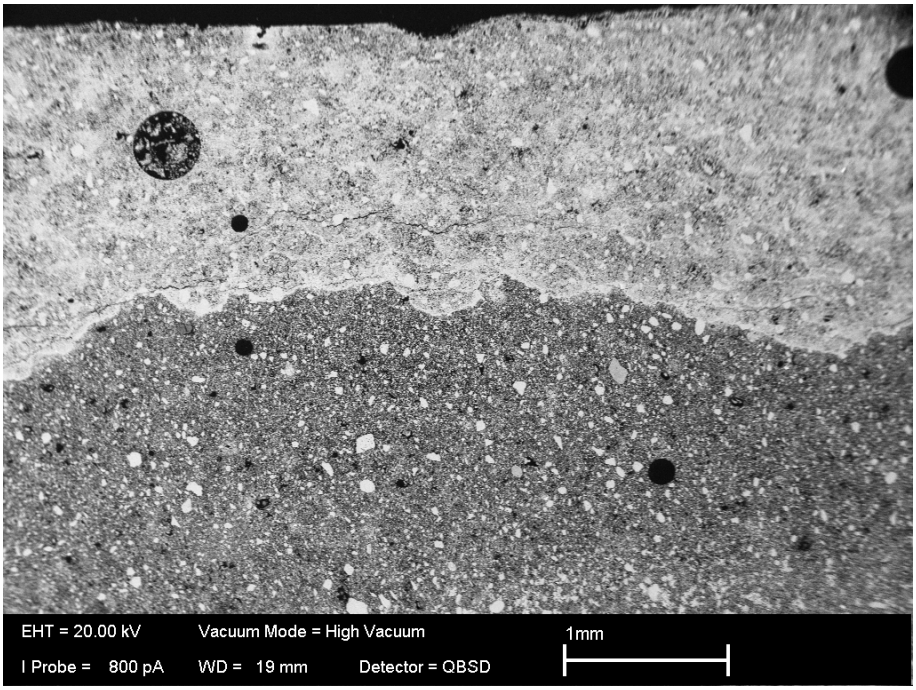

Plate 29. BSEM photomicrograph showing the very sharply-defined main carbonation reaction front demarcating the inner region of partially-carbonated cement (dull grey) from the outer reaction zone of intensely carbonated cement (light grey). The reaction front is defined by a narrow zone of intense precipitation of dense microcrystalline calcite (see Plate 30), with a sharp ragged leading edge, and a more diffuse tail. 'ENFG + liquid CO_2', 40 days at 20°C under 80 bar pressure experiment.

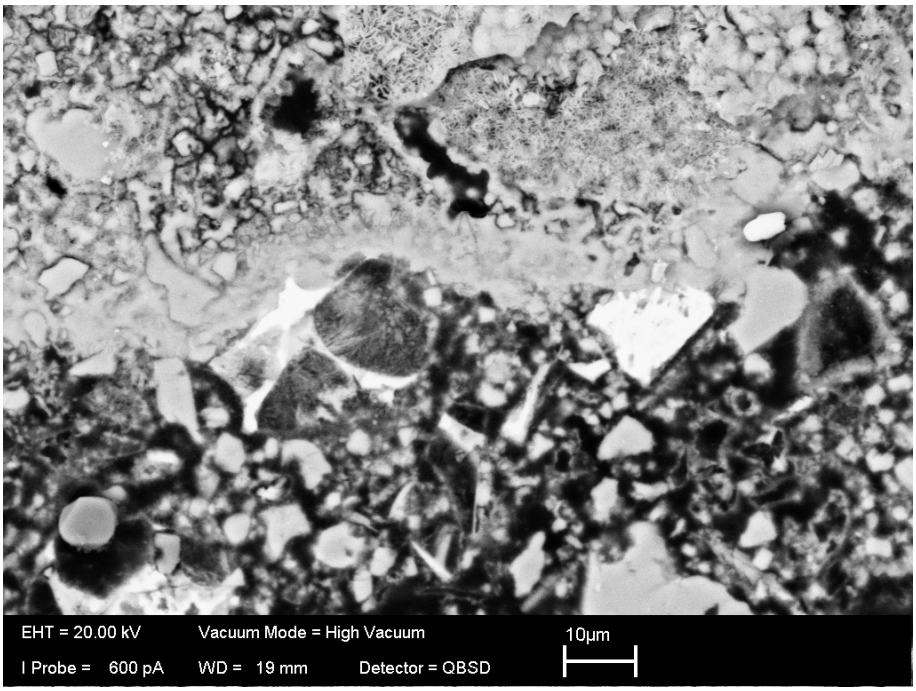

Plate 30. BSEM photomicrograph showing detail of the very sharply-defined main carbonation reaction front. The reaction front is defined by a narrow zone of intense precipitation of dense microcrystalline calcite with fibrous calcium carbonate (possible aragonite) precipitated in the intensely carbonated cement behind the reaction front. 'ENFG + liquid CO_2', 40 days at 20°C under 80 bar pressure experiment.

8. Implications for repository performance

Information in the proceeding sections allowed identification and quantification of processes occurring during cement carbonation, and this will help inform predictive modelling of repository evolution. The buffer/backfill cement appears to have coped with carbonation well, generally remaining intact, with samples showing no evidence of overall shrinkage or swelling.

Carbonation was identifiable by a colour change of the cement samples (dark grey to light brown), and this progressed from the outside of the samples towards their centres. Carbonation was rapid, especially early in the experiments, with some samples showing at least partial carbonation through to the centres of the samples (12.5 mm minimum travel distance) within 40 days. Most of the carbonation observed was relatively uniform on greater than mm scales. However, a small number of (mainly diffusion) samples showed some evidence for carbonation along specific zones. This may have been aided in certain cases by heterogeneities within the samples. These appear to have been caused by segregation of cement grains during casting/setting. The coarser layers had their pore space filled with $Ca(OH)_2$ and this was more susceptible to carbonation than the finer-grained CSH phases. Similar features could form in a repository setting, and could provide preferential routes for CO_2 migration if they occurred on a large scale. Such cement heterogeneity could be minimised through the use of organic additives (superplasticisers) to enhance cement flow behaviour. However, Francis *et al.* (1997) and Young *et al.*, (2013) note that the presence of such organics may enhance the mobility of some radionuclides. Without them however, some degree of grain segregation and hetergoenious carbonation may be a feature within a repository. It will be important therefore, to consider carefully the pros and cons of adding additives to repository buffer/backfill cement.

In terms of bulk samples, carbonation was not associated with a sample volume change that meant that overall NRVB density increased. In detail however, this density change was not uniform. At microscopic scales carbonation resulted in a patchwork of low-density domains composed mainly of silica gel enclosed by higher density zones of secondary carbonate. The low-density domains had higher porosity, and the higher density zones had lower porosity. These higher density zones may have formed as the carbonation front moved through the sample, with initial local microcracking that was subsequently infilled by carbonate precipitation. Potentially, the many thin 'walls' of carbonate precipitate might reduce sample permeability (see Purser *et al.*, 2013; Rochelle *et al.*, 2013). Reductions in permeability could be beneficial in terms of containment, as they would act to limit radionuclide migration. At a somewhat larger (millimetric) scale, there was some evidence that unconfined samples could develop stress cracking in the partly-carbonated cement close to the carbonation reaction fronts, though these features were very localised and could be filled by secondary carbonates as the reaction fronts moved through the sample. It is possible however, that there might be a dynamic zone of increased permeability that moves just ahead of the main carbonation front.

Carbonation resulted in a reaction zone several mm wide, within which were several reaction fronts delineating 4 main reaction zones. These were:

Zone 1: Unreacted cement

Zone 2: Partially carbonated cement

Zone 3: Fully carbonated cement

Zone 4: Leached cement (where slightly acidic CO_2-rich water had re-dissolved some of the secondary carbonate).

The visually most apparent reaction front occurred between Zones 2 and 3. Note that Zone 4 probably formed relatively early in the experiment when waters surrounding the NRVB samples were not fully saturated with carbonate minerals, and as such may not occur in a repository

setting. It is apparent however, that multiple reaction zones are likely to form within a repository setting as a consequence of carbonation.

Carbonation resulted in the degradation of the high pH buffering capacity of the NRVB cement. Given that many metallic radionuclides have low solubility under alkaline conditions, but increased solubility as pH decreases, carbonation may potentially lead to increased metal corrosion rates and consequent increased potential for radionuclide migration. That said, if as seems likely, the repository contained an excess of cement that was more than sufficient to react with all the produced CO_2, overall pH buffering to alkaline conditions could still be effective for many parts of the repository. Whilst we did not measure the porewater pH in the fronts directly, their presence can be determined by the abrupt nature of the reactions fronts and removal of portlandite and CSH phases due to the migration of lower pH conditions associated with the CO_2.

In the experiments carbonation and uptake of CO_2 increased the weight of the cement by up to 8.5%. This has two potential benefits:

1) Reduction in potential for pressure increases due to gas production due to consumption of CO_2.
2) As some wastes contain ^{14}C, it provides a mechanism for released $^{14}CO_2$ to be immobilised in secondary carbonate minerals.

One less expected observation concerning solute migration was the enhanced localised uptake of dissolved chloride (Cl^-) by the cement. ^{36}Cl presents particular issues within repositories, due to its long half-life, ease of uptake into biological systems, and relative mobility in many settings. Uptake of Cl^- was most clearly revealed by significant decreases in dissolved Cl^- in the experiments using more 'evolved' porewater compositions (i.e. porewaters reflecting interaction between saline groundwater and the cement) (see Figure 13).

Many of the experiments showed decreases in dissolved Cl^-, not just those pressurised with CO_2. The NRVB cement appeared to be immobilising Cl^-, especially at lower temperatures (in this study 20°C) where Cl^- uptake was especially favoured. Smaller, but still significant, amounts of additional Cl^- were taken up in equivalent experiments pressurised with CO_2. The additional stability provided by the presence of CO_2 possibly suggests that it may exist as part of a solid-solution series with Cl- and CO_3-endmembers.

Detailed mineralogical observations in the region around carbonation fronts revealed the presence of small amounts of two fine-grained, Cl-rich solid phases. One was a gel-like Cl-rich CSH, the other was only found in the 20°C experiments and occurred as fine-grained radial fibrous crystal aggregates of a calcium chloroaluminate phase, probably hydrocalumite ($Ca_4Al_2O_6Cl_2.10H_2O$) (Rochelle *et al.*, 2013; Milodowski *et al.*, 2013) (Figure 16).

Element mapping clearly showed that these Cl-rich phases were found on the largely unreacted cement-side of the reaction front (Figure 17). It would appear that they are only stable under higher pH conditions (i.e. where CSH phases were still present). It is thought that they have progressively broken down as the carbonation reactions progressively consume the CSH around them. The released Cl^- then diffused towards the remaining CSH and re-precipitated. This dissolution/precipitation process would continue until all of the CSH is reacted (in the case of a limited quantity of cement), at which point the Cl^- would be released back into solution.

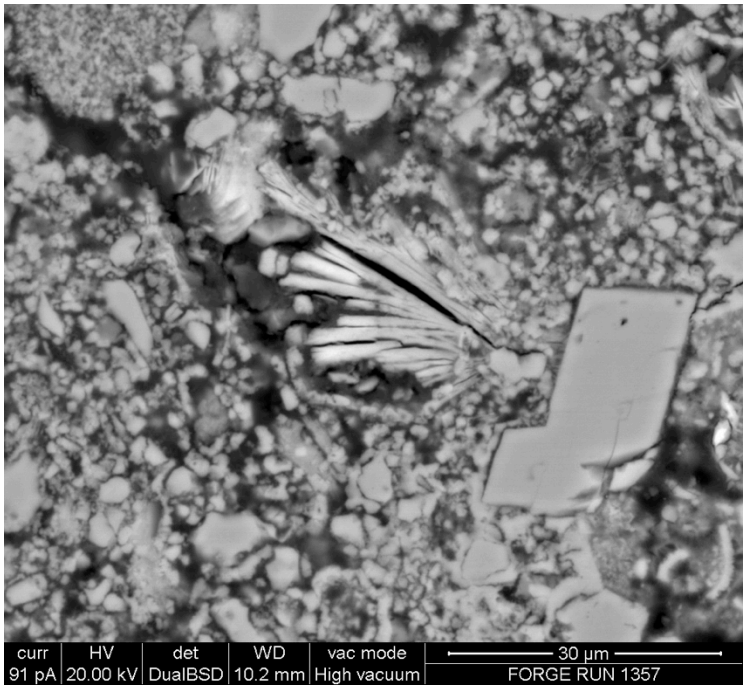

Figure 16. BSEM photomicrograph of radial fibrous secondary calcium chloroaluminate phase. This formed within altered cement just behind the leading edge of the carbonation front.

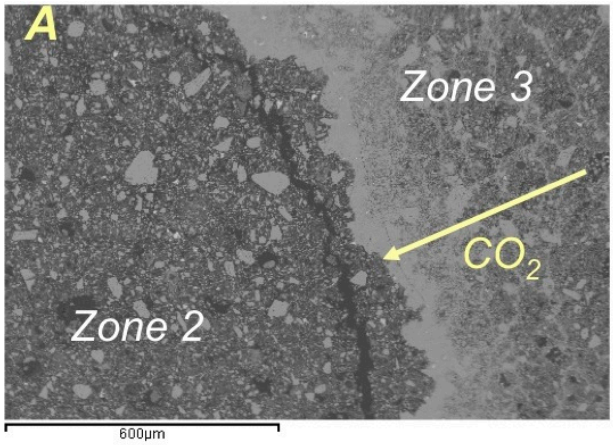

A) Backscattered SEM image of main carbonation reaction front.

B) Map of Ca abundance (high Ca = pink). Note the high abundance at the carbonation front, and also the limestone grains in cement.

C) Map of Cl abundance (High Cl = green). Note its abundance at the edge of Zone 2, just in advance of the main carbonation front.

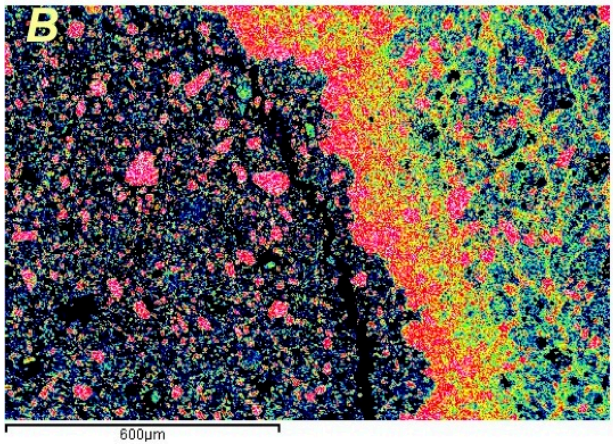

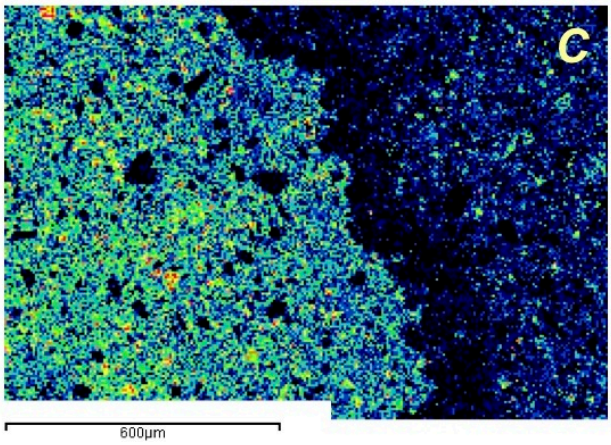

Figure 17. High resolution images of a cement carbonation front. Note the abundance of Cl on the partly-carbonated side of the reaction front, and its near absence in the fully-carbonated cement.

The uptake of Cl^- in CO_2-free cement systems concurs with observations undertaken as part of previous experimental buffer/backfill cement studies (Glasser *et al.*, 1998). Cl^- uptake in CO_2-rich systems has also been previously noted as part of borehole stability studies for the deep underground storage of CO_2. Rochelle *et al.* (2006, 2009) found increased Cl^- uptake in CO_2-rich experiments compared to CO_2-free experiments, and Carey *et al.* (2007) report a Cl-rich secondary phase in recovered samples of borehole cement that had been exposed to CO_2-rich fluids for 30 years.

The apparent likely occurrence of Cl-rich phases within cementitious repositories, raises the question of whether performance assessment calculations could include them (many current approaches assume conservative, i.e. non-reacting, behaviour of Cl^-). Inclusion of such phases would likely retard the overall predicted migration of ^{36}Cl, lowering eventual releases to the biosphere, and hence improving safety calculations. Equally, they may allow for higher initial loadings of ^{36}Cl in the waste. It would be useful to investigate these Cl-rich phases further.

Carbonation features and secondary phases observed in these experiments using a relatively porous/permeable cement, bear many similarities to those found in far lower porosity/permeability borehole cements used in CO_2-storage operations (e.g. Rochelle and Milodowski, 2013). There are also similarities to samples of naturally-occurring CSH phases which have been naturally-carbonated over prolonged timescales (Milodowski *et al.*, 1989, 2009, 2011). A number of common carbonation processes may be operating in all these systems, and consideration of all these sources of information is needed to help provide an overall picture of cement carbonation over a range of temporal and spatial scales.

9. Conclusions

Thirty-two static batch experiments were pressurised with either CO_2, or with N_2 for 'non-reacting' comparison tests at 20°C or 40°C, and 40 or 80 bar. The aim of them was to help investigate mineralogical and fluid chemical changes due to the diffusional ingress of CO_2 into unconfined samples of Nirex Reference Vault Backfill measuring 2.5 cm in diameter and 5 cm long.

The cement blocks remained intact, even after prolonged exposure to CO_2-rich fluids. Carbonation was associated with an increase in weight of up to 8.5% during CO_2 uptake, though the samples did not change in overall size. Free phase CO_2 gave slightly more reaction than dissolved CO_2, possibly because of its higher concentration and greater ability to penetrate the samples. In terms of major reactions during carbonation, these were the breakdown of portlandite and calcium silicate hydrate (CSH) phases and the formation of carbonate phases (calcite, aragonite and vaterite) and silica gel. All the cement samples showed rapid reaction with CO_2, manifested by a colour change from grey to light brown due to the formation of finely-disseminated free ferric oxide (probably hematite, Fe_2O_3). Carbonation features and secondary phases observed in these experiments using a relatively porous/permeable cement, bear many similarities to those found in far lower porosity/permeability borehole cements used in CO_2-storage operations. There are also similarities to samples of naturally-occurring CSH phases which have been naturally-carbonated over prolonged timescales. Petrographic analyses also revealed that some heterogeneities were generated within the cement samples as a result of cement plug casting, leading to heterogeneous reaction and faster carbonation in some parts of the cement samples. Such features may be present within a repository, and should be taken into account when assessing repository performance.

Carbonation resulted in a series of reaction fronts that moved through the cement over time. These fronts separated several reaction zones: Zone 1 = minor carbonation with minimal apparent volume change, Zone 2 = partial carbonation and very localised shrinkage, Zone 3 = complete conversion of portlandite and CSH with localised shrinkage associated with the

development of calcium carbonate-sealed microfractures, Zone 4 = dissolution of initially-formed carbonate minerals in the outermost parts of the sample by the surrounding, slightly-acidic water. The shrinkage in Zone 2 was expressed as small fractures (typically several mm long), though these do not appear to extend beyond this zone. Zone 3 contained an anastomising '3D chickenwire' meshwork of interconnected, higher-density, carbonate-filled microfractures (typically on a 10s-100s μm scale) that separated silica-rich areas having lower-density and high porosity, and sub-parallel 'relic' reaction fronts. The small fractures of Zone 2 appear to have filled with secondary precipitates in Zone 3. It would be useful to understand how these reaction zones evolve over longer timescales, and investigate whether they have the potential to become narrower (or even merge together), with more efficient sealing of porosity that might 'armour' the cement from further carbonation.

In terms of radionuclide immobilisation, a mixed picture was found. Cement carbonation led to loss of high pH buffering, and as a consequence might be expected to enhance solubility of metallic radionuclides. Conversely, precipitation of $CaCO_3$ and densification of the cement would be expected to reduce permeability and lower the potential for radionuclide mobility. In terms of specific radionuclides, carbonation would immobilise $^{14}CO_2$ if that were present. The formation of Cl-rich phases within the cement could be beneficial as it might help to immobilise ^{36}Cl leaching from the waste.

The study highlighted several areas where further investigations could be useful. These include:

- Assessing the likelihood for compositional heterogeneity within the cement as a consequence of settling during and after pouring.
- Quantifying the longevity of the reaction zones identified, and whether they evolve into a single reaction front over long timescales.
- Better defining the likelihood of cement micro-fracturing during carbonation, mechanisms controlling the formation of narrow carbonate precipitation zones, and their impact on permeability.
- Quantifying how efficient secondary phases are at 'armouring' cement from further carbonation, and how the permeability of this carbonated zone changes over time.
- Precise identification of the Cl-rich phases forming within the altered cement, and consideration of the impact such phases could have on ^{36}Cl retardation and repository safety functions.

Carbonation features and secondary phases observed in these experiments using a relatively porous/permeable cement, bear many similarities to those found in far lower porosity/permeability borehole cements used in CO_2-storage operations. There are also similarities to samples of naturally-occurring CSH phases which have been naturally-carbonated over prolonged timescales. A number of common carbonation processes may be operating in all these systems, and consideration of all these sources of information is needed to help provide an overall picture of cement carbonation over a range of temporal and spatial scales.

10. Acknowledgements

The research leading to these results has received funding from the European Atomic Energy Community's Seventh Framework Programme (FP7/2007-2011) under Grant Agreement no. 230357, the FORGE project.

The Nuclear Decommissioning Authority (NDA) are also thanked for funding that has helped support the research that led to the results presented here.

References

ALLEN, J.R.L. 1982. *Sedimentary Structures, Their Character and Physical Basis*. Vol. 2.: Elsevier Scientific Publications, Amsterdam.

BOND, K.A., MORETON, A.D. AND TWEED, C.J. 1995. Water compositions of relevance to a deep cementitious-based repository at Sellafield: Evaluation using thermodynamic modelling, Nirex Report NSS/R310, 25p.

BOND, K.A. AND TWEED, C.J. (1995). Groundwater compositions for the Borrowdale Volcanic Group, Boreholes 2, 4 and RCF3, Sellafield, evaluated using thermodynamic modelling, Nirex Report NSS/R397, 34p.

CAREY, J.W., WIGAND, M., CHIPERA, S.J., WOLDEGABRIEL, G., PAWAR, R., LICHTNER, P.C., WEHNER, S.C., RAINES, M.A. AND GUTHRIE, J. 2007. Analysis and performance of oil well cement with 30 years of CO_2 exposure from the SACROC Unit, West Texas, USA. *International Journal of Greenhouse Gas Control*, 1, 75-85.

CZERNICHOWSKI-LAURIOL, I., SANJUAN, B., ROCHELLE, C., BATEMAN, K., PEARCE, J. AND BLACKWELL, P. 1996. Area 5: Inorganic Geochemistry, Chapter 7 in 'The underground disposal of carbon dioxide' (S. Holloway ed.). Final report for the CEC, contract number JOU2-CT92-0031. Published by the British Geological Survey.

ELLIS, A.J. ~~AND~~ GOLDING, R.M. 1963. The solubility of carbon dioxide above 100°C in water and in sodium chloride solutions. *American Journal of Science*, 261, 47-60.

FRANCIS, A.J., CATHER, R. AND CROSSLAND, I.G. 1997. Development of the Nirex reference vault backfill; report on current status in 1994. Nirex Science Report S/97/014, United Kingdon Nirex Limited, 57p.

GLASSER, F.P., TYRER, M., QUILLIN, K., ROSS, D., PEDERSEN, J., GOLDTHORPE, K., BENNETT, D. AND ATKINS, M. 1998. The chemistry of blended cements and backfills intended for use in radioactive waste disposal. United Kingdom Environment Agency R&D Technical Report P98, ISBN: 1857 05 157 2, 332pp.

GOLDSTEIN, J.I., NEWBURY, D.E., ECHLIN, P., JOY, D.C., FIORI, C. AND LIFSHIN, E. 1981. *Scanning Electron Microscopy and X-Ray Microanalysis*. Plenum Press, New York, 673pp.

GUNTER, W.D., PERKINS, E.H., BACHU, S., LAW, D., WIWCHAR, B., ZHOU, Z. AND MCCANN, T.J., 1993. Aquifer disposal of CO_2-rich gases. Alberta Research Council report, C-1993-5.

MILLS, P.C. 1983. Genesis and diagnostic value of soft-sediment deformation structures – a review. *Sedimentary Geology,* 35, 83-104.

MILODOWSKI, A.E., LACINSKA, A. AND WAGNER, D. 2009. JRAP-14: Reactions between CO_2 and borehole infrastructure. Deliverable JRAP-14/2: A natural analogue study of CO_2-cement interaction: Carbonate alteration of calcium silicate hydrate-bearing rocks from Northern Ireland. European Commission FP6 Project Number SES6-CT-2004-502816, Network of Excellence on Geological Storage of CO_2 (CO_2GeoNet), 28pp.

MILODOWSKI, A.E., NANCARROW, P.H.A. AND SPIRO, B. 1989. A mineralogical and stable isotope study of natural analogues of Ordinary Portland Cement (OPC) and Cao-SiO_2-H_2O (CSH) compounds. United Kingdom Nirex Safety Studies Report, NSS/R240.

MILODOWSKI, A.E., ROCHELLE, C.A., LACINSKA, A. AND WAGNER, D. 2011. A natural analogue study of CO_2-cement interaction: Carbonation of calcium silicate hydrate-bearing rocks from Northern Ireland. *Energy Procedia,* 4, 5235-5242.

MILODOWSKI, A.E., ROCHELLE, C.A. AND PURSER, G. 2013. Uptake and retardation of Cl during cement carbonation. *Procedia Earth and Planetary Science*, 7, 594-597.

PURSER, G., MILODOWSKI, A.E., HARRINGTON, J.F., ROCHELLE, C.A. BUTCHER, A. and Wagner, D. 2013. Modification to the flow properties of repository cement as a result of carbonation. *Procedia Earth and Planetary Science*, 7, 701-704.

REARDON, E.J., JAMES, B.R. AND ABOUCHAR, J., 1989. High pressure carbonation of cementitious grout. Cement and Concrete Research, 19, 385-399.

ROCHELLE, C.A., BATEMAN, K., COOMBS, P., PEARCE, J.M. AND WETTON, P.D. 1994. The evaluation of chemical mass transfer in the disturbed zone of a deep geological disposal facility for radioactive wastes. IX. Further reactions involving discs of Borrowdale Volcanic Group lithologies with synthetic evolved near-field groundwater. British Geological Survey Technical Report WE/94/44, 30p.

ROCHELLE, C.A., BATEMAN, K., COOMBS, P., PEARCE, J.M. AND WETTON, P.D. 1998. The evaluation of chemical mass transfer in the disturbed zone of a deep geological disposal facility for radioactive wastes. VIII. Further reactions involving powdered Borrowdale Volcanic Group lithologies with synthetic evolved near-field groundwater. Nirex Report NSS/R393, 33p.

ROCHELLE, C.A., BATEMAN, K., MACGREGOR, R., PEARCE, J.M., PRIOR, S.V., SAVAGE, D. AND WETTON, P.D. 1998. The evaluation of chemical mass transfer in the disturbed zone of a deep geological disposal facility for radioactive wastes. VI. The hydrothermal aging of discs of bulk rock and near-fracture Borrowdale Volcanic Group lithologies with a synthetic evolved near-field groundwater. Nirex Report NSS/R390, 34p, 1998.

ROCHELLE, C.A., BATEMAN, K., MACGREGOR, R., PEARCE, J.M., SAVAGE, D. AND WETTON, P.D. 1998. The evaluation of chemical mass transfer in the disturbed zone of a deep geological disposal facility for radioactive wastes. V. Reaction of powdered Borrowdale Volcanic Group lithologies with synthetic evolved near-field groundwater. Nirex Report NSS/R382, 24p.

ROCHELLE, C.A., BATEMAN, K., MILODOWSKI, A.E., KEMP, S.J. AND BIRCHALL, D. 2006. Geochemical interactions between CO_2 and seals above the Utsira Formation: An experimental study. British Geological Survey Commissioned Report, CR/06/069. 86 pp.

ROCHELLE, C.A. AND MILODOWSKI, A.E. 2013. Carbonation of borehole seals: comparing evidence from short-term lab experiments and long-term natural analogues. *Applied Geochemistry*, 30, 161-177.

ROCHELLE, C.A., MILODOWSKI, A.E., LACINSKA, A., RICHARDSON, C., SHAW, R., TAYLOR, H., WAGNER, D., BATEMAN, K., LÉCOLIER, E., FERRER, N., LAMY, F., JACQUEMET, N., SHI, JI-Q., DURUCAN, S. AND SYED, A.S. 2009. JRAP-14: Reactions between CO_2 and borehole infrastructure, report on laboratory experiments and modelling. CO_2GeoNet project report for the European Commission, deliverable JRAP-14/3, 138p.

ROCHELLE, C.A., MILODOWSKI, A.E., SHI, J-Q., MUNOZ-MENDEZ, G., JACQUEMET, N. AND LECOLIER, E. 2007. A review of the potential impact of CO_2 on the integrity of well infrastructure for underground CO_2 storage. British Geological Survey Commissioned Report, CR/07/204, 83p.

ROCHELLE, C.A., PEARCE, J.M., BATEMAN, K., BIRCHALL, D.J., CHARLTON, B.D., REEDER, S., SHAW, R.A., TAYLOR, H. AND TURNER, G. 2004. Geochemical interactions between supercritical CO_2 and borehole cements used at the Weyburn oilfield. British Geological Survey Commissioned Report, CR/04/009, 22 p.

ROCHELLE, C.A., PEARCE, J.M., BATEMAN, K., COOMBS, P. AND WETTON, P.D. 1997. The evaluation of chemical mass transfer in the disturbed zone of a deep geological disposal facility for radioactive wastes. X. Interaction between synthetic cement porefluids and BVG: Observations from experiments of 4, 9 and 15 months duration. British Geological Survey Technical Report, WE/97/16C, 79p.

ROCHELLE, C.A., PURSER, G., MILODOWSKI, A.E., NOY, D.J., WAGNER, D., BUTCHER, A. AND HARRINGTON, J.F. 2013. CO_2 migration and reaction in cementitious repositories: A summary of work conducted as part of the FORGE project. British Geological Survey Open Report, OR/13/004, 30pp.

SAVAGE, D., BATEMAN, K, HILL, P., HUGHES, C., MILODOWSKI, A., PEARCE, J., RAE, E. AND ROCHELLE, C. 1992. Rate and mechanism of the reaction of silicates with cement pore fluids. *Applied Clay Science*, 7, p 33-45

SCHREMP, F.W. AND ROBERSON, G.R. 1975. Effect of supercritical carbon dioxide (CO_2) on construction materials. *Soc. of Petroleum Engineers Journal*, June edition, p. 227-233.

STEWART, P.B. AND MUNJAL, P.K. 1970. The solubility of carbon dioxide in pure water, synthetic sea water and synthetic sea-water concentrates at –5 to 25°C and 10 to 45 atm pressure. *Journal of Chemical Engineering Data*, 15(1), 67-71.

TOEWS, K.L., SHROLL, R.M. AND WAI, C.M. 1995. pH-defining equilibrium between water and supercritical CO_2. Influence on SFE of organics and metal chelates. *Analytical Chemistry*, 67, 4040-4043.

YOUNG, A.J., WARWICK, P., MILODOWSKI, A.E. AND READ, D. 2013. Behaviour of radionuclides in the presence of superplasticiser. *Advances in Cement Research*, 25, 32-43 [DOI: 10.1680/adcr.12.00032].

Appendix 1

The following pages contain information about, and data from the 40 day long batch experiments.

Part A: Experiments run at 20°C and 80 bar.

Digestion vessel experiments to react Nirex Reference Vault Backfill (NRVB) with synthetic cement pore fluids ± CO_2
40 day long experiments at 20°C and 80 bar

	Starting solutions		CO_2 experiments			N_2 experiments		
	Young fluid	Evolved fluid	Young fluid	Evolved fluid	Dry	Young fluid	Evolved fluid	Dry
Start date	-	-	1/8/10 16:00	8/1/10 16:00	8/1/10 16:00	8/1/10 16:00	8/1/10 16:00	8/1/10 16:00
End date	-	-	17/2/10 08:25	17/2/10 18:20	17/2/10 16:00	17/2/10 08:15	17/2/10 18:10	17/2/10 16:00
Time (days)	0	0	40	40	40	40	40	40
Run temperature	-	-	20	20	20	20	20	20
Run pressure	-	-	80	80	80	80	80	80
Run number	-	-	**1364**	**1362**	**1360**	**1365**	**1363**	**1361**
Vessel number	-	-	BGS048	BGS047	BGS022	BGS056	BGS049	BGS029
Experimental charge	-	-	NRVB	NRVB	NRVB	NRVB	NRVB	NRVB
Cement core number	-	-	2I	2H	2G	2L	2K	2J
Weight of cement core before	-	-	40.466	40.415	39.9855	40.2322	40.2544	40.4071
Weight of cement core after	-	-	42.5902	41.8581	No weight available	40.6207	41.0836	39.1821
Weight difference of cement core	-	-	2.1242	1.4431	-	0.3885	0.8292	-1.225
Fluid type	YNFP 1 starting solution	ENFG starting solution	YNFP 1	ENFG	-	YNFP 1	ENFG	-
Initial weight of fluid	-	-	231.234	230.943	N/A	229.898	230.025	N/A
BGS fluid LIMS code	12389-0002	12389-0001	12389-0015	12389-0013	-	12389-0016	12389-0014	-
Comments	Filtered to 0.2 μm	Filtered to 0.2 μm	Filtered to 0.2 μm	Filtered to 0.2 μm	-	Filtered to 0.2 μm	Filtered to 0.2 μm	-
pH at 20 °C	12.06	12.05	6.71	6.55	-	12.69	12.87	-
Sample Code	YNFP 1 Starting fluid	ENFG Starting fluid	1364/1	1362/1	-	1365/1	1363/1	-
TDS	-	-	-	-	-	-	-	-
Ca^{2+} (mg l^{-1})	40.4	2087	1589	2734	-	70.8	2142	-
Mg^{2+} (mg l^{-1})	<1.93	<1.92	311	284	-	<1.89	<1.89	-
Na^{+} (mg l^{-1})	2674	9445	1777	11899	-	2250	10090	-
K^{+} (mg l^{-1})	4316	314	2840	354	-	3215	259	-
OH^{-} (mg l^{-1})			-	-	-	-	-	-
CO_3^{2-} (mg l^{-1})			-	-	-	422.0	813.0	-
HCO_3^{-} (mg l^{-1})			1923	2059.0	-	-323.000	-802.000	-
Total Alk (mg l^{-1})			-	-	-	-	-	-
Cl^{-} (mg l^{-1})	5797	16391	966.5	3182.3	-	1495.2	3773.1	-
SO_4^{2-} (mg l^{-1})	<24.1	927	14.5	165.9	-	3.96	72.7	-
NO_3^{-} (mg l^{-1})	9.93	19.1	0.369	0.535	-	0.516	0.770	-
Cat1 meq l^{-1}	228.7	523.0	254.8	686.4	-	183.6	552.4	-
Cat2 meq l^{-1}	0.000	0.558	0.000	0.474	-	0.000	0.600	-
Ani1 meq l^{-1}	163.7	482.0	#N/A	#N/A	-	#N/A	#N/A	-
Ani2 meq l^{-1}	0.000	0.378	#N/A	#N/A	-	#N/A	#N/A	-
AniTIC meq l^{-1}	163.7	482.0	#N/A	#N/A	-	#N/A	#N/A	-
Cation Total meq l^{-1}	228.7	523.6	254.8	686.9	-	183.6	553.0	-
Anion Total meq l^{-1}	163.7	482.4	#N/A	#N/A	-	#N/A	#N/A	-
Balance %	16.57	4.09	#N/A	#N/A	-	#N/A	#N/A	-
S Balance	-	-	-	-	-	-	-	-
TIC Balance	-	-	-	-	-	-	-	-
Br^{-} (mg l^{-1})	<9.65	30.2	ND	6.06	-	3.23	7.55	-
NO_2^{-} (mg l^{-1})	<4.82	<4.76	#N/A	#N/A	-	#N/A	#N/A	-
HPO_4^{2-} (mg l^{-1})	<48.2	<47.6	#N/A	#N/A	-	#N/A	#N/A	-
F^{-} (mg l^{-1})	<4.82	<4.76	#N/A	#N/A	-	#N/A	#N/A	-
Total P (mg l^{-1})	<1.93	<1.92	<1.93	<1.89	-	<1.89	<1.89	-
Total S (mg l^{-1})	<48.2	362	<48.2	357	-	<47.3	135	-
S Diff %	83.32	14.50	#N/A	#N/A	-	#N/A	#N/A	-
Si (mg l^{-1})	35.8	<14.4	35.3	44.7	-	36.2	<14.2	-
SiO_2 (mg l^{-1})	76.5	<30.8	75.5	95.6	-	77.5	<30.4	-
Ba (mg l^{-1})	<0.386	<0.384	<0.385	<0.377	-	<0.378	1.15	-
Sr (mg l^{-1})	<0.965	24.5	<0.963	20.8	-	<0.946	25.6	-
Mn (mg l^{-1})	<0.386	<0.384	<0.385	<0.377	-	<0.378	<0.379	-
Total Fe (mg l^{-1})	<1.93	<1.92	<1.93	<1.89	-	<1.89	<1.89	-
Oxidised Fe (mg l^{-1})	<1.93	<1.92	<1.93	<1.89	-	<1.89	<1.89	-
Al (mg l^{-1})	<1.93	<1.92	<1.93	<1.89	-	<1.89	<1.89	-
Co (mg l^{-1})	<0.386	<0.384	<0.385	<0.377	-	<0.378	<0.379	-
Ni (mg l^{-1})	<0.965	<0.960	<0.963	<0.943	-	<0.946	<0.947	-
Cu (mg l^{-1})	<0.965	<0.960	<0.963	<0.943	-	<0.946	<0.947	-
Zn (mg l^{-1})	<0.965	<0.960	<0.963	<0.943	-	<0.946	<0.947	-
Cr (mg l^{-1})	<0.386	<0.384	0.548	0.587	-	<0.378	1.23	-
Mo (mg l^{-1})	<2.89	<2.88	<2.89	<2.83	-	<2.84	<2.84	-
Cd (mg l^{-1})	<0.386	<0.384	<0.385	<0.377	-	<0.378	<0.379	-
Pb (mg l^{-1})	<1.93	<1.92	<1.93	<1.89	-	<1.89	<1.89	-
V (mg l^{-1})	<1.93	<1.92	<1.93	<1.89	-	<1.89	<1.89	-
Li (mg l^{-1})	<4.82	<4.80	<4.82	<4.71	-	<4.73	<4.73	-
B (mg l^{-1})	<4.82	<4.80	<4.82	<4.71	-	<4.73	<4.73	-
As (mg l^{-1})	<2.89	<2.88	<2.89	<2.83	-	<2.84	<2.84	-
Se (mg l^{-1})	<4.82	<4.80	<4.82	<4.71	-	<4.73	<4.73	-

Part B: Experiments run at 40°C and 40 bar.

Digestion vessel experiments to react Nirex Reference Vault Backfill (NRVB) with synthetic cement pore fluids ± CO_2
40 day long experiments at 40°C and 40 bar

	Starting solutions		CO_2 experiments			N_2 experiments		
	Young fluid	Evolved fluid	Young fluid	Evolved fluid	Dry	Young fluid	Evolved fluid	Dry
Start date	-	-	2/10/09 15:00	2/10/09 15:00	2/10/09 15:00	2/10/09 15:00	2/10/09 15:00	2/10/09 15:00
End date	-	-	10/11/09 10:30	10/11/09 10:45	10/11/09 11:00	10/11/09 16:05	10/11/09 16:00	10/11/09 16:10
Time (days)	0	0	40	40	40	40	40	40
Run temperature	-	-	40	40	40	40	40	40
Run pressure	-	-	40	40	40	40	40	40
Run number	-	-	**1353**	**1357**	**1355**	**1352**	**1356**	**1354**
Vessel number	-	-	BGS047	BGS048	BGS022	BGS049	BGS050	BGS029
Experimental charge	-	-	NRVB	NRVB	NRVB	NRVB	NRVB	NRVB
Cement core number	-	-	2A	2C	2B	2D	2F	2E
Weight of cement core before	-	-	40.5500	40.6665	40.4661	40.6397	40.8163	40.4923
Weight of cement core after	-	-	41.5868	41.7148	43.7841	40.3360	41.0549	39.5256
Weight difference of cement core	-	-	1.0368	1.0483	3.3180	-0.3037	0.2386	-0.9667
Fluid type	YNFP starting solution	ENFG starting solution	YNFP	ENFG	-	YNFP	ENFG	-
Initial weight of fluid	-	-	231.7	231.2	N/A	232.2	233.2	-
BGS fluid LIMS code	12389	12389	12389-0010	12389-0012	-	12389-0009	12389-0011	-
Comments	Filtered to 0.2 µm	Filtered to 0.2 µm	Filtered to 0.2 µm	Filtered to 0.2 µm	-	Filtered to 0.2 µm	Filtered to 0.2 µm	-
pH at 20 °C	12.06	12.05	7.07	7	-	12.81	12.72	-
Sample Code	YNFP Starting fluid	ENFG Starting fluid	1353/1	1357/1	-	1352/1	1356/1	-
TDS	12810	29180	19925		-	9908	-	-
Ca^{2+} (mg l^{-1})	40.4	2087	974	2006	-	705	1589	-
Mg^{2+} (mg l^{-1})	<1.93	<1.92	205	54.3	-	<1.91	<1.89	-
Na^{+} (mg l^{-1})	2674	9445	2205	8819	-	2309	8710	-
K^{+} (mg l^{-1})	4316	314	3524	148	-	3867	184	-
OH^{-} (mg l^{-1})	-	-	-	-	-	-	-	-
CO_3^{2-} (mg l^{-1})	-	-	-	-	-	73.5	44.7	-
HCO_3^{-} (mg l^{-1})	-	-	5263.0	3230.0	-	641.0	541.0	-
Total Alk (mg l^{-1})	-	-	-	-	-	-	-	-
Cl^{-} (mg l^{-1})	5797	16391	3166	11325	-	4515	13074	-
SO_4^{2-} (mg l^{-1})	<24.1	927	<97.8	564	-	<98.1	218	-
NO_3^{-} (mg l^{-1})	9.93	19.1	42.2	<38.8	-	<39.2	<38.4	-
Cat1 meq l^{-1}	228.7	523.0	251.5	492.0	-	234.5	462.9	-
Cat2 meq l^{-1}	0.000	0.558	0.056	0.597	-	0.147	0.612	-
An1 meq l^{-1}	163.7	482.0	90.0	331.2	-	127.4	373.4	-
An2 meq l^{-1}	0.000	0.378	0.000	0.000	-	0.000	0.000	-
AnTIC meq l^{-1}	163.7	482.0	90.0	331.2	-	127.4	373.4	-
Cation Total meq l^{-1}	228.7	523.6	251.5	492.6	-	234.7	463.5	-
Anion Total meq l^{-1}	163.7	482.4	90.0	331.2	-	127.4	373.4	-
Balance %	16.57	4.09	47.30	19.59	-	29.64	10.77	-
S Balance	17.3	3.75	47.7	-	-	30.0	-	-
TIC Balance	16.6	4.09	47.3	-	-	29.6	-	-
Br (mg l^{-1})	<9.65	30.2	<39.1	<38.8	-	<39.2	<38.4	-
NO_2^{-} (mg l^{-1})	<4.82	<4.76	<19.6	<19.4	-	<19.6	<19.2	-
HPO_4^{2-} (mg l^{-1})	<48.2	<47.6	<196	<194	-	<196	<192	-
F^{-} (mg l^{-1})	<4.82	<4.76	<19.6	<19.4	-	<19.6	<19.2	-
Total P (mg l^{-1})	<1.93	<1.92	<1.90	<1.89	-	<1.91	<1.89	-
Total S (mg l^{-1})	<48.2	362	<47.6	238	-	<47.8	90.2	-
S Diff %	83.32	14.50	31.39	20.84	-	31.51	19.18	-
Si (mg l^{-1})	35.8	<14.4	43.7	42.5	-	<14.3	<14.2	-
SiO_2 (mg l^{-1})	76.5	<30.8	93.5	91.0	-	<30.7	<30.4	-
Ba (mg l^{-1})	<0.386	<0.384	0.421	<0.379	-	1.84	1.61	-
Sr (mg l^{-1})	<0.965	24.5	2.17	26.2	-	5.26	25.8	-
Mn (mg l^{-1})	<0.386	<0.384	<0.381	<0.379	-	<0.382	<0.379	-
Total Fe (mg l^{-1})	<1.93	<1.92	<1.90	<1.89	-	<1.91	<1.89	-
Oxidised Fe (mg l^{-1})	<1.93	<1.92	<1.90	<1.89	-	<1.91	<1.89	-
Al (mg l^{-1})	<1.93	<1.92	<1.90	<1.89	-	<1.91	<1.89	-
Co (mg l^{-1})	<0.386	<0.384	<0.381	<0.379	-	<0.382	<0.379	-
Ni (mg l^{-1})	<0.965	<0.960	<0.952	<0.947	-	<0.956	<0.947	-
Cu (mg l^{-1})	<0.965	<0.960	<0.952	<0.947	-	<0.956	<0.947	-
Zn (mg l^{-1})	<0.965	<0.960	<0.952	<0.947	-	<0.956	<0.947	-
Cr (mg l^{-1})	<0.386	<0.384	<0.381	<0.379	-	0.855	1.06	-
Mo (mg l^{-1})	<2.89	<2.88	<2.86	<2.84	-	<2.87	<2.84	-
Cd (mg l^{-1})	<0.386	<0.384	<0.381	<0.379	-	<0.382	<0.379	-
Pb (mg l^{-1})	<1.93	<1.92	<1.90	<1.89	-	<1.91	<1.89	-
V (mg l^{-1})	<1.93	<1.92	<1.90	<1.89	-	<1.91	<1.89	-
Li (mg l^{-1})	<4.82	<4.80	<4.76	<4.73	-	<4.78	<4.73	-
B (mg l^{-1})	<4.82	<4.80	<4.76	<4.73	-	<4.78	<4.73	-
As (mg l^{-1})	<2.89	<2.88	<2.86	<2.84	-	<2.87	<2.84	-
Se (mg l^{-1})	<4.82	<4.80	<4.76	<4.73	-	<4.78	<4.73	-

Digestion vessel experiments to react Nirex Reference Vault Backfill (NRVB) with synthetic cement pore fluids ± CO_2
40 day long experiments at 40°C and 80 bar

	Starting solutions		CO_2 experiments				N_2 experiments			
	Young fluid	Evolved fluid	Young fluid	Evolved fluid	Dry	Deionised water	Young fluid	Evolved fluid	Dry	Deionised water
Start date	-	-	2/10/09 15:00	24/9/09 14:00	2/10/09 15:00	2/10/09 15:00	2/10/09 15:00	24/9/09 14:00	2/10/09 15:00	2/10/09 15:00
End date	-	-	10/11/09 11:30	3/11/09 13:45	10/11/09 16:30	10/11/09 11:15	10/11/09 10:20	3/11/09 13:30	10/11/09 11:45	10/11/09 16:15
Time (days)	0	0	40	40	2/10/04 0:00	2/10/04 0:00	2/10/04 0:00	2/10/04 0:00	2/10/04 0:00	2/10/04 0:00
Run temperature	-	-	40	40	40	40	40	40	40	40
Run pressure	-	-	80	80	80	80	80	80	80	80
Run number	-	-	**1347**	**1343**	**1348**	**1351**	**1346**	**1342**	**1349**	**1350**
Vessel number	-	-	BGS043	BGS057	BGS020	BGS046	BGS044	BGS056	BGS018	BGS045
Experimental charge	-	-	NRVB	NRVB	NRVB		NRVB	NRVB	NRVB	
Cement core number	-	-	3I	3F	3L	-	3J	3E	3K	-
Weight of cement core before	-	-	41.1453	42.0064	41.9013	-	41.4214	41.5020	41.7220	-
Weight of cement core after	-	-	41.1960	43.8972	45.0965	-	44.6017	41.4852	40.0921	-
Weight difference of cement core	-	-	0.0507	1.8908	3.1952	-	3.1803	-0.0168	-1.6299	-
Fluid type	YNFP starting solution	ENFG starting solution	YNFP	ENFG	-	Deionised water	YNFP	ENFG	-	Deionised water
Initial weight of fluid	-	-	235.1	240.0	N/A	240.0	236.7	237.1	N/A	240.0
BGS fluid LIMS code	12389	12389	12389-0006	12389-0004	-	12389-0008	12389-0005	12389-0003	-	12389-0007
Comments	Filtered to 0.2 µm	Filtered to 0.2 µm	Filtered to 0.2 µm	Filtered to 0.2 µm	-	Filtered to 0.2 µm	Filtered to 0.2 µm	Filtered to 0.2 µm	-	Filtered to 0.2 µm
pH at 20 °C	12.06	12.05	6.97	7.04	-	5.53	12.19	12.69	-	9.56
Sample Code	YNFP Starting fluid	ENFG Starting fluid	1347/1	1343/1	-	1351/1	1346/1	1342/1	-	1350/1
TDS	12810	29180	6580	16328	-	4285	11621	26200	-	164
Ca^{2+} (mg l^{-1})	40.4	2087	837	2345	-	73.8	485	1826	-	<19.5
Mg^{2+} (mg l^{-1})	<1.93	<1.92	522	348	-	<1.96	<1.91	<1.90	-	<1.95
Na^{+} (mg l^{-1})	2674	9445	2084	8370	-	<68.7	2552	10397	-	<68.2
K^{+} (mg l^{-1})	4316	314	3023	148	-	<98.2	4165	333	-	<97.4
OH^{-} (mg l^{-1})		-	-	-	-	-	-	-	-	-
CO_3^{2-} (mg l^{-1})		-	-	-	-	-	-	540	-	-
HCO_3^{-} (mg l^{-1})		-	1109.0	1192.0	-	42.9	675.1	<50	-	<5
Total Alk (mg l^{-1})		-	-	-	-	-	-	-	-	-
Cl^{-} (mg l^{-1})	5797	16391	4557	12636	-	<96.8	4569	13408	-	253
SO_4^{2-} (mg l^{-1})	<24.1	927	<98.5	587	-	<96.8	<97.3	277	-	326
NO_3^{-} (mg l^{-1})	9.93	19.1	<39.4	<39.1	-	<38.7	<38.9	<38.9	-	122
Cat1 meq l^{-1}	228.7	523.0	252.7	513.6	-	3.68	241.8	551.9	-	0.000
Cat2 meq l^{-1}	0.000	0.558	0.000	0.323	-	0.000	0.078	0.663	-	0.000
An1 meq l^{-1}	163.7	482.0	128.6	368.7	-	0.000	128.9	384.0	-	15.9
An2 meq l^{-1}	0.000	0.378	0.000	0.000	-	0.000	0.000	0.000	-	0.000
AnTIC meq l^{-1}	163.7	482.0	128.6	368.7	-	0.000	128.9	384.0	-	15.9
Cation Total meq l^{-1}	228.7	523.6	252.7	513.9	-	3.7	241.8	552.6	-	0.0
Anion Total meq l^{-1}	163.7	482.4	128.6	368.7	-	0.0	128.9	384.0	-	15.9
Balance %	16.57	4.09	32.56	16.45	-	100.00	30.46	18.00	-	-100.00
S Balance	17.3	3.75	32.9	16.1	-	180.0	30.8	17.8	-	-100.000
TIC Balance	16.6	4.09	32.6	16.5	-	100.0	30.5	18.0	-	-100.000
Br^{-} (mg l^{-1})	<9.65	30.2	<39.4	<39.1	-	<38.7	<38.9	<38.9	-	<38.7
NO_2^{-} (mg l^{-1})	<4.82	<4.76	<19.7	<19.6	-	<19.4	<19.5	<19.4	-	<19.4
HPO_4^{2-} (mg l^{-1})	<48.2	<47.6	<197	<196	-	<194	<195	<194	-	<194
F^{-} (mg l^{-1})	<4.82	<4.76	<19.7	<19.6	-	<19.4	<19.5	<19.4	-	<19.4
Total P (mg l^{-1})	<1.93	<1.92	<1.93	<1.92	-	<1.96	<1.91	<1.90	-	<1.95
Total S (mg l^{-1})	<48.2	362	<48.4	242	-	<49.1	<47.7	119	-	<48.7
S Diff %	83.32	14.50	32.07	19.19	-	34.18	31.95	22.54	-	323.11
Si (mg l^{-1})	35.8	<14.4	44.6	43.7	-	<14.7	<14.3	<14.2	-	<14.6
SiO_2 (mg l^{-1})	76.5	<30.8	95.5	93.6	-	<31.5	<30.6	<30.4	-	<31.3
Ba (mg l^{-1})	<0.386	<0.384	<0.387	<0.384	-	<0.393	1.42	1.82	-	<0.390
Sr (mg l^{-1})	<0.965	24.5	<0.967	14.1	-	<0.982	2.51	27.9	-	<0.974
Mn (mg l^{-1})	<0.386	<0.384	<0.387	<0.384	-	<0.393	<0.382	<0.379	-	<0.390
Total Fe (mg l^{-1})	<1.93	<1.92	<1.93	<1.92	-	<1.96	<1.91	<1.90	-	<1.95
Oxidised Fe (mg l^{-1})	<1.93	<1.92	<1.93	<1.92	-	<1.96	<1.91	<1.90	-	<1.95
Al (mg l^{-1})	<1.93	<1.92	<1.93	<1.92	-	<1.96	<1.91	<1.90	-	<1.95
Co (mg l^{-1})	<0.386	<0.384	<0.387	<0.384	-	<0.393	<0.382	<0.379	-	<0.390
Ni (mg l^{-1})	<0.965	<0.960	1.00	<0.960	-	<0.982	<0.954	<0.948	-	<0.974
Cu (mg l^{-1})	<0.965	<0.960	<0.967	<0.960	-	<0.982	<0.954	<0.948	-	<0.974
Zn (mg l^{-1})	<0.965	<0.960	<0.967	<0.960	-	<0.982	<0.954	<0.948	-	<0.974
Cr (mg l^{-1})	<0.386	<0.384	1.56	0.811	-	<0.393	0.474	1.45	-	<0.390
Mo (mg l^{-1})	<2.89	<2.88	<2.90	<2.88	-	<2.95	<2.86	<2.84	-	<2.92
Cd (mg l^{-1})	<0.386	<0.384	<0.387	<0.384	-	<0.393	<0.382	<0.379	-	<0.390
Pb (mg l^{-1})	<1.93	<1.92	<1.93	<1.92	-	<1.96	<1.91	<1.90	-	<1.95
V (mg l^{-1})	<1.93	<1.92	<1.93	<1.92	-	<1.96	<1.91	<1.90	-	<1.95
Li (mg l^{-1})	<4.82	<4.80	<4.84	<4.80	-	<4.91	<4.77	<4.74	-	<4.87
B (mg l^{-1})	<4.82	<4.80	<4.84	<4.80	-	<4.91	<4.77	<4.74	-	<4.87
As (mg l^{-1})	<2.89	<2.88	<2.90	<2.88	-	<2.95	<2.86	<2.84	-	<2.92
Se (mg l^{-1})	<4.82	<4.80	<4.84	<4.80	-	<4.91	<4.77	<4.74	-	<4.87